NEUTRAL AND IONIC FLUORESCENCE OF MOLECULAR GASES BY PHOTON IMPACT

SYED MAQBOOL AHMED

PH.D. THESIS
JULY 1990

PHYSICAL RESEARCH LABORATORY

NEUTRAL AND IONIC FLUORESCENCE OF MOLECULAR GASES

BY PHOTON IMPACT

by

SYED MAQBOOL AHMED

A THESIS
SUBMITTED FOR THE DEGREE OF

DOCTOR OF PHILOSOPHY

OF THE GUJARAT UNIVERSITY

JULY   1990

PHYSICAL RESEARCH LABORATORY
AHMEDABAD -   380 009
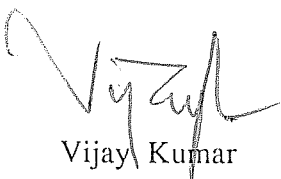INDIA

Dedicated
To
My Parents

CERTIFICATE

I hereby declare that the work presented in this thesis is original and has not formed the basis for the award of any degree or diploma by any University or Institution.

Syed Maqbool Ahmed

Certified by :

Vijay Kumar

Ahmedabad.

July, 1990.

STATEMENT

The basic aim of the work presented in this thesis is, to study the neutral and ionic fluorescence of molecular gases as a function of incident photon energies. The measurement of fluorescence quantum yield of neutral species by photon impact has been carried out for both SO_2 and CS_2 whereas, the fluorescence spectra of these target gases have been studied at the incident photon wavelengths of 121.6, 73.6-74.4, and 58.4 nm. The total photoabsorption and fluorescence cross sections are the required quantities to be measured for determining the fluorescence quantum yield of a molecule at an incident photon wavelength. The knowledge of these cross sections provides a better insight into the primary photochemical process of absorption . Also, these physical quantities are required to understand some of the important reactions occurring in the planetary atmospheres. Similarly the studies of fluorescence spectrum of the ionic species/dissociated fragments are of great importance in the areas of aeronomy and astrophysics.

A new method has been developed for the measurement of absolute photoabsorption cross section of neutral species. This includes a modified design for the beam splitter and an additional monochromator used at the end of absorption chamber to reject the fluorescence signals along the optic axis, arising due to the absorption of target molecules. The total fluorescence cross sections for the target molecules are also measured in the same experiment perpendicular or along the optic axis depending upon the strength of the fluorescence signals. Another experiment has been designed and fabricated to study the fluorescence spectra of target molecules at incident photon wavelengths less than 100 nm and also at 121.6 nm. In this case, the total fluorescence is

dispersed using a monochromator. The relative production cross sections for the product states are also obtained in the present experiment, at different incident wavelengths.

A sophisticated experimental set-up has been designed and fabricated in the laboratory to measure the fluorescence quantum yield of neutral species. An intense line-free UV continuum (185-350 nm) was produced from an argon mini-arc light source, and the radiation was monochromatised using a 1 meter near normal incidence evacuable monochromator. An instrumental bandwidth of about 0.2 nm was selected so as to accommodate the low fluorescence signals obtained in a few spectral regions. A beam splitter between the exit slit of the monochromator and the absorption/fluorescence chamber was used to monitor the incident photon intensity during the experiment. The absorption region, 24.8 cms long is evacuated to a pressure of 10^{-5} Torr and the other end is sealed by another quartz plate. An additional 0.2 meter monochromator was used after the absorption/fluorescence chamber to avoid the detection of fluorescent emission produced by the excited target molecules in the direction of the optic axis. All the light intensity measurements were made by thermoelectrically cooled photomultipliers. A MKS capacitance manometer was employed to measure the absolute pressure of the target gas.

The experimental set-up for the ionic fluorescence studies includes a micro-wave discharge light source to produce resonant lines of helium, nitrogen, and hydrogen, a differential pumping unit to remove the source gases entering into the fluorescence chamber , an evacuable fluorescence chamber with an appropriate outlet to study the fluorescence in a direction perpendicular to the incident photon beam, a 0.2 meter monochromator to disperse the fluorescence ,a thermoelectrically cooled photomultiplier , and a fast data acquisition system. This is a windowless experiment, and hence differential pumping is needed to maintain a high degree of vacuum inside the fluorescence chamber. The experimental set-up for neutral fluorescence and absorption studies has been discussed in Chapter 2 of the thesis,

whereas, the experiment on the ionic fluorescence has been described in Chapter 6. The subject of photoabsorption, photodissociation, fluorescence, ionic fluorescence, and dissociative photoionization has been introduced in Chapter 1.

An analytical method has been developed to compute the photoabsorption cross sections for neutral species using Beer-Lambert law. Methods have also been developed to calculate the fluorescence cross sections of target molecules in two configurations. In the first configuration, the fluorescence intensity is measured perpendicular to the optic axis whereas in the other geometry, the fluorescence signals are detected along the optic axis. The analytical methods developed to compute photoabsorption, and fluorescence cross section for the neutral species have been discussed in Chapter 3.

The major errors considered in the present experimental measurement are the errors arising from the pressure measurement, thermal transpiration effects, uncertainty in the measurement of optical path length, and counting statistics. The coherent sum of all these errors acted as an upper limit to the actual error, whereas the incoherent sum represented the most probable error. All the errors and their estimated magnitudes in the measurement of photoabsorption and fluorescence cross section for the neutral species of the target gases have been discussed in Chapter 4.

Total photoabsorption and fluorescence cross sections for sulphur dioxide have been measured in the 188-231 and 278.7-320 nm regions using argon mini arc light source with the monochromator resolution of 0.2 nm. The absorption cross sections have been measured with an accuracy of $\pm 3.1\%$ whereas the most probable error estimated in the case of fluorescence cross section is $\pm 4.6\%$. The fluorescence quantum yields for SO_2 have also been obtained in the two spectral regions. The photoabsorption cross sections measured in the present work

have been compared with data reported by other researchers in the field. A comparison in case of fluorescence cross sections is not possible as no quantitative measurements have been reported so far in these spectral regions. Presence of a predissociating state in SO_2 has been confirmed in the present experiment. The threshold energy of incident photons responsible for predissociation has been found to be in the range between 218.9 and 220.6 nm.

Total photoabsorption and fluorescence cross sections for carbon disulphide have been measured in the 188.2-213 and 287.5-339.5 nm spectral regions. The absorption cross sections have been measured with an accuracy of $\pm$ 4.2 % whereas the most probable error estimated in the case of fluorescence cross section is $\pm$ 5.1%. The fluorescence quantum yields for CS_2 have also been obtained in the two spectral regions. The photoabsorption cross sections measured in the first spectral region have been found to be pressure dependent. The mechanism for such a pressure dependence has also been put forward in the present work. The fluorescence cross section in the present experiment, were measured along the photon beam axis. In the spectral region 300-320 nm, the fluorescence cross section measured at the peaks of the vibrational bands have been fond to have different values at low and high pressures. A complex process which seems to occur in this case has been suggested. The process may involve vibrational relaxation of the upper emitting state prior to normal quenching. All these results have been discussed in detail in Chapter 5.

The fluorescence spectra of CS_2 and SO_2 have been studied at three incident photon wavelengths of 121.6, 73.6-74.4 and 58.4 nm and relative production cross sections for different product states have been measured. The $CS(A\ ^1\Pi \rightarrow X\ ^1\Sigma^+)$ system between 240 to 290 nm has been obtained when CS_2 is photoexcited at 121.6 nm whereas $CS_2^+(B\ ^2\Sigma_u^+ \rightarrow X\ ^2\Pi_g)$ and $CS_2^+(A\ ^2\Pi_u \rightarrow X\ ^2\Pi_g)$ systems have been produced between 276 to 295 and 437 to 555 nm respectively when excited by both the incident photon wavelengths of 73.6-74.4

and 58.4 nm. The fluorescence spectra of SO_2 obtained at 121.6 and 73.6-74.4 nm include the vibrational bands of $SO(A\ ^3\Pi \rightarrow X\ ^3\Sigma)$ and $SO\ (B\ ^2\Sigma^- \rightarrow X^3\ \Sigma^-)$ systems from 240 to 268 and 268 to 442 nm respectively whereas the emission spectrum at 58.4 nm, has contributions from the two SO systems and $SO^+(A\ ^2\Pi \rightarrow X\ ^2\Pi)$ system. In all these emission spectra, the fluorescence bands of different systems have been analyzed and their relative production cross sections have been measured. The results for both the target gases have been discussed in detail in Chapter 6, while conclusion and scope for future work has been taken up in Chapter 7.

ACKNOWLEDGEMENT

Our group members have offered their help whole heartily throughout my thesis work, and I would like to take this opportunity to thank them. I am grateful to Mr.A.P.Gohil for the help he has rendered to me in various capacities particularly in handling the data acquisition system (DAS) and making the arrangements in interfacing the DAS to the Computer. The power supply for the argon mini-arc source was designed and fabricated by Mr.I.T.Kripalani. I owe a lot to him for this and also for his help in making the manuscript of my thesis on the PC. Mr.Ishwarbhai's help was invaluable in the fabricating and setting up of my experiment on ionic fluorescence. His rich experience and sincere help went a long way in making the experiment a success. I express my sincere gratitude to him. I am thankful to Mr.R.S.Patel for his help in maintaining the vacuum instruments. Mr.J.K.Dave was always helpful in various kinds of jobs in the laboratory. My thanks are due to him. I am also thankful to Mr.C.S.Philips for his help in typing the scientific papers. Mr.V.K.Lodha was offering a helping hand throughout my experimental work. I gratefully acknowledge his contribution.
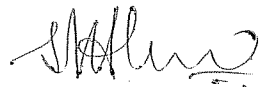
Thanks are due to Messrs H.N.Chandel and M.N.Trivedi for their help in the construction of the experimental set-up. I offer my thanks to the staff of workshop, carpentry, glass blowing and photographic section, liquid nitrogen plant and computer center for various helps during the course of my work. The ever cheerful library staff has always been cooperative. I thank Mrs.U.Ghiya and the entire staff for their valuable support. I am also thankful to the draftsman Mr.S.C.Bhavsar for making the various figures and diagrams.

It would be impossible for me to name all the people and friends whose association kept me happy and cheerful during all the past six years. A few names that comes to my mind immediately are Dr.Amarendra, Messrs Banerjee, Kishku, Kameshwar Rao, V.Ramani, Janardhan, Shakti, Gufran, Viju, Mathew, Swetkethu, Subrat, Gurubaran, Krishnan, Manohar lal,

Debashish, Somesh and Guru Prasad. I extend them my gratitude.

Discussions with my colleague and friend Miss P.Seema were very interesting and proved to be a great source of inspiration. I offer my thanks to her. I am indebted to my parents, brothers and sisters for their patience and enthusiastic support. I am particularly thankful to my father for his regular letters which kept me cheerful and in a positive state of mind throughout the thesis work.

Finally I thank once again all my friends and well wishers who have directly or indirectly helped me in completing this work successful.

(Syed Maqbool Ahmed)

July,1990
Ahmedabad

CONTENTS

CHAPTER - 2 : EXPERIMENTAL SET - UP

CHAPTER - 3   :   METHOD

CHAPTER - 4 : ERROR ANALYSIS

CHAPTER - 5 : RESULTS AND DISCUSSION

CHAPTER - 6 : IONIC FLUORESCENCE

CHAPTER - 7 :   CONCLUSION AND SCOPE FOR FUTURE WORK

LIST OF PUBLICATIONS

REFERENCES

CHAPTER - 1

INTRODUCTION

1.1 Photochemical Processes

Interaction of light with atoms and molecules leading to absorption of a light quantum is called *photochemical process*. The photochemical reaction comprises of series of events starting from the initial act of light absorption and ending in the production of stable molecule. The resultant products are, in general , different from the reactants.

Photochemical processes could conveniently be divided into *primary* and *secondary processes*. The primary process may be defined, following Noyes and Leighton (1966), as the initial act of light absorption leading to the formation of electronically excited state and other processes immediately following this initially formed excited state. The latter process may include unimolecular reactions such as fluorescence, dissociation, isomerisation and photoionization as well as bimolecular processes such as deactivation and reaction of the excited state by collisions with the same or different kind of molecules. The secondary process includes the reaction of atoms and radicals produced in the primary process either directly from the excited molecule or by collisions of the excited molecule with the same or different kind of molecules. The secondary reactions are the reactions of atoms and radicals with each other and the reaction of atoms and radicals with molecules.

1

When ultraviolet or vacuum ultraviolet radiation is incident on diatomic or simple polyatomic molecules, the following primary photochemical reactions may take place :

1. $AB_2 + h\nu \longrightarrow AB_2^{**}$ (Photoexcitation)

$AB_2^{**} \longrightarrow AB_2^{*} + h\nu'$ (Neutral Fluorescence)

$AB_2 + h\nu \longrightarrow AB^{**} + B$

                                   (Photodissociation)

$\longrightarrow AB + B^{*}$

$AB^{**} \longrightarrow AB^{**} + h\nu'$ (Fluorescence from

                                     photofragmented

$B^{**} \longrightarrow B^{*} + h\nu'$ products)

2. $AB_2 + h\nu \longrightarrow (AB_2^{+})^{**} + e^{-}$ (Photoionization)

$(AB_2^{+})^{**} \longrightarrow (AB_2^{+})^{*} + h\nu'$ (Ionic fluorescence)

$AB_2 + h\nu \longrightarrow AB^{+} + B^{-}$

                                   (Dissociative

                                   photoionization)

$\longrightarrow AB^{-} + B^{+}$
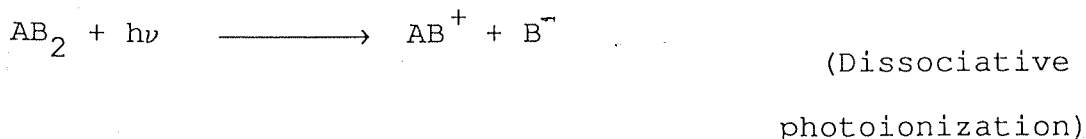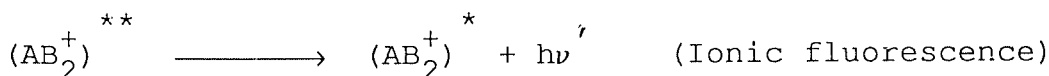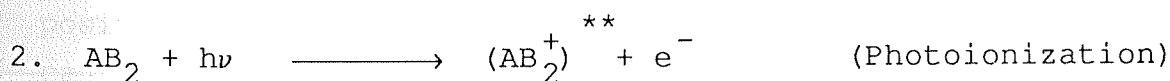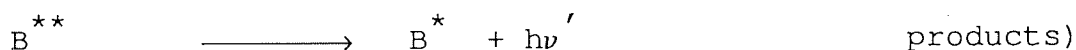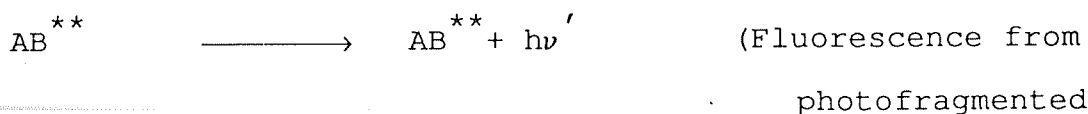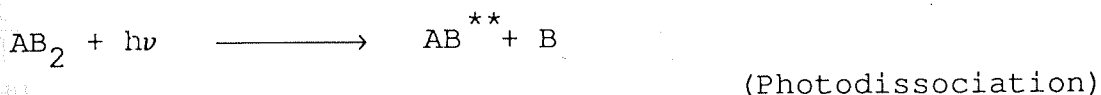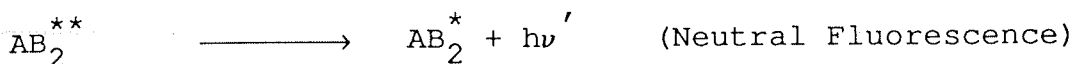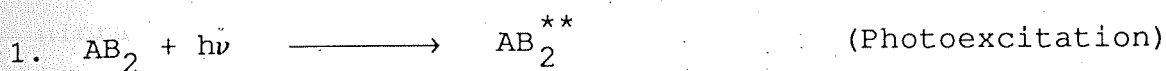
The double asterisk (**) indicates the higher electronically excited state whereas the single asterisk (*)

denotes lower electronically excited state. In the above example, a typical triatomic molecule AB_2 has been chosen. ν and ν' are the frequencies of the incident and emitted radiation respectively. It may be interesting to note that most simple molecules with the exception of O_3 and NO_2 absorb light only in the ultraviolet (200 - 400 nm) and vacuum ultraviolet (below 200 nm) regions. The molecules O_3 and NO_2, however, can absorb visible light even at longer wavelengths.

1.2 Quantum States of Molecules

Although, the target gases used in the present experiment were triatomic molecules, the discussion on diatomic molecules will be helpful in understanding the various quantized energies available in a triatomic molecule.

1.2.1 Diatomic molecules

It is well known that atoms can exist only in certain discrete states. These states may also be represented by various orbits of electrons moving about a nucleus of positive charge. The energy values for various atomic states can in principle be obtained by solving Schrödinger equation using appropriate potential energies for electrons. In the case of diatomic molecule two additional features, the vibration and rotation of the molecule, have to be considered.

1.2.1.1 Rotational energy levels of diatomic molecules

A diatomic molecule can rotate about an axis perpendicular to the internuclear axis and passing through the center of gravity. Assuming that the distance 'r' between masses m_1 and m_2 does not change with rotation (a rigid

rotator model) the energy levels of such a rigid rotator can be found by solving the Schrödinger equation of a form :

$$\sum_{i=1,2} \frac{1}{m_i} \left[\frac{\partial^2 \psi}{\partial x_i^2} + \frac{\partial^2 \psi}{\partial y_i^2} + \frac{\partial^2 \psi}{\partial z_i^2} \right] + \frac{8\pi^2}{h^2} E\psi = 0 \quad \longrightarrow (1.1)$$

where ψ is a wave function of the coordinates alone; x_i, y_i, z_i are the cartesian coordinates; m_i is the mass of the atom 'i' and E is the total energy. By solving the Schrödinger equation, the energies are given by

$$E = \frac{h^2 \, J \, (J+1)}{8\pi^2 \, \mu r^2} \quad \longrightarrow (1.2)$$

where h is the Planck's constant, $\mu r^2 = I$ is the moment of inertia, μ is the reduced mass and J is the rotational quantum number, which can take the integral values.

If the wave number is used instead of energy, Eq. (1.2) becomes

$$F(J) = \frac{E}{hc} = B \, J(J+1) \quad \longrightarrow (1.3)$$

where $$B = \frac{h}{8\pi^2 \, cI} \quad cm^{-1} \quad \longrightarrow (1.4)$$

The constant B is called the rotational constant and F(J) in cm^{-1} gives the rotational term value. In actual practice, the internuclear distance changes periodically with time near the

equilibrium distance. Also, because of the action of the centrifugal force, the internuclear distance increases with increasing rotation of molecules. A detailed calculation shows that the actual rotational term value is given by

$$F(J) = B \; J(J+1) - D \; J^2 \; (J+1)^2 \qquad\qquad \longrightarrow (1.5)$$

where D is a constant much smaller than B.

1.2.1.2 Vibrational energy levels of diatomic molecules

When two atoms combine to form a stable covalent molecule, they may be said to do so because of internal electronic re-arrangement. On one hand there is a repulsion between the positively charged nuclei of both atoms and between the negative electron *clouds*; on the other, there is an attraction between the positively charged nucleus of one atom and the electrons of the other and vice versa. The two atoms settle at a mean internuclear distance such that these forces are just balanced and the energy of the whole system is at a minimum. Attempt to squeeze the atoms more closely together leads to rapid increase in repulsive forces, whereas attempt to pull them further apart is restricted by the attractive forces. In either case an attempt to distort the bond requires an input of energy and so the relation between potential energy versus internuclear distance can be plotted as given in Fig.(1.1).

The compression and extension of a bond may be considered, as the behaviour of a spring, which follows Hook's law. This may be written as

$$F = - k \; (r-r_{eq}) \qquad\qquad \longrightarrow (1.6a)$$

where F is the restoring force, k the force constant and 'r'
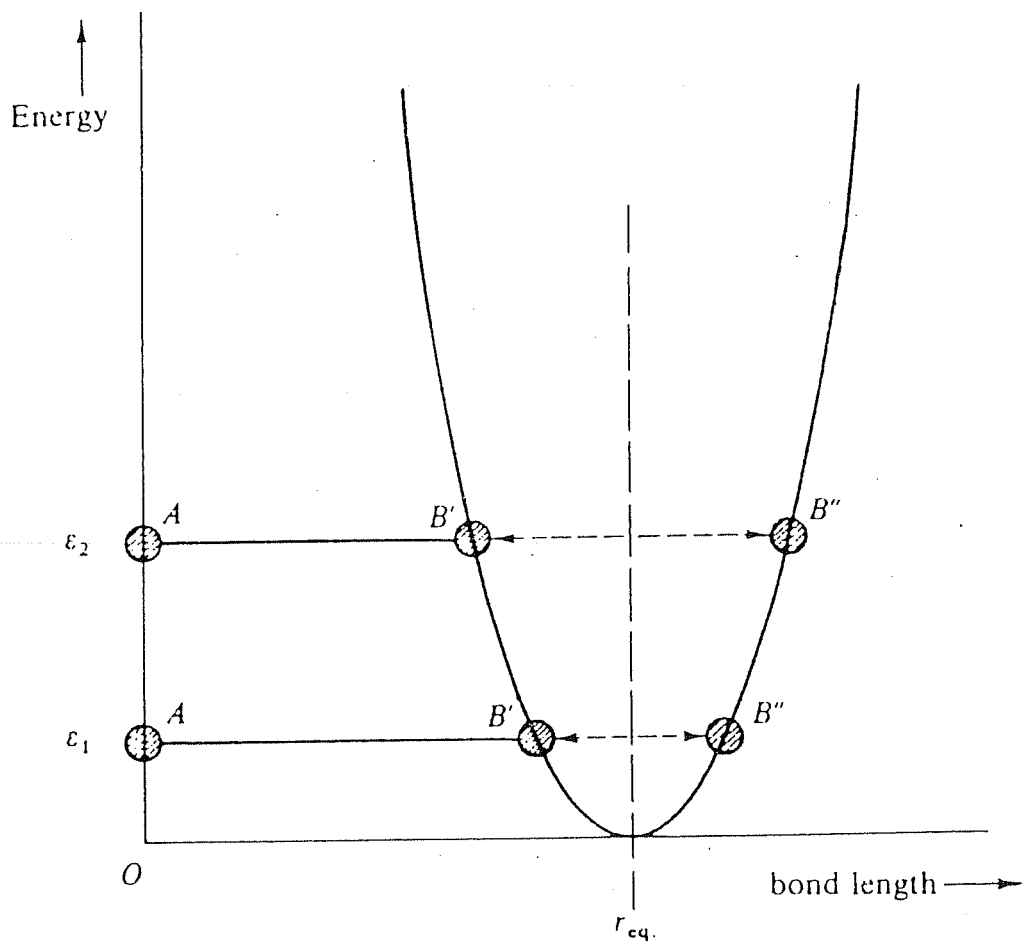
Figure 1.1 Parabolic curves of energy plotted against the extension or compression of a spring obeying Hook's law.

the internuclear distance.

The energy curve is parabolic and has the form

$$E = \frac{1}{2} k (r-r_{eq})^2 \quad\quad\quad \longrightarrow \text{(1.6b)}$$

This model of vibrating diatomic molecule, the so-called simple harmonic oscillator model, is only an approximation. Figure (1.1) shows that if one atom A is considered to be stationary on the $r = 0$ axis; the other will oscillate between B' and B''. Classically, the oscillating frequency is given by

$$\omega_{osc} = \frac{1}{2\pi} \sqrt{\frac{k}{\mu}} \quad \text{Hz.} \quad\quad\quad \longrightarrow \text{(1.6c)}$$

where μ is reduced mass of the system.

Vibrational energies, like all other molecular energies, are quantized and the allowed vibrational energies for any particular system may be calculated by substituting the form of potential energy Eq.(1.6b) into the Schrödinger equation. For the simple harmonic oscillator these turned out to be

$$E_v = (v + 1/2) h\omega_{osc} \quad \text{joules} \quad\quad (v=0,1,2,..)$$

or $\quad\quad\quad\quad\quad\quad\quad\quad\quad\quad\quad\quad\quad\quad \longrightarrow \text{(1.7a)}$

$$G_v = \frac{E_v}{hc} = (v + 1/2) \bar{\omega}_{osc} \quad \text{cm}^{-1} \quad\quad \longrightarrow \text{(1.7b)}$$

6

where $\bar{\omega}_{osc} = \dfrac{1}{2\pi c} \sqrt{\dfrac{k}{\mu}}$ is in cm^{-1} and v is the vibrational quantum number.

Real molecules do not obey exactly the laws of simple harmonic motion; real bonds although elastic, are not so homogeneous as to obey Hook's law. If the bond between atoms is stretched, for instance, there comes a point at which it will break into atoms. Thus although for small compressions and extensions the bond may be taken as perfectly elastic, for larger amplitudes, greater than 10% of the bond length, a much more complicated behaviour must be assumed. Figure (1.2) shows diagrammatically, the shape of the energy curve for a typical diatomic molecule, together with (dotted) the ideal, simple harmonic parabola.

A purely empirical expression which fits this curve to a good approximation was derived by P.M.Morse and is called *Morse Function*:

$$E = D_{eq} \left[1 - \exp\{-a(r_{eq} - r)\} \right]^2 \qquad \longrightarrow (1.8a)$$

where 'a' is a constant for a particular molecule and D_{eq} is the dissociation energy.

When Eq.(1.8a) is used instead of Eq.(1.6b) in the Schrödinger equation, the pattern of the allowed vibrational energy level is found to be

$$G(v) = (v + 1/2)\,\bar{\omega}_e - (v + 1/2)^2\,\bar{\omega}_e x_e + \ldots \longrightarrow (1.8b)$$

7
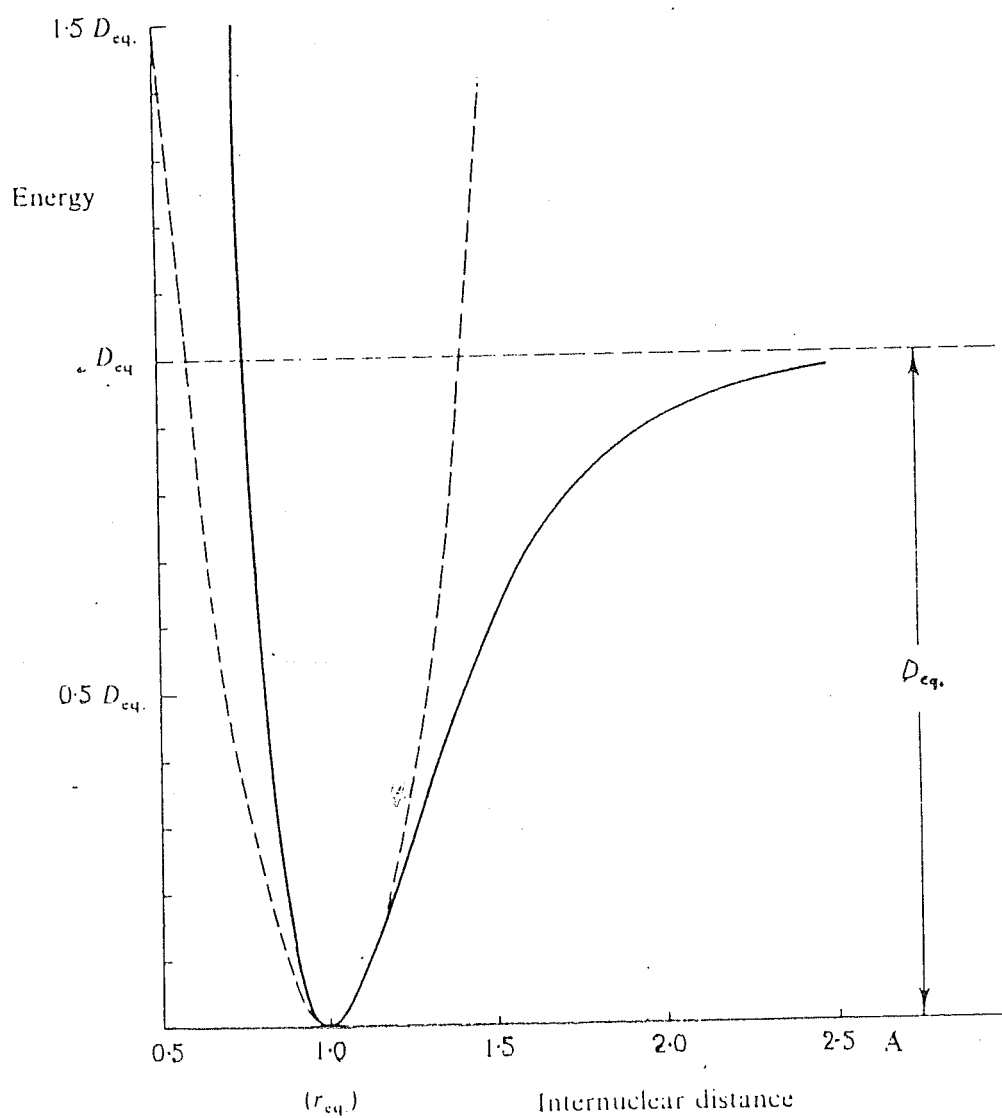
Figure 1.2 The Morse curve : the energy of a diatomic molecule undergoing anharmonic extension and compressions.

where $\bar{\omega}_e$ is oscillating frequency (in cm^{-1}) and x_e is the corresponding anharmonicity constant.

1.2.1.3 Electronic states of diatomic molecules

In contrast with atoms where electrons rotate about a spherically symmetric field, electrons in a diatomic molecule move about a field that is cylindrically symmetric with respect to the internuclear axis. As a result, the orbital angular momentum of the electrons is defined along the internuclear axis. The spectroscopic term symbols for the diatomic molecular orbitals can be obtained as in the case of atoms, by the summation of all λ's, the quantum number of the component of the orbital angular momentum of the electrons, to give the total angular momentum number in the direction of the bond axis, and is denoted by L. A precession of L takes place about the internuclear axis with constant component M_L (h/2Π), where M_L can take only the values

$$M_L = L, \ L-1, \ L-2, \ldots \ldots \ -L \qquad \longrightarrow (1.9)$$

The term Λ represents the component of the electronic orbital angular momentum along the internuclear axis and is given as:

$$\Lambda = |\ M_L\ | \qquad \longrightarrow (1.10)$$

Similarly the total spin quantum number of the molecule S, can be had by adding the spin of individual electrons. For $\Lambda \neq 0$ there is an internal magnetic field in the direction of internuclear axis resulting from the orbital motion of electrons. This magnetic field causes a precession of S about

the field direction (the internuclear axis) with a constant component of M_S (h/2π). For molecules M_S is denoted by Σ (this quantum number Σ is different than the term symbol Σ used for $\Lambda = 0$), and from quantum theory the allowed values for Σ are

$$\Sigma = S, \ S-1, \ S-2, \ldots \ldots \ -S \qquad\qquad \longrightarrow (1.11)$$

The two quantities combine to give the resultant angular momentum $\Omega = |\Lambda + \Sigma|$. The total multiplicity is given by (2S+1). The term symbol for $\Lambda = 0, \pm 1, \pm 2, \ldots$ etc., respectively are Σ, Π, Δ, Φ ....etc., . The states Π, Δ, Φ, are doubly degenerate, since Λ can both be positive and negative; Σ states are non-degenerate. The spectroscopic terms are represented by

$$^{2S+1}\Lambda_{\Omega} \qquad\qquad \longrightarrow (1.12)$$

For example the ground state of hydrogen molecule can be written as

$$^1\Sigma_g^+$$

Here the superscript + (or -), subscript g (or u) provides further information regarding the symmetry properties of the orbital. In any diatomic molecule any plane drawn through both nuclei is a plane of symmetry i.e, electron density, shape, force fields are quite unchanged by reflection in the plane. However the wave function of the electron, Ψ, may either be completely unchanged (symmetrical, +) or changed in sign only (antisymmetrical, -) with respect to such a reflection. The subscript letters 'g' and 'u' stand for *gerade* or symmetric and *ungerade* or antisymmetric functions

respectively under the operation of inversion at the point of symmetry located at the bond axis. In the case of homonuclear molecule the mid-point of the bond between two (identical) atoms is the center of symmetry. If the molecule is heteronuclear, then there is no center of symmetry and the odd-even classification of orbitals does not arise.

For molecular orbitals, the principal quantum number n has no meaning. According to convention, the ground state is denoted by the symbol X, higher excited states of the same multiplicity as the ground state by A, B, C etc., and those of different multiplicity by small letters a, b, c etc. For example, the ground state of oxygen is $X^3\Sigma_g^-$ and the higher excited states are $a^1\Delta_g$ and $b^1\Sigma_g^+$.

1.2.2   Quantum States of Polyatomic Molecules

The following discussion restricts to simple polyatomic molecules.

1.2.2.1   Rotational levels of polyatomic molecules

In the case of diatomic molecules, rotational energy levels are given in terms of the moment of inertia about the axis perpendicular to the internuclear axis and going through the center of mass. In polyatomic molecules, three mutually perpendicular axes, called the principal axes, must be considered about which the moment of inertia is maximum or minimum. According to international nomenclature, the rotational constants are designated as

$$A > B > C$$

and the corresponding axes are called a *axis*, b *axis*, *and* c *axis*. If B = C, the molecule is called a prolate symmetric

top, whose rotational term values are given by

$$F(J,K) = B\ J(J+1) + (A-B)K^2 \qquad\longrightarrow (1.13)$$

where $A = h/8\pi^2cI_A$, $B = h/8\pi^2cI_B$ and K is the quantum number of the component of the angular momentum along the top axis. On the other hand if $A = B$, the molecule is called an oblate symmetric top and its rotational term values are given by

$$F(J,K) = B\ J(J+1) - (B-C)K^2 \qquad\longrightarrow (1.14)$$

where $C = h/8\pi^2cI_C$. Since K is a component of J, K can not be greater than J. For each K, J takes a series of values $J = K,\ K+1,\ K+2, \ldots$.

1.2.2.2 Vibrational levels of polyatomic molecules

In the case of polyatomic molecules, there are 3N-6 vibrational degrees of freedom for nonlinear molecules and 3N-5 vibrational degrees of freedom for linear molecules, where N is the number of atoms in the molecule. The vibrational term values without degenerate vibrations are

$$G(v_1, v_2, \ldots) = \sum_i \omega_i(v_i+1/2) + \sum_i \sum_{k>i} x_{ik}(v_i+1/2)(v_k+1/2) + \ldots$$

$$\longrightarrow (1.15)$$

here ω_i is the frequency (cm^{-1}) of the ith normal vibration corresponding to ω_e of diatomic molecules, v_i is the vibrational quantum number of the ith normal vibration or

harmonic motion and x_{ik} is the anharmonicity constant corresponding to $\omega_e x_e$ for diatomic molecule.

1.2.2.3 Electronic states of polyatomic molecules

The electronic states of the polyatomic molecules are generally classified according to the symmetry properties of the molecules in the equilibrium position. The electronic eigen function either changes sign or remains unchanged by the symmetry operations allowed for the point group to which the molecule belongs. The symmetry property of the electronic eigen function is important to determine whether a given transition is allowed and also to obtain the direction of transition moment.

Another expression of the electronic states of polyatomic molecules is the so-called molecular orbital rotation. In this notation, each electron is associated with the eigen function corresponding to the motion of the electron in the field of the fixed nuclei and the average field of other electrons. The eigen function has the same symmetry properties as one of the symmetry species of the point group to which the molecule belongs. For example, for the point group C_{2v}, molecular orbitals are represented by a_1, a_2, b_1 and b_2. Electronic energies of the molecular orbitals can be estimated from the correlation between the united atom and separated atoms.

Symmetry properties of a molecule are of utmost importance in understanding its chemical and physical behaviour, in general, and spectroscopy and photochemistry in particular. A symmetry operation is one which leaves frame work of a molecule unchanged. There are five kind of symmetry operations which are necessary for classifying a point group :

1. Rotation about an axis of symmetry   : C_p

2. Reflection in a plane of symmetry   : σ

3. Inversion through a center of symmetry   : i

4. Rotation about an axis followed by
   reflection in a plane perpendicular to it   : S

5. Identity operation   (or)
   leaving the molecule unchanged   : I

The axes, plane, and center of symmetry are known as the *elements of symmetry*. All these elements intersect at one point, the center of gravity of the molecule, which does not change during these operations. Hence the designation point group.

In the molecular orbital theory, wave function of molecules plays a significant role. Since each of these symmetry operations of the point group carries the molecule into a physically equivalent configuration, any physically observable property, such as the energy, of the molecule must remain unchanged by the symmetry operation. The only possible wave functions of the molecules are those which are either symmetric or antisymmetric towards the symmetry operation of the point group.

If there is only one element of symmetry (as in point group C_2 and C_s) there are only two types of electronic states, those whose eigen functions are symmetric with respect to that element of symmetry. These symmetry types are designated A and B for C_2 and A$'$ and A$''$ for C_s.

13

In point groups with two independent elements, of symmetry there are four types of electronic states which may be designated as ++, +-, -+, and -- where the first and the second sign represent the behaviour with respect to the two possible symmetry operations. This applies to the point groups C_{2v} and C_{2h} for which the symmetry types are designated by A_1, A_2, B_1, B_2 and A_g, A_u, B_u, B_g respectively.

If a molecule has a two-fold axis C_{2v}, and two planes of symmetry σ_2 through the axis, then it belongs to the point group C_{2v}. In considering the symmetry of the molecule it is always assumed that an axis of symmetry is set up vertically. In this case, therefore, the planes through the axis are "vertical" planes. That is why they are called σ_v. On the other hand the molecule with an infinite-fold axis (C_∞), an infinite number of C_2's perpendicular to the C_∞, an infinite number of planes through the C_∞, and a plane of symmetry perpendicular to the C_∞ belongs to $D_{\infty h}$ point group.

In the present experiment the gases used to measure the fluorescence quantum yield are SO_2 and CS_2. The ground state of sulphur dioxide is $\tilde{X}\ ^1A_1$ of C_{2v} point group and that of carbon disulphide is $\tilde{X}\ ^1\Sigma_g^+$ belonging to $D_{\infty h}$ point group.

1.3 Primary Processes in Diatomic Molecules

The primary processes following light absorption by diatomic molecules should illustrate the simplest case of photochemical processes since there is only one bond to be broken and the resulting products are two atoms. The molecule may, upon light absorption, undergo immediate dissociation or may perform many vibrations before it dissociates into atoms. Sometimes the molecule is raised to a stable excited state from which it fluoresces if it suffers no collisions.

The absorption spectra of diatomic molecules are in some cases continuous, without any fine structure, while in other cases they show discrete structure followed by a continuum. The spectra may be explained with the aid of the potential energy curves. Figure (1.3a) shows the potential energy curves for direct dissociation by absorption of a light quantum $h\nu$. The upper repulsive curve has no minimum and a dissociation results from light absorption at all wavelengths.

Figure (1.3b) presents the potential energy curves showing that a molecule dissociates into one ground and one excited atom above energies corresponding to the convergence limit. v' signifies the vibrational levels of the upper state and v'' means those of the ground state. The absorption spectrum in this case will have a discrete structure corresponding to the transitions $v_i' \leftarrow v_i''$.

After a molecule has undergone an electronic transition into an excited state there are several processes by which its excess energy may be lost. Some of them are discussed here

(i)   **Dissociation**: The excited molecule breaks into two fragments. No spectroscopic phenomena, beyond the initial absorption spectrum, are observed unless the fragments radiate energy by one of processes mentioned below

(ii) **Re-Emission**: If the absorption process takes place as shown schematically in Fig (1.4 a), then the re-emission called 'Resonance fluorescence' is just the reverse of this, as in (b) of the figure.

(iii) **Fluorescence**: If, as in Fig (1.4a), the molecule is in a higher vibrational state after electronic excitation, then excess vibrational energy may be lost by inter-molecular collisions; this is illustrated in (c) of the figure. The
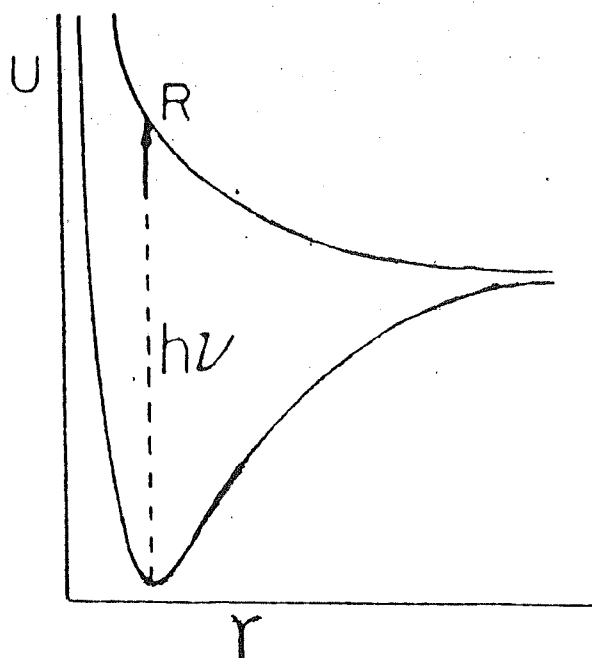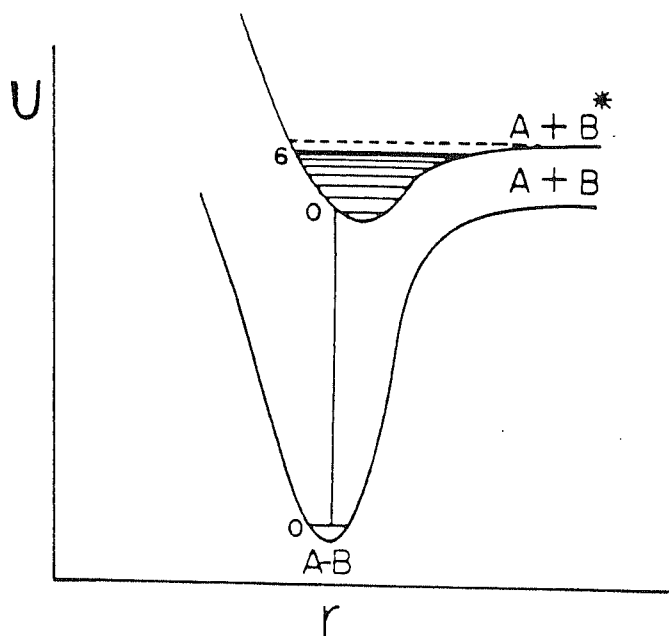
Figure 1.3 (a) Potential energy curves showing absorption continuum.

(b) Potential energy curves showing convergence limit.

(a) absorption   (b) Re-emission   (c) Fluorescence   (d) Phosphorescence
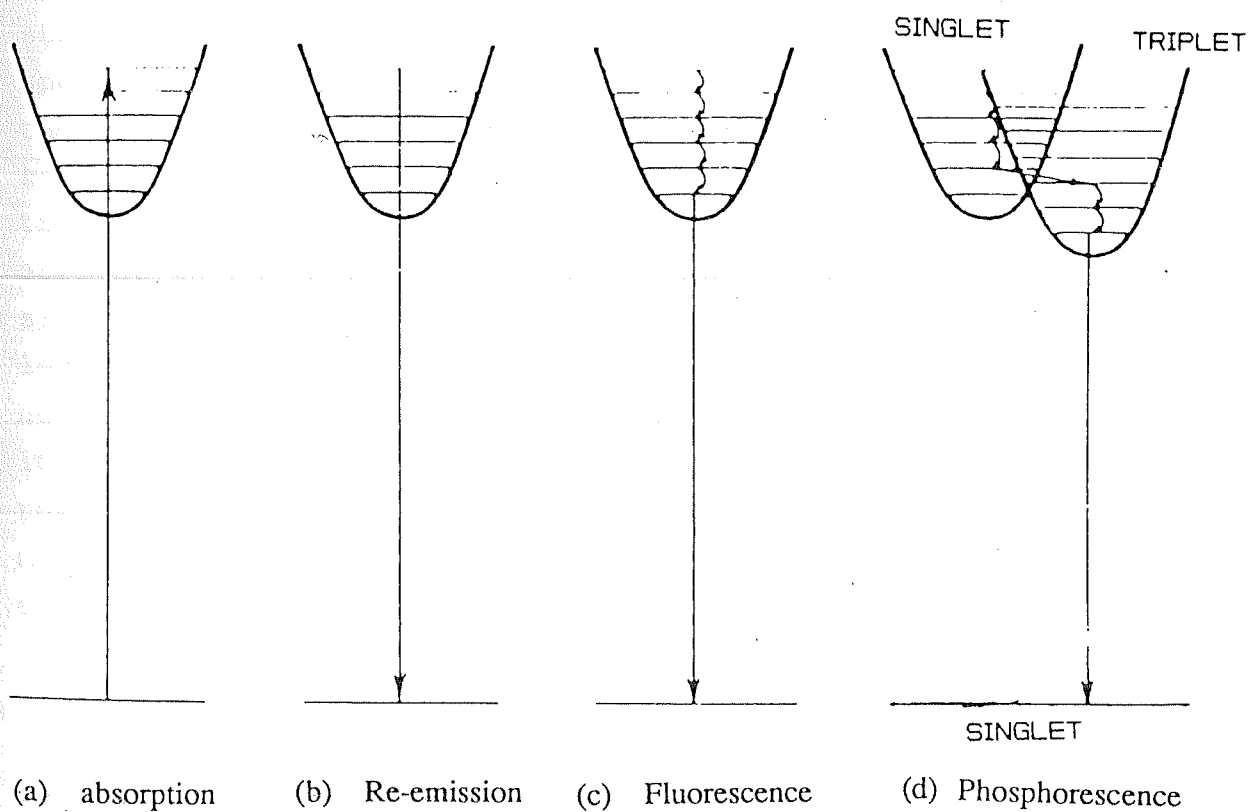
Figure 1.4 Showing the various ways in which an electronically excited molecule can lose energy.

vibrational energy is converted to kinetic energy and appears as heat in the sample; such transfer between energy levels is referred to as *radiationless*. When the excited molecule has reached a lower vibrational state (e.g. $v' = 0$), it may then emit radiation and revert to the ground state. The radiation emitted, called the fluorescence spectrum, is normally of lower frequency than that of initial absorption.The time between initial absorption and return to the ground state is very small, of the order of 10^{-8} sec.

(iv) **Phosphorescence:** This can occur when two excited states of different total spin have comparable energies. Thus in (d) of Fig (1.4), the ground state and one of the excited states are singlet ($S = 0$) states, while the neighbouring excited state is a triplet ($S = 1$). Although the rule $\Delta S = 0$ forbids spectroscopic transitions between singlet and triplet states, there is no prohibition if the transfer between the excited states occurs kinetically, i.e., through radiationless transition induced by collisions. Once the molecule has arrived in the triplet state, it cannot return to the excited singlet state. It will, therefore, eventually reach the $v' = 0$ level of the triplet state. Now although a transition from here to the ground state is forbidden by dipole transition, it may take place via other channels but much more slowly than allowed transition. Thus, this is why a phosphorescent material will continue to emit radiation seconds, minutes or even hours after the initial absorption.

1.3.1 Predissociation in diatomic molecules

If the incident photon energy exceeds the bond energy, the primary process is either the complete dissociation or the simultaneous occurrence of dissociation and fluorescence. The former case is represented in Fig.(1.5a), where the two upper states, R_1, and R_2 are both repulsive. The R_1 state is
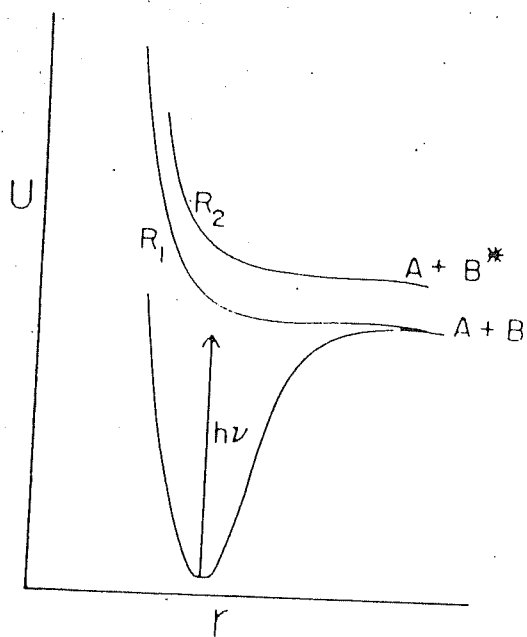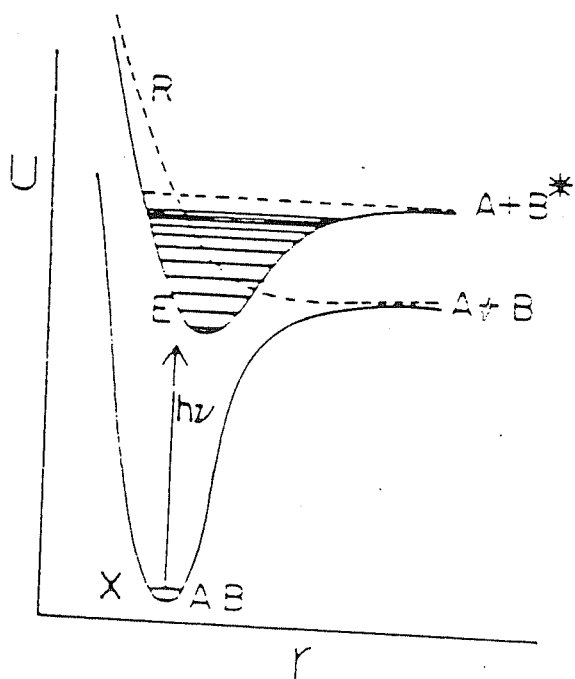
Figure 1.5 (a) Potential energy curves showing continuous absorption. R_1 and R_2 are two upper repulsive curves.

(b) Potential energy curves showing predissociation.

correlated with ground state atoms A and B, while R_2 state is associated with one ground and one excited atom, A and B^*.

The latter case, that is, the simultaneous occurrence of dissociation and fluorescence, is shown in Fig.(1.5b). It shows the upper state A correlated with one ground and one excited state atom, A and B^*, and the repulsive state R arising from ground state atoms, A and B. If the photon energy slightly exceeds the bond energy of the ground electronic state X, the molecule may cross over to the repulsive state R and dissociate immediately or it may be brought into the stable state A by light absorption from which the molecule may either fluoresce or predissociate into A + B by a radiationless transition to the repulsive state R.

1.4 Primary Processes in the Triatomic Molecules

If the incident photon energy is below that of the weakest bond, an electronically excited molecule formed by light absorption may give rise to fluorescence. The lifetime of the radiative transition to the ground state is related to the integrated absorption coefficient as given by:

$$\tau^{-1} = A(v^{'}) = 2.8 \times 10^{-8} \sum_{v^{''}} \bar{\nu}^{-3} (v^{'}, v^{''}) \ q(v^{'}, v^{''}) \int \frac{k_{\bar{\nu}}}{\bar{\nu}} \ d\bar{\nu}$$

$$\longrightarrow (1.16)$$

where $v^{'}$ and $v^{''}$ are vibrational states of excited and ground states respectively, τ is the radiative lifetime, $q(v^{'}, v^{''})$ is the Franck-Condon factor, $\bar{\nu}$ is the wave number corresponding to the absorbed radiation, $k_{\bar{\nu}}$ is the absorption coefficient, and $A(v^{'})$ is the spontaneous emission probability of an excited state.

.It has been found for simple molecules, such as CS_2, SO_2 and NO_2 that the observed fluorescence lifetimes are much longer than those expected from the integrated absorption coefficient. Common to these molecules are the extensive perturbation of rotational structure observed in the ultraviolet and visible regions. Douglas (1966) was the first who suggested that the anomalous lifetime can be explained on the basis of an extensive interaction between the initially formed excited state by light absorption and another state that does not combine with the ground state. Figure (1.6) shows a schematic energy level diagram that illustrates the *Douglas mechanism.*

The molecule is brought into a certain rotational level below the dissociation energy D_0 of the excited state E_1 by light absorption (Fig. 1.6). The rotational level interacts with many adjacent levels belonging to another excited state E_2. The E_2 state may be a metastable state located between the ground state and E_1, or it can be the ground state. If the E_2 state is the ground state, the level density at the energy corresponding to hν may be much larger than that of the E_1 state. In other words, the level in the E_1 state is diluted many times by the levels of the ground state. Since the transition from these levels (of E_2 state) are forbidden, the radiative life is many times greater than that expected from the integrated absorption coefficient. It may also be stated that the molecule, initially in the E_1 state, goes over to the E_2 state where it spends most of its time before it comes back to the E_1 state and fluoresce.

1.4.1 Photodissociation in triatomic molecule

The photodissociation commonly occurs by absorption of light with energies exceeding the weakest bond. The most common type of photodissociation in triatomic molecules XYZ is a dissociation at the weaker of the two bonds
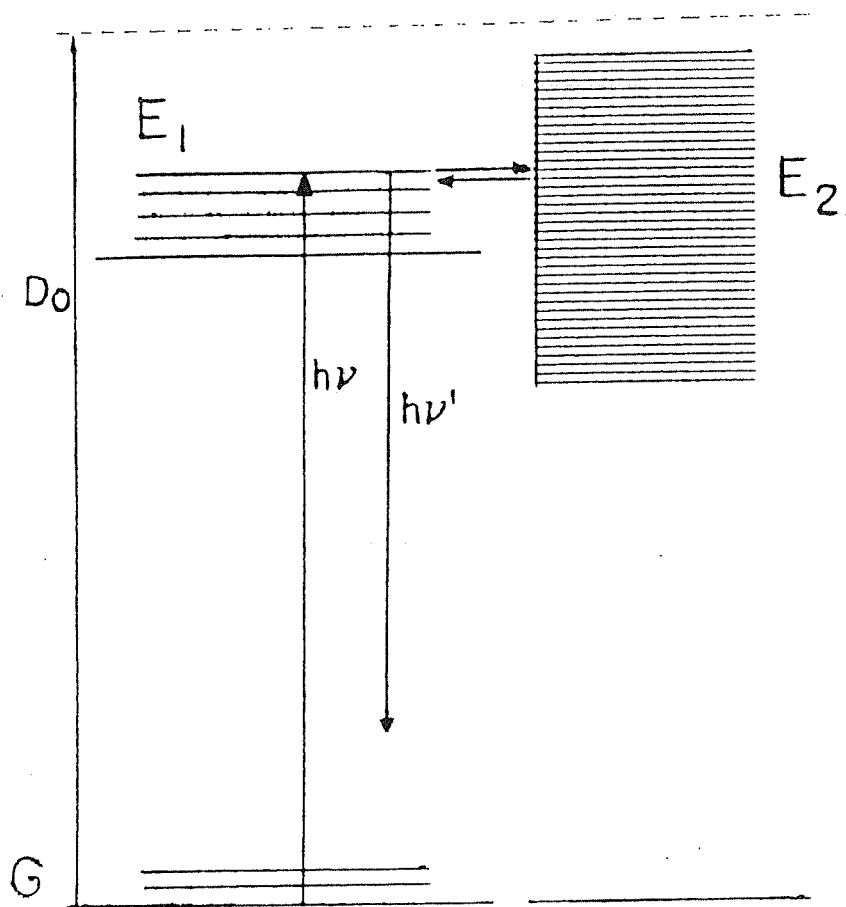
Figure   1.6   The   anomalously   long   radiative   life.   Explaining
          Douglas mechanism.

$$XYZ \;+\; h\nu \;\longrightarrow\; X + YZ \qquad\qquad \longrightarrow \;(1.17)$$
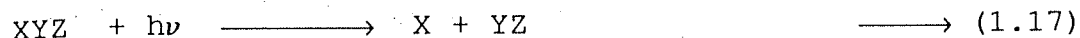
where the X - Y bond is weaker than the Y - Z bond. Typical examples are

$$OCS \;+\; h\nu \;\longrightarrow\; S + CO$$

$$NOCl \;+\; h\nu \;\longrightarrow\; Cl + NO$$
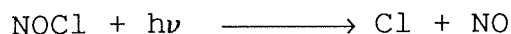
Another type of dissociation is the simultaneous scission of the two bonds and the formation of a new bond

$$XYZ \;+\; h\nu \;\longrightarrow\; XZ + Y \qquad\qquad \longrightarrow \;(1.18)$$

This type of dissociation appears to be common in vacuum ultraviolet photolysis but less common in near ultraviolet, indicating a large potential barrier for such a process. The photolysis of H_2O at 123.6 nm leads partially to the formation of H_2 molecule

$$H_2O \;+\; h\nu \;\longrightarrow\; H_2 + O$$
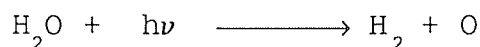
An upper state responsible for the dissociation must have an equilibrium configuration with an H - O - H angle much smaller than that in the ground state.

A still less common type of dissociation is the production of three atoms

$$XYZ + h\nu \longrightarrow X + Y + Z \longrightarrow (1.19)$$
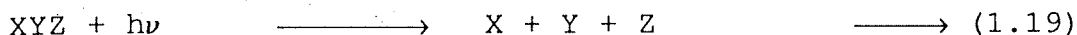
This type of dissociation is energetically possible in the vacuum ultraviolet photolysis; no such examples have clearly been demonstrated.

1.4.2 Predissociation in triatomic molecules

When a discrete upper state is above the dissociation limit, a molecule in the discrete upper state raised by light absorption may dissociate into products through the interaction with an overlapping dissociation continuum and at the same time give rise to fluorescence or it may cross over to another metastable state. The situation is similar to the predissociation in diatomic molecules as discussed earlier, although some clear-cut cases have been found in absorption spectra of polyatomic molecules.

The predissociation is, in general, followed by sudden weakening of fluorescence above the dissociation limit. This has been obtained in the SO_2 fluorescence near 220 nm by Okabe (1971) and also confirmed in the present work (Chap.5).

1.5 Photoabsorption

The knowledge of the extent of absorption in the molecular system is important in photochemistry since the absorption coefficient must be known to obtain the quantum yield, the oscillator strength of the bands, and the lifetime of the electronically excited state. Therefore, the absorption coefficient (or absorption cross section) is an

important quantity which should be measured in the laboratory with a fair degree of accuracy.

The discovery that light was absorbed exponentially was first enunciated by Pierre Bouguer (1729). But, Bouguer's work is generally little known and credit for describing the law of absorption is frequently given to Lambert (1760). According to Lambert's law, if a parallel beam of monochromatic radiation passed through a homogeneous absorbing medium, the intensity of the radiation I was reduced by the same fractional amount $-\Delta I/I$ for each element of path length Δx traversed. That is

$$-\Delta I = I \mu \Delta x \longrightarrow (1.20)$$

where the proportionality constant μ depends only on the properties of the medium at that particular monochromatic wavelength. Integration of (1.20) gives

$$I_\lambda = I_{0\lambda} \exp (-\mu x) \longrightarrow (1.21)$$

where $I_{0\lambda}$ is the intensity of the incident beam, I_λ is the intensity transmitted through a distance x of the medium, and μ is referred to as the *liner absorption coefficient*.

In 1852, Beer found that the absorption coefficient was proportional to the concentration of the absorbing medium. This resulted in expressing the value of μ in Eq.(1.21) at some standard conditions of temperature and pressure (STP), namely, at 273 K and 1 atmosphere (760 Torr) pressure. Therefore, from Beer's law

21

$$\mu = \sigma_{T\lambda} \, n = \sigma_{T\lambda} \, n_0 \times \frac{p}{760} \times \frac{273}{T} \qquad \longrightarrow (1.22)$$

combination of Eqns.(1.21) and (1.22) is known as *Beer - Lambert* law, and is given by

$$I_\lambda = I_{0\lambda} \, \exp(-\sigma_{T\lambda} \, nl) \qquad \longrightarrow (1.23)$$

where the concentration or density of the gas n_0 is given by Loschmidt's number ($n_0 = 2.687 \times 10^{19}$ molecules cm^{-3}) when μ is measured at STP. The constant of proportionality in Eq.(1.22) $\sigma_{T\lambda}$ has the units of an area and is, therefore, referred to as the total absorption cross section. When μ is given at STP, the path length x is related to the actual measured distance l of the absorption cell by

$$x = \frac{p}{760} \times \frac{273}{T} \times l \qquad \longrightarrow (1.24)$$

Various units are used to express the absorption coefficients. Different forms of Beer-Lambert law are given by:

$$I_\lambda = I_{0,\lambda} \, \exp(-k_\lambda \, pl) \qquad \longrightarrow (1.25)$$

$$I_\lambda = I_{0,\lambda} \, \exp(-\sigma_{T\lambda} \, nl) \qquad \longrightarrow (1.26)$$

22

$$I_\lambda = I_{0,\lambda} \exp\left(-\epsilon_\lambda \, cl\right) \qquad\qquad \longrightarrow (1.27)$$

In Eq.(1.25), the absorption coefficient is denoted by k_λ and it has the units of $atm^{-1} cm^{-1}$. In this expression p is the pressure in atmospheres at a reference temperature (0 or 25 ^{O}C). In Eq. (1.26), $\sigma_{T\lambda}$, is called absorption cross section having the units of cm^2, and the concentration of the absorbing medium is given in molecules per cm^3. The absorption coefficient ϵ_λ, called the molar absorption coefficient (Eq. 1.27), is expressed in $dm^3 \, mol^{-1} \, cm^{-1}$, when the concentration is given in mol dm^{-3}.

1.5.1 Validity of Beer-Lambert law

The Beer-Lambert law given by Eq.(1.23) is valid only under certain conditions. The discussions outlined in this section have to be fulfilled for the validity of Beer-Lambert law to measure absorption coefficient of the medium under study.

The radiation used for the purpose of attenuation in the absorbing medium must be parallel beam of monochromatic type. The absorbing medium is assumed to be homogeneous, in other words, the atoms and molecules are sufficiently separated so that the intermolecular forces are negligible. In the case of homogeneous medium, chances of multiple scattering are also minimized.

When the absorbing medium consists of discrete bands, the absorption cross section will not remain constant over a range of pressures of the absorbing medium. Figure (1.7) shows a plot of log $(I_{0\lambda}/I_\lambda)$ against pressure. The slope is linear at low pressure $(p < p_0)$, but it deviates from linearity at high pressures.

23
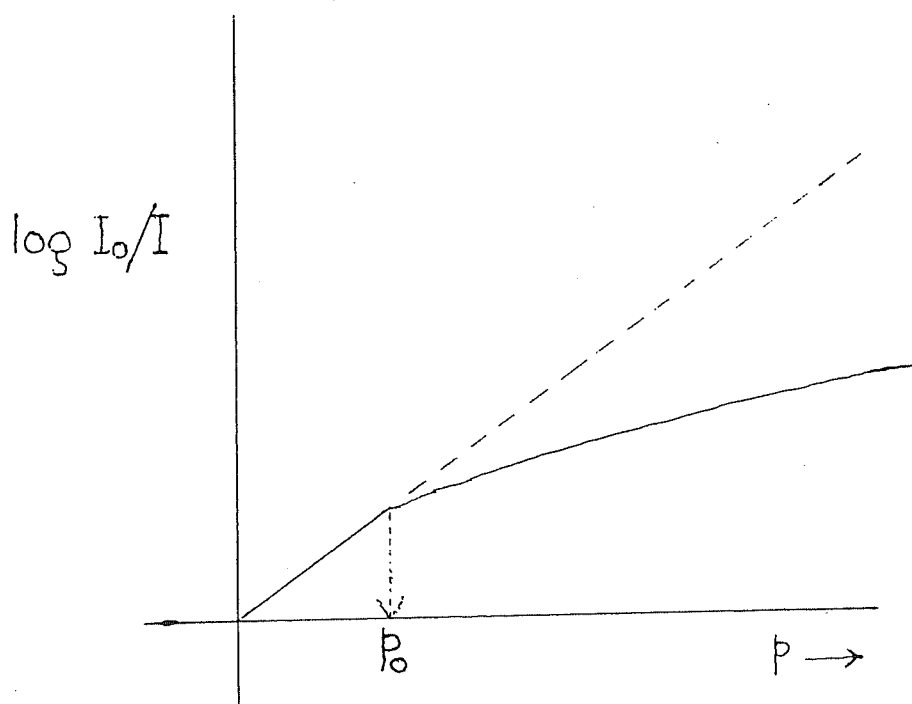
Figure 1.7 Deviation from the Beer-Lambert law.

The deviation from the Beer-Lambert law results in part due to the lack of instrumental resolution. Qualitative explanation may be given using Fig.(1.8), which shows three rotational absorption lines with widths much narrower than the width ($\Delta\omega$) of a monochromatic line emerging from the exit slit of a monochromator. The Beer-Lambert law holds up to a pressure shown in Fig.(1.8b), as the quantity log ($I_{0\lambda}/I_{\lambda}$) is proportional to the pressure. When the pressure is increased further the deviation occurs, since the absorption at the line center is complete and only the off-center portion of the absorption lines contribute to an increase of absorption (Fig. 1.8c).

At a fixed pressure and path length the apparent absorption coefficient some times decreases as the slit width increases. Figure (1.8a) explains that the area taken by the absorption lines becomes proportionately smaller as the slit width is increased. Hence the transmitted intensity is increased, resulting in the reduction of absorption coefficient.

1.6   Photoionization

The process of ejecting an electron from an atom or molecule due to its interaction with energetic photon, was termed *electrification of gas* prior to the discovery of photoelectric effect in 1887. In the 1900's it was called *photoelectric ionization* of a gas. However, it soon took on its permanent name of *photoionization*. Most of the molecules when irradiated at photon wavelengths less than 100 nm are photoionized with the result that the molecules get populated in different electronic states of the ion.

The photoionization cross section for a molecule is given by
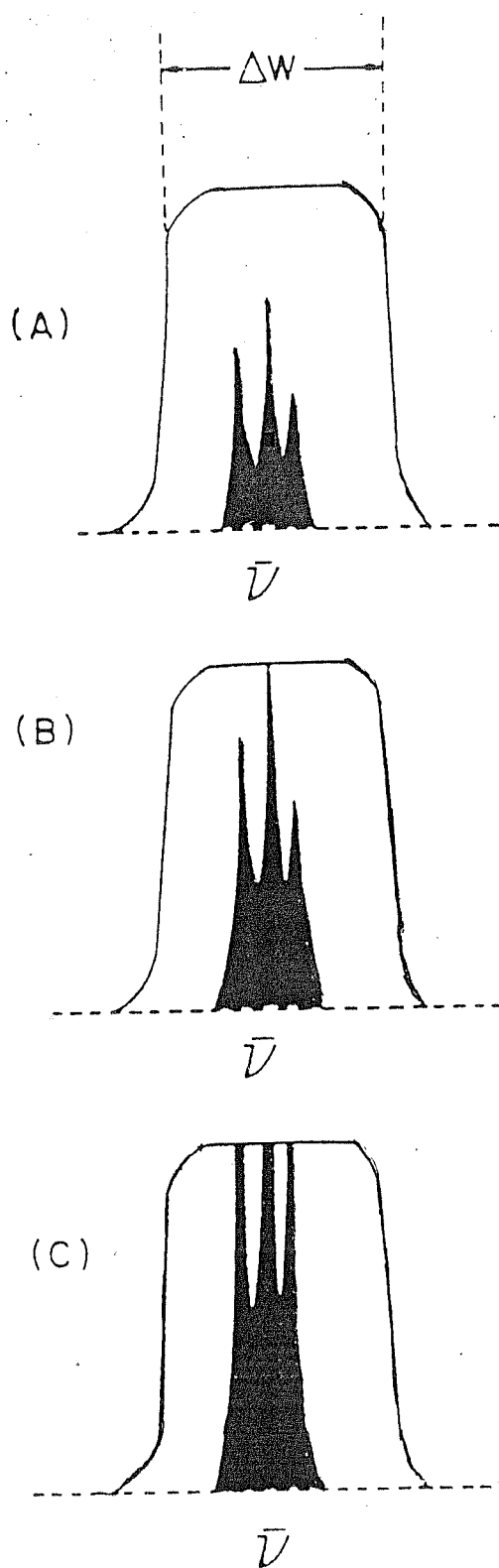
Figure 1.8 Deviation from the Beer-Lambert law due to the lack of spectral resolution.

$$\sigma_i = \gamma_i \, \sigma_T \qquad\qquad\qquad \longrightarrow (1.28)$$

where γ_i , called the photoionization efficiency, is defined as the number of ions produced per photon absorbed. σ_i and σ_T are the photoionization and total absorption cross sections respectively. In case of atoms at photon energies greater than the ionization threshold, the only primary absorption mechanism other than ionization, is absorption by discrete energy levels that lie in the ionization continuum. In nearly all cases, autoionization occurs and the net result is ionization. Thus for atoms, γ_i can be considered to be unity and $\sigma_i = \sigma_T$. For molecules, this is not true. Many of the super excited levels simply decay by fluorescence or cross over into a dissociative state, while others will autoionize.

γ_i, has been defined as the number of ions produced per absorbed photon. The ion may be singly, doubly, or multiply charged but it is still a single ion. Thus, σ_i refers to the total ionization cross section which can not exceed σ_T, that is $\gamma_i \leq 1$.

1.7 Fluorescence

Absorption of light in visible and ultraviolet regions of the electromagnetic spectrum leads to excitation of target molecules from ground state to higher electronic states. The energy of photons in visible and ultraviolet is in the range 2-6 eV, and it would be energetically possible to promote the molecules in their higher electronic excited states. The photon energy in vacuum ultraviolet region (energy > 12 eV) is sufficient to ionize the target molecules; as a result, the different electronic states of the molecular ions would get populated. In both the cases, the electronic transition

would take place from higher excited state to lower excited state, provided selection rules are allowed. The emission from photoexcited products is called *neutral fluorescence*, the one from ionic species is known as *ionic fluorescence*.

1.7.1 Fluorescence from neutral molecules

The simplest mechanism for a molecule in excited electronic state to lose the excess energy is by re-emission of radiation at the same wavelength which produced the excitation. This is termed as *resonance fluorescence*. This phenomenon is possible in the vapour phase of the target molecules at very low pressures where the intermolecular collisions are rare, and the target molecule is said to be isolated. The pressure needed to achieve the condition of *isolation* can be obtained from the kinetic theory of gases and has been found to be of the order of 10^{-1} to 10^{-2} Torr.

If the number density of the target molecules is considerably large (pressure $\simeq$ 1 Torr), the phenomenon called *normal fluorescence* occurs. In a high density concentration collisions occur between excited molecules and other; usually the ground state molecules. Such collisions will lead to exchange of vibrational and rotational energy , the so-called internal conversion, and the molecule will settle in lower vibrational states of the excited electronic states. Now, if the selection rules are allowed, transition will take place from the lower vibrational state of the excited electronic state to the various vibrational levels of the ground electronic state of the molecule. This emission at frequencies smaller than that of absorbed photon is called *normal fluorescence*. Here it should be pointed out that, this type of emission, can also be defined in a different way in relation to the total spin of the two states in which the transition is taking place. If during the emission process,

26

the electron undergoing the transition does not change its spin, the emission is referred to as fluorescence.

1.7.1.1 Fluorescence and other competing process

Not all electronically excited states of the molecules give rise to observable emission. There is always a possibility of the excited state being de-activated by other competing processes which are non-radiative in nature.

The average decay period, τ , of fluorescing molecules (i.e., the time required for the intensity of the emitted light to fall to 1/e of its initial value) is of the order of 10^{-6} to 10^{-9} sec, thus indicating that this is the order of magnitude of the lifetime of excited molecule. For molecules which do not fluoresce, some other competing process occurs in period shorter than 10^{-6} to 10^{-9} sec. Several such processes have been reported in literature.

One of these processes, known as predissociation, has been discussed in detail in Section (1.3.1) and (1.4.2). Another mechanism for non-radiative deactivation of molecules is the conversion of excess energy into vibrational energy and is called internal conversion. This process is extremely rapid in many molecules, and appears to occur to some extent in all molecules.

A third mechanism of non-radiative deactivation consists of energy transfer to other molecules and is called external conversion.

1.7.2 Ionic Fluorescence

Observation of fluorescence in molecular ions is the most direct evidence for the stability of excited states of the ions formed. When fluorescence can be detected, radiationless transitions and dissociative processes must be at least weakly forbidden.

The information reported in literature about the fluorescence of the large number of diatomic or polyatomic molecular ions, though sparse, clearly indicates that non-radiative transitions do not dominate radiative transitions in all cases. Even when dissociation channels are open, fluorescence is sometimes observed. Since it is difficult to generate molecular ions in large concentration as compared to neutral species, it is likely that those radiative transitions reported for molecular ions must be the dominant decay modes in most instances. However, for neutral species it is possible to observe radiative decay when competition from non-radiative process is strong. It has also been suggested that in competition between radiative and non-radiative processes, the latter are favoured as the size of the molecular ion increases. This is implied by the theory for radiationless transitions.

The total photoionization cross sections for the molecular systems could be apportioned in two ways :

i) The relative cross sections for formation of the various electronic states of the molecular ion.

ii) The other type of partial cross section which is a measure of the state of the products resulting from ionization.

The first type of partial cross sections could be deduced primarily with the aid of photoelectron spectroscopic data

whereas, the second type of relative cross section could be obtained from photoionization mass spectrometry or photoelectron-photoion coincidence studies. Alternatively, the two types of relative cross sections could be studied in detail using a single technique i.e. ionic fluorescence. This could be obtained by measuring the total fluorescence cross sections as a function of incident photon wavelength and also by studying the dispersed fluorescence spectrum of parent molecular ion and photofragmented species at a few incident photon wavelengths taken one at a time.

1.8 Fluorescence Quantum Yield

The fluorescence quantum yield of a molecule at a certain incident photon wavelength is defined as the number of photons emitted per absorbed photon. In the total absorption process some of the absorbed photons ΔI_n will be lost in excitation or dissociation process, some ΔI_i, will cause ionization, and a certain number ΔI_s will be scattered out of the incident beam. If ΔI represents the total number of photons absorbed from the incident beam, then $\Delta I = \Delta I_n + \Delta I_i + \Delta I_s$, and thus

$$\sigma_T = \frac{\Delta I_n}{\Delta I} \sigma_T + \frac{\Delta I_i}{\Delta I} \sigma_T + \frac{\Delta I_s}{\Delta I} \sigma_T \qquad \longrightarrow (1.29)$$

or

$$\sigma_T = \sigma_n + \sigma_i + \sigma_s \qquad \longrightarrow (1.30)$$

where σ_n, σ_i, σ_s represent, the cross section for producing neutral products, ionized products, and scattering

respectively. The fractions $\Delta I_n/\Delta I$, etc., are the yields or efficiencies for the production of excited states usually denoted by γ_n etc.

In the spectral region from 100 nm to longer wavelengths, the ionic production is absent; also the contribution of scattering cross section is negligible. Therefore, from eqns. (1.29) and (1.30) σ_n can be written as

$$\sigma_n = \frac{\Delta I_n}{\Delta I} \, \sigma_T = \gamma_n \, \sigma_T \qquad\qquad \longrightarrow (1.31)$$

If the excited neutral products fluoresce as explained in the preceding section, Eq. (1.31) can be termed as

$$\sigma_f = \gamma_f \, \sigma_T \qquad\qquad \longrightarrow (1.32)$$

where σ_f is the total fluorescence cross section, γ_f is the fluorescence quantum yield, and σ_T is the total absorption cross section. From Eq. (1.32) it can be seen that the fluorescence quantum yield can be obtained by measuring the total fluorescence and absorption cross section at a given wavelength and taking the ratio of these quantities.

At photon wavelengths shorter than 100 nm, the molecules would get photoionized with the result that the molecular ions would get populated in different electronic states, at these wavelengths

$$\sigma_i = \frac{\Delta I_i}{\Delta I} \, \sigma_T \qquad\qquad \longrightarrow (1.33)$$

If the excited ionic molecules fluoresce as explained previously, Eq.(1.33) could be written as

$$\sigma_{if} = \gamma_{if} \sigma_T \quad\quad\quad \longrightarrow (1.34)$$

where σ_{if} is the total ionic fluorescence cross section, and γ_{if} is the ionic fluorescence quantum yield. In general, at photon wavelengths shorter than 100 nm, there is a small contribution from neutral photoexcited, photodissociated molecules. The total fluorescence at these wavelengths, however would include the fluorescence component from both the neutral molecules as well as molecular ions. A much better insight about the fluorescence and nature of products at these wavelengths could be obtained if the total fluorescence is dispersed and energy analysis of the dispersed fluorescence is carried out as a function of incident wavelengths.

1.9 Selection Rules for Molecular Transitions

For molecules, the rules governing the transition between two given energy states are

1. $\Delta\Lambda = 0, \pm 1$: allowed changes in the component of the total orbital angular momentum in the direction of molecular axis.

2. $\Delta S = 0$: the spin conservation rule.

3. Symmetry properties of the energy states must be conserved.

The rule governing the transition between the states of like multiplicities is most stringently obeyed. Transition between ideal singlet and triplet states are strictly forbidden. But, such transitions do occur under the influence of intramolecular and intermolecular perturbations which can mix pure singlet and pure triplet states. Also, symmetry forbidden transitions do occur sometimes though with very low intensities. The restriction of the symmetry selection rule can be broken down by vibration-electronic interactions.

1.10 Survey of Experimental Methods

The measurement of total photoabsorption cross section, fluorescence cross section and hence fluorescence quantum yield for a molecule at any incident photon wavelength requires the quantities such as the ratio of the light incident upon a sample to that transmitted by the sample or to that emitted as fluorescence signal from the sample in the direction of the fluorescence detector. The accuracy of this method depends strongly upon the light source intensity remaining constant at each wavelength during the entire measurement. Thus, techniques to measure incident, transmitted, and fluorescence intensity over very small time intervals are used or these are measured simultaneously. The techniques for carrying out absorption and fluorescence studies in the ultraviolet region are described below.

a) Double Beam

This method involves a mechanical oscillation of a mirror or detector which actually intercepts the entire incident beam. One of the methods, is shown in Fig.(1.9), where wedge shaped mirror is forced to oscillate about the incident beam. The intercepted beam is focused into the

32

PM 2

GAS
FILLED CELL

PM 3

$h\nu$

EMPTY CELL

PM 1
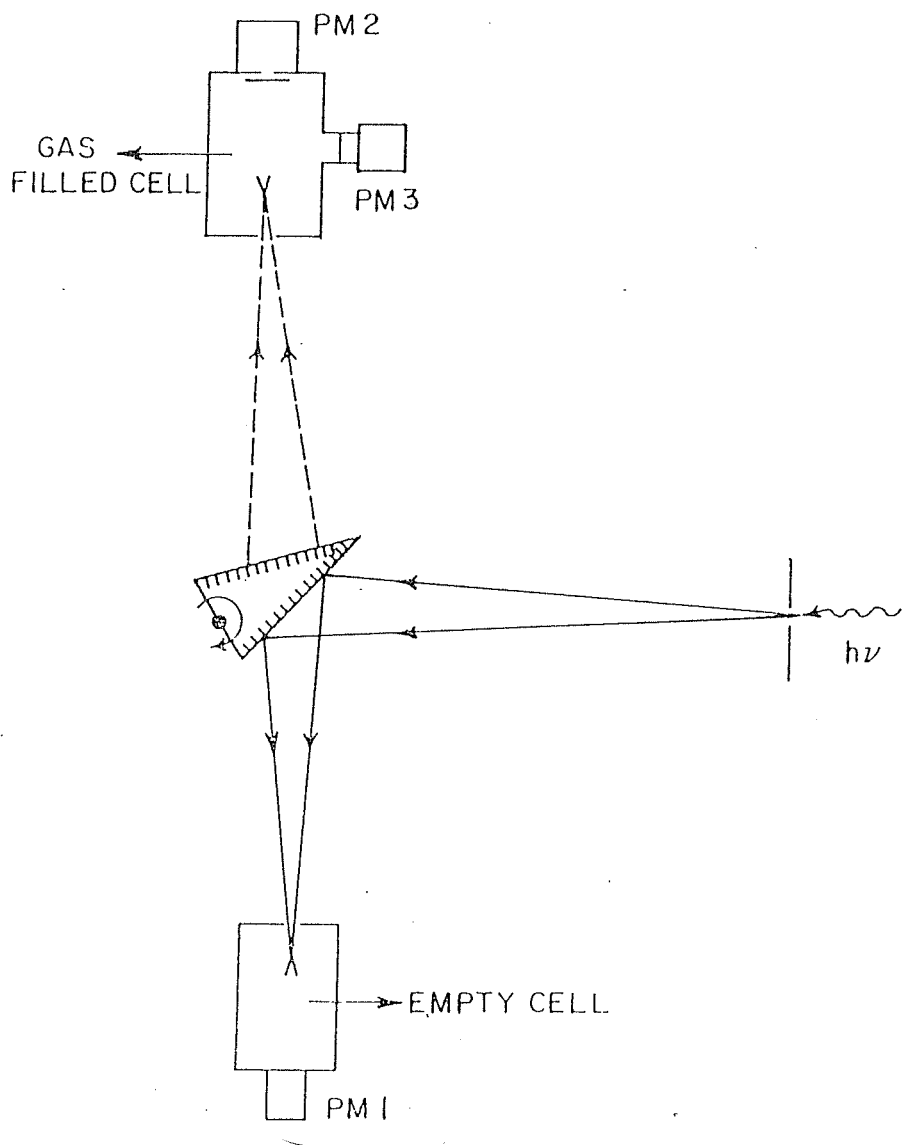
Figure 1.9 Double-beam absorption measurements.

entrance slit (or window) of the gas filled cell during one-half of the cycle and then focused onto an empty reference cell during the next half cycle. The signals from the two photomultipliers are adjusted to be identical when both cells are empty. This method has been used in McPherson double beam instrument (McPherson - Sheffield Instrument Company, Acton, MA). A similar device is reported by Schmitt and Brehm (1966).

b) Split Beam

No moving parts are involved in this method. However, the technique is similar to the double-beam method. In split-beam method, a portion of the incident beam is reflected into PM1 (Fig. 1.10) giving a signal proportional to incident photon intensity. The remainder of the incident beam is transmitted to PM2. The photomultiplier tubes (PM1, PM2) must be balanced when there is no gas in the cell.

The splitting of the beam can be achieved with a reflecting mesh intercepting part of the incident beam. Because of poor reflectance of most of the materials in the UV and vacuum UV, it is often preferable to coat the mesh directly with sodium salicylate and focus the fluorescent radiation onto a photomultiplier tube either with a lens or a light pipe. This method, or variations there of , have been reported by Hudson and Carter (1965), Codling et al (1977), Boursey et al (1971), and Castex et al (1969).

The other methods like a double ionization chamber (Samson, 1964) and a modified double-ion chamber with cylindrical cross section (Samson and Haddad,1974) could also be used to measure total absorption cross sections and ionization efficiency only in the wavelength region shorter than 100 nm.
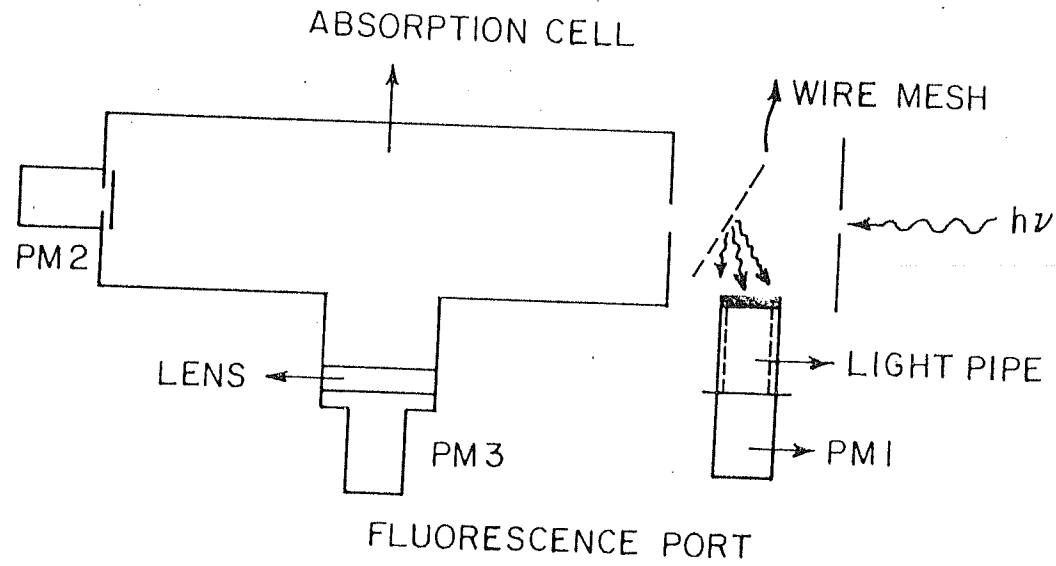
Figure 1.10 Split-beam absorption measurements.

In both the above arrangements, the fluorescence port is used to study the quantitative fluorescence spectroscopy of molecules. As a matter of fact, the fluorescence intensity can be detected, both in the direction perpendicular to the photon beam axis and along the beam axis using some appropriate colour glass filters.

In the measurement of absorption and fluorescence cross sections of elements, it is necessary to vapourize the element by the use of some type of furnace. Atomic beams emerging from the furnace would form an ideal system for this purpose. But in the present experiment, the cross sections are being measured for molecules in gas phase only; therefore, the systems using heat pipes and atomic beams would not be described here.

1.11 Need for a New Experimental System

The need for having an entirely new experimental system for measuring absorption and fluorescence cross sections can only be ascertained by knowing the advantages and disadvantages of the two experimental system described above. In case of double-beam method, the wedge shaped mirror is allowed to oscillate about the incident photon beam. The reflecting material used for the mirror surface is aluminum-MgF_2 for the spectral region 115 to 300 nm and gold or platinum for wavelengths shorter than 100 nm. The reflactance of such a mirror especially in the first spectral region deteriorates with time. Also, this mirror is a moving part which is quite cumbersome to handle in the experiment. As the mirror has to oscillate focussing the photon beam at the two cells alternately, the data acquisition system in the experiment becomes some what complicated. If all these problems could be handled using sophisticated technology, this method would be quite useful. But, unfortunately, not

many researchers in this field have cared to use this method because of the complications described above.

Moving parts have been avoided in the split-beam method. The reflecting mesh used for splitting the beam is coated with the scintillator, sodium salicylate, so that the incident UV or VUV photon beam is converted into visible, and the reflected visible beam is allowed to pass through a light pipe. In another arrangement, the UV or VUV photon beam is reflected from the tungsten wire mesh and is focused on a glass substrate coated with sodium salicylate. In both the arrangements, the reflected intensity is very small. The fluorescent quantum efficiency of sodium salicylate is about 36% (Kumar and Dutta, 1979) and the light losses in the light pipe are appreciable. The net result is that about 1 to 2% of the total incident photon beam enters the photomultiplier of the beam splitter. There would, therefore, be large errors in the measurement of incident intensity and this in turn, would introduce larger errors in the measurement of photoabsorption and fluorescence cross section of molecules. The situation would deteriorate further with time, as sodium salicylate is known to age and its fluorescent quantum efficiency would change for the worse.

There is another major drawback in the two systems described above. The scintillator-photomultiplier combination or any other detector used to measure transmitted intensity in the UV or VUV region is not opaque to radiations at higher wavelengths extending to visible region. When the target gas molecules are introduced in the absorption chamber, the transmitted intensity is supposed to be reduced due to absorption of incident UV or VUV radiation by target species. Because of absorption, the target molecules would get populated in higher electronic states and the fluorescence would take place from higher to lower states. The fluorescence would be at wavelengths higher than the incident photon wavelength. There would be a fluorescent component

along the photon beam axis which would be detected along with the transmitted intensity. In otherwords, a transmitted intensity would show a value much larger than its true value. As a result, the absorption cross section would show a value smaller than its real value.

In light of the points mentioned above, it is evident that a new experimental system is needed for measuring the absorption and fluorescence cross sections accurately. This has been achieved in the present work. The new system takes care of the drawbacks mentioned above. The two problems have been taken care of, as described below:

1) In the present experiment, the cross sections are measured in the spectral region 180-340 nm. That is why, it was very convenient to replace the tungsten wire mash in the beam splitter by a quartz plate placed at 45° to the optic axis. In this case, the reflectance of the quartz plate is very large and the use of both sodium salicylate and light pipe could be avoided. A photomultiplier with extended S-20 spectral response (180 to 800 nm) could be used to measure the incident photon beam intensity. This, relatively simple, change incorporated in our new experimental system has helped to obtain large incident intensity, thereby reducing error in the measurement of absorption and fluorescence cross sections.

2) As discussed above, the transmitted intensity included the fluorescent component produced along the optic axis because of the absorption of photon beam by the target molecule. To avoid this, another monochromator has been used after the absorption chamber and the gratings of the two monochromators are co-rotated so as to have the same wavelength. This type of arrangement has helped to measure absorption cross sections of target molecules with better accuracy.

The new experimental system designed and fabricated in the laboratory to measure the photoabsorption and fluorescence cross section of molecules has been discussed in detail in Chapter 2. Another experiment to measure ionic fluorescence has also been fabricated in the laboratory and has been discussed in chapter 7 along with some interesting results on the dispersed fluorescence from the target ions. In both the cases, the target molecules chosen are SO_2 and CS_2.

1.12   Choice of the Target Gas Molecules

Sulphur dioxide and carbon disulphide have been chosen in the present experiment to study the quantitative absorption and fluorescence spectroscopy of both neutral molecules and molecular ions. Such a study provides the necessary basic data for many fields such as atomic and molecular physics, aeronomy, astrophysics, and plasma physics.

Sulphur dioxide and carbon disulphide are important molecules present as reactive trace constituents in the troposphere and stratosphere of the earth. Extensive data on Venus atmospheric sulphur dioxide have been obtained from recent planetary and inter-planetary probes (Conway et al, 1979) and from earth-based observations (Barker, 1979). The evidence of SO_2 on Io was made available from in-situ UV observations by Bertaux and Belton (1979) while the detection of SO_2 frost on the Io surface was reported by Smythe et al (1979) from ground based infra-red measurement. The presence of CS_2 in the Venusian atmosphere has been proposed by Young (1978), even though the observational evidence for a clean detection is, at present, marginal at best. In the recent past, the CS radical has been found to be abundant in the interstellar medium (Dalgarno and Black, 1976; Linke and Goldsmith, 1980). The radical is most likely produced by

photodissociation of carbon disulphide. A fair idea about the concentration of SO_2 and CS_2 in the terrestrial troposphere and stratosphere; Venusian and Io's atmospheres can be obtained from the in-situ and ground based measurements mentioned above along with other data like photoabsorption and fluorescence cross sections etc., measured in the laboratory, as a function of incident photon energy. In view of this it is clear that more measurements in this direction, are needed, possibly by using better techniques.

CHAPTER - 2

EXPERIMENTAL SET - UP

2.1 Introduction

The experimental set-up for the measurement of absorption cross section, fluorescence cross section and fluorescence quantum yield for molecules by photon impact includes an ultraviolet light source for the production of line free continuum, a beam splitter to monitor light intensity during the experiment, a dispersing unit for wavelength selection, the collision chamber for carrying out absorption and fluorescence studies, photon detectors and fast data acquisition system. The schematic view of the entire experimental assembly is given in Fig.(2.1).

In the conventional method for studying the quantitative absorption, the transmitted photon beam is measured just after the absorption chamber. There is a notable change in the present experiment. An additional 0.2-meter monochromator has been introduced after the absorption chamber as shown in the Fig.(2.1). The gratings for the main and the additional monochromator are co-rotated so as to have the same wavelength. This was done to avoid detection of any fluorescence signals produced along the direction of the optic axis by the target molecule, excited because of photoabsorption. The detailed description of each sub-system used in the overall experimental assembly is given in the following sections.
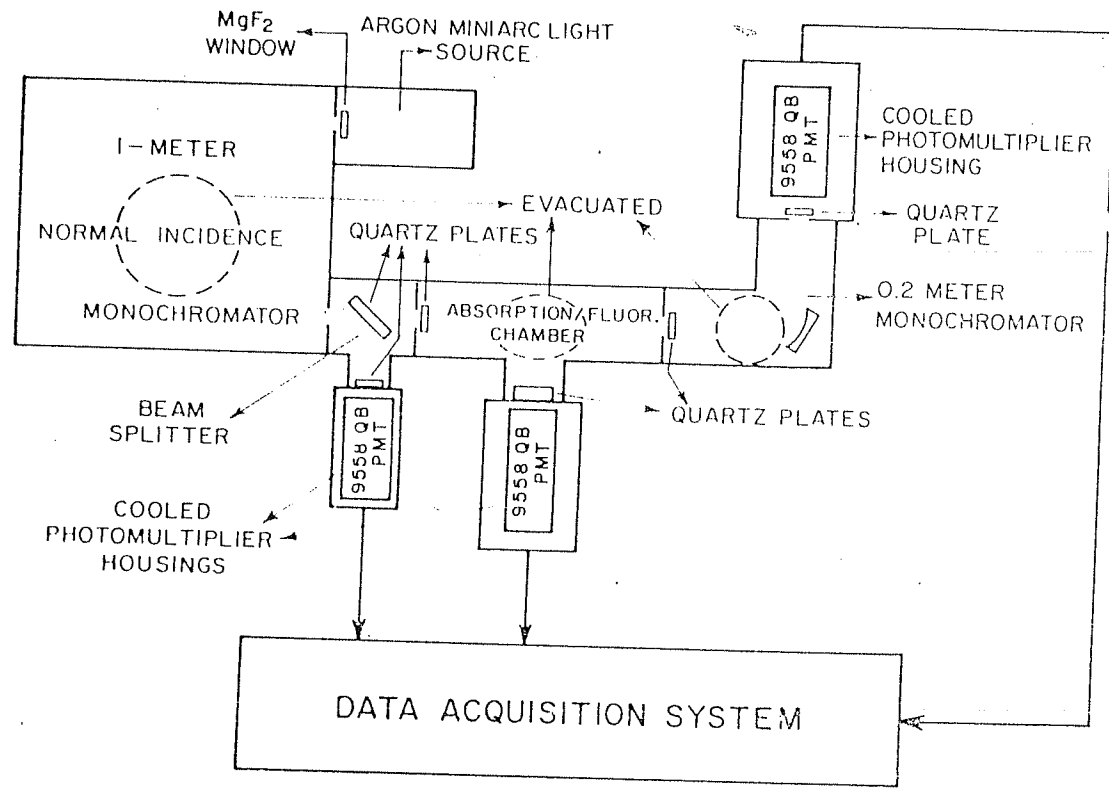
Figure 2.1 Schematic of the experimental arrangement.

2.2 Argon Mini-arc Source

The argon mini-arc developed at National Bureau of standards, USA., by Bridges and Ott (1977) has been used in the present experiment as a background light source. This source has been powered by a high current home made power supply. The mini-arc provides an intense, stable and reproducible UV continuum covering the spectral region from 114 nm to wavelengths larger than 350 nm with DC power requirements of less than 1.5 KW. A schematic of the argon mini-arc light source is shown in Fig.(2.2). The arc source consists essentially of three copper plates separated by insulating rings and clamped together to form a gas tight enclosures. The central plates form a channel which guides and constricts the discharge. The outer two plates are the anode and the cathode. All three plates are water cooled. The water flows inside each piece independently through holes drilled into the sides (not shown in Fig.). The arc constricting section is 6.3 mm thick with a 4.0 mm dia hole. The diameter is designed in such a way that the discharge remains stable and the output radiation is optimized. The electrodes and the arc chamber are cooled by a continuous flow of water from a closed network water chiller. Other than the argon mini-arc light source, the most widely used UV sources to date are commercially available deuterium, mercury and mercury-xenon lamps. These lamps have certain advantages such as relatively strong continuum, low power requirements and small size. But there are serious limitations also. In deuterium lamp the drawback is, a variability related to how the discharge positions itself on the electrodes following each ignition. Hence the lamp alignment must be checked every time a new spectral scan has to be started. This adjustment to get maximum signal is time consuming. Also, the deuterium lamp has aging characteristics. Conflicting views about the aging have been reported in literature by Pitz (1969), Ott and Bartoe (1972) and Stuck and Wende (1974). In the case of
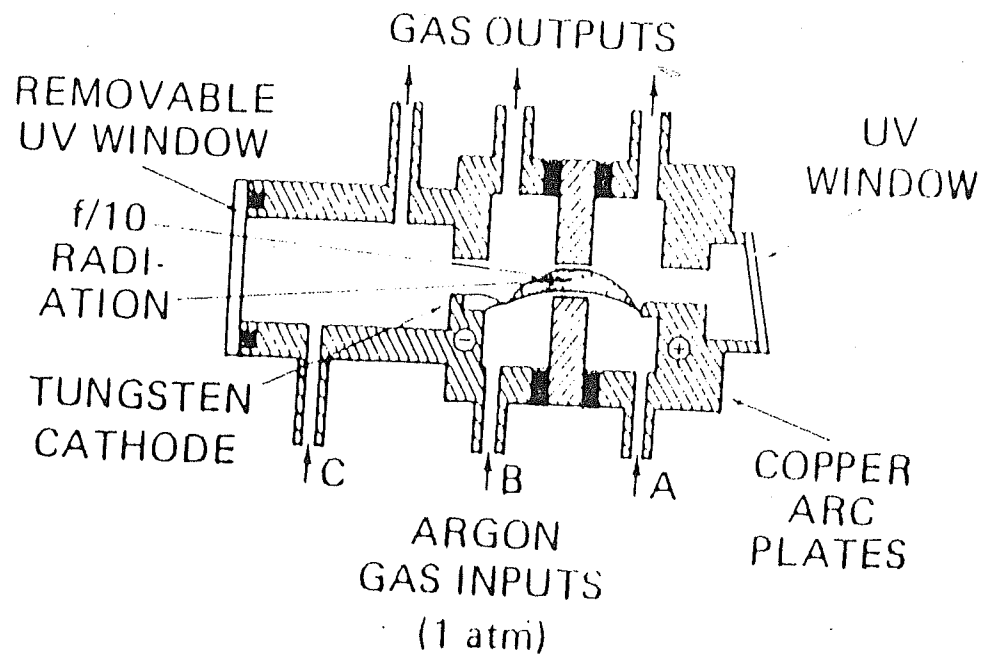
Figure 2.2 Schematic of the argon mini-arc light source.

mercury lamp, the region of applicability is limited to a very narrow spectral range (270-600 nm). Another disadvantage in this lamp is the presence of many lines super imposed over the continuum.

The comparison of argon mini-arc lamp with few other lamps is given in Fig.(2.3). Argon mini-arc covers a wide spectral region and has the following features (Bridges and Ott, 1977) :

     i.   Intense line-free continuous spectrum between 110-350 nm

    ii.   Stability and reproducibility over many hours of operation.

  iii.   Uniform output power over a large solid angle.

   iv.   Radiant power output adjustment over a range of several decades.

    v.   Simple alignment and operation.

2.2.1 Operation of the source

The gas purity is necessary to maintain the arc stability and reproducibility of the continuum emission is insured by operating with a continuous flow of argon at around 1 atmosphere pressure. Maintaining high degree of purity within the arc chamber also minimizes the radiant power of atomic resonance lines in the spectrum which arise from small (ppm) concentrations of oxygen, nitrogen, carbon and hydrogen. These elements are present as air and water vapour impurities in the arc chamber and gas handling system.

The arc discharge is initiated simply by applying voltage between the electrodes, and inserting a tungsten rod which is externally connected to the anode potential, until it touches the cathode. The discharge is transferred from the tip of the external rod to the anode as the rod is withdrawn.
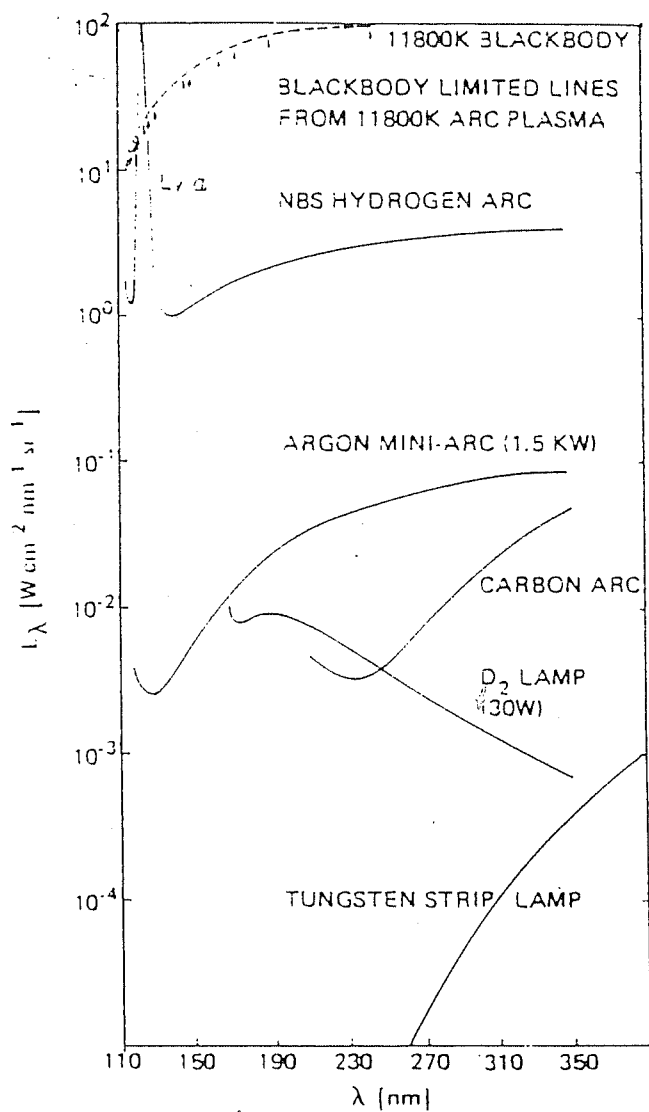
Figure 2.3 Comparison of the spectral radiance of several
UV sources.

2.2.2 Power supply

A low voltage of 40V and high current of 40A is needed for the argon mini-arc source to sustain the discharge. To meet these requirements, a current regulated power supply has been designed and fabricated in the laboratory (Kripalani and Misra, 1988). The circuit diagram is given in Fig.(2.4). To extract high currents up to 50A, an air cooled three phase transformer with the primary of 440V and secondary of 40 volts is used. Voltage rectification is done by the diodes D1 to D6 having a high rating of 200V and 100A. After rectification, the DC voltage of 56V having ripple factor up to 4.5 % is fed to the positive end of the light source through a 0.6 Ohms (200W) resistance. This resistance limits the over all circuit current to 100A. A voltage regulator IC-723, featuring high ripple rejection, excellent temperature stability is used. The 10K ohms potentiometer on pin No. 5 is used to vary the output voltage of the IC from 2 to 12V which corresponds to 30-50 Amps of current across the discharge. Any fluctuations in the discharge current arising due to the instability of gas pressure, line voltage etc, can be handled by the inverted feed back given to IC-723 in the current regulated circuit and hence a stable current is sustained. Great care has been taken in deciding the power ratings of the transformer, power transistors and other components used, so as to achieve a rugged and trouble free power source.

2.2.3 Performance and spectrum of the light source

The current regulated power supply is designed to work for hours together. The output flux of the mini-arc source has been found to be approximately constant during 3-4 hours of continuous operation. However, due to high consumption of power ($\simeq$ 1.6KW) in the discharge region of the mini-arc lamp,

0.6 Ω
200 W

40V A/C

D1

D2

D3

D4

D5

D6

0.05 OHMS
40W

M1

T1

ARGON
SOURCE

12
T2
D7

230V A/C

0

12

D8

3.3 K

500 PF

+
1000 μF
25V

723
14 13 12 11 10 9 8
1 2 3 4 5 6 7

.001

3.9K

10K

1K

33 Ω

2N 2222
Tr₁

1K

D9

D10

2N 2222
Tr₂

2N 3055
Tr₃

2N 3055
Tr₄

0.2 Ω
SW

2N 3055
Tr₁₈

0.2 Ω
SW

0.1 Ω
200 W
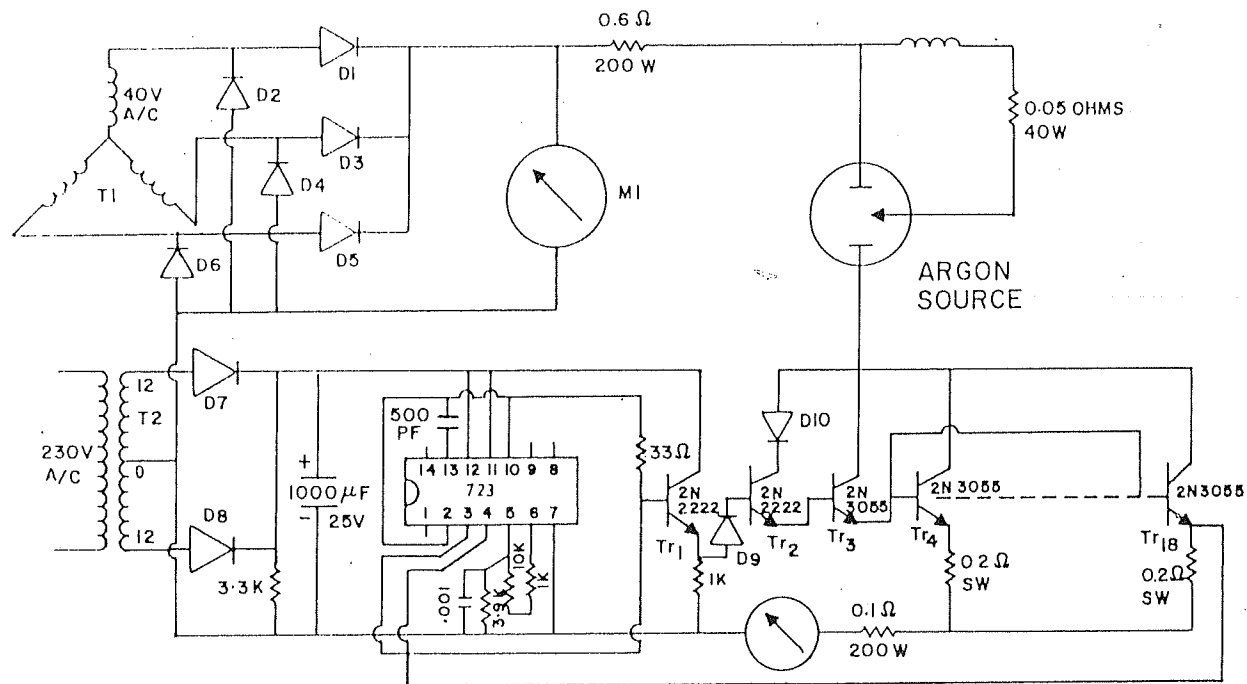
Figure 2.4 (a) Circuit diagram of the mini-arc power supply.

```
┌──────────────┐    ┌──────────────┐    ┌──────────────┐    ┌──────────────────┐
│ SINGLE PHASE │    │ FULL WAVE    │    │ VOLTAGE      │    │ PARALLEL         │
│ STEP DOWN    │───▷│ RECTIFIER    │───▷│ REGULATOR    │───▷│ COMBINATION OF   │
│ TRANSFORMER  │    │ SECTION      │    │ CIRCUIT      │    │ POWER TRANSISTOR │
│ 12-0-12V     │    │ 16 V DC      │    │ I/C 723      │    │ 2N 3055          │
└──────────────┘    └──────────────┘    └──────────────┘    └──────────────────┘
```

SINGLE PHASE STEP DOWN TRANSFORMER 12-0-12 V

FULL WAVE RECTIFIER SECTION 16 V DC

VOLTAGE REGULATOR CIRCUIT I/C 723

PARALLEL COMBINATION OF POWER TRANSISTOR 2N 3055

3 PHASE STEP DOWN TRANSFORMER 440 TO 40V A/C

FULL WAVE RECTIFIER SECTION FOR DC 56 V DC

0.6 Ω 200 ω

ARGON SOURCE

M2

0.1 OHMS 200 ω

Figure 2.4 (b) Block digram of the circuit.

deposition of tungsten and other impurities takes place on the electrodes clogging the arc constricting hole land also contaminating the M_gF_2 window. All these results in the deterioration of the source performance. Therefore, after every 100 hours of operation, the mini-arc source was opened and the electrodes and the M_gF_2 window were thoroughly cleaned.

The complete spectrum of the mini-arc source is shown in Fig.(2.5) covering the spectral region 145-350 nm. The spectrum has been sub-divided in three convenient spectral regions. The details of the spectra covering smaller wavelength regions from 145 to 200 nm, 200 to 260 nm and 260 to 350 nm are shown in Figs.(2.6), (2.7) and (2.8) respectively. It has been observed that at wavelengths shorter than 200 nm (Fig. 2.6), there are several atomic lines in the spectrum, associated with impurity atoms like nitrogen, carbon and oxygen. At wavelengths longer than 200 nm, the spectrum was, more or less, continuous in nature as seen in Figs.(2.7) and (2.8).

The effect of change in arc current on intensity of argon mini-arc light source has been studied in detail. For this purpose, a small spectral region, 220 to 235 nm, has been chosen and the change in intensity has been studied in this spectral region for five arc currents 34, 38, 40 and 42 amperes (Fig. 2.9). The intensity seems to be a linear function of arc current. At wave lengths shorter than 200 nm, the output radiance of the mini-arc is low. That is why an arc current of 42A is used whenever experiments are carried out at these wavelengths. At wavelengths larger than 290 nm, the output radiance is very large and an arc current of about 34A was used to run the experiment. For intermediate wavelengths, an arc current of 38A is sufficient to have good statistics in any experiment. For higher wavelengths (more than 290 nm), even a low value of 34A of arc current, is enough to saturate the detectors and in this case, there is a
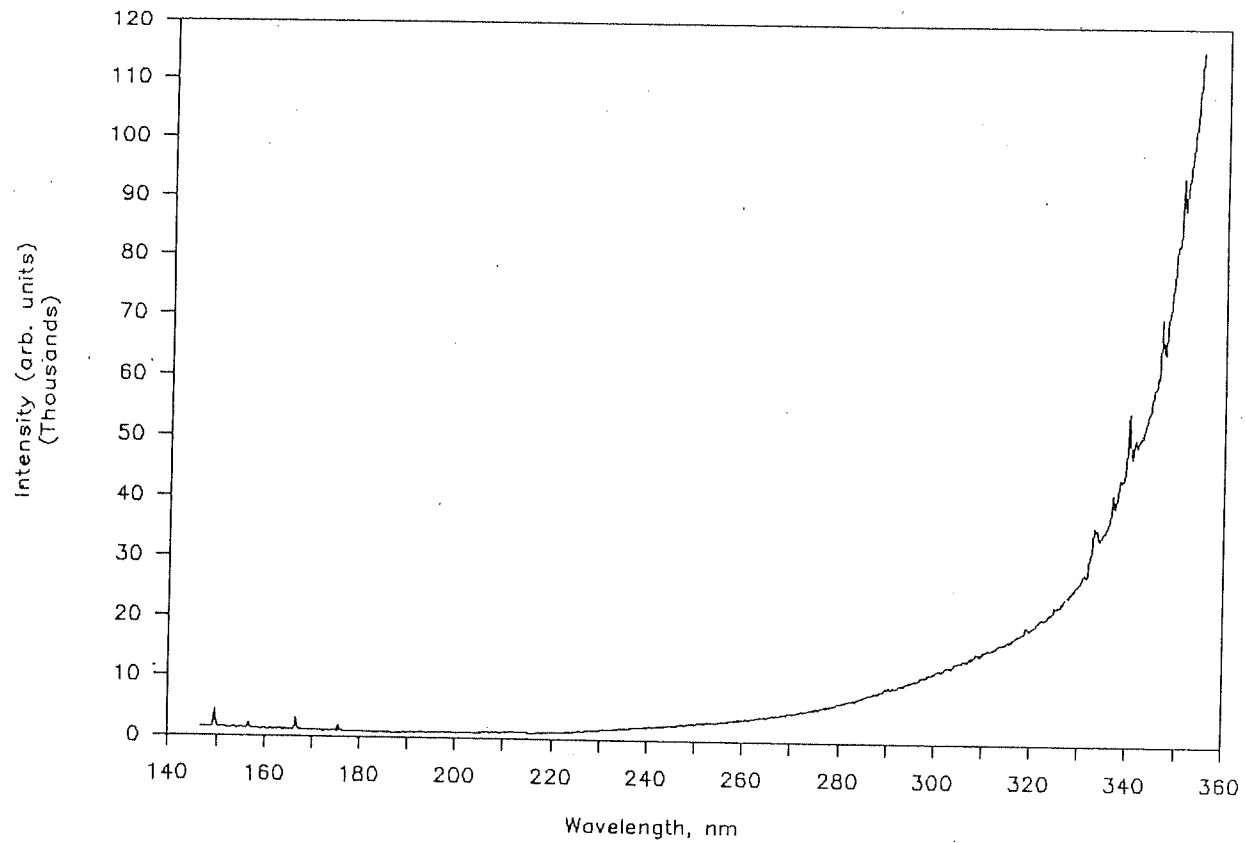
Figure 2.5 Complete mini-arc spectrum in 145-350 nm region.
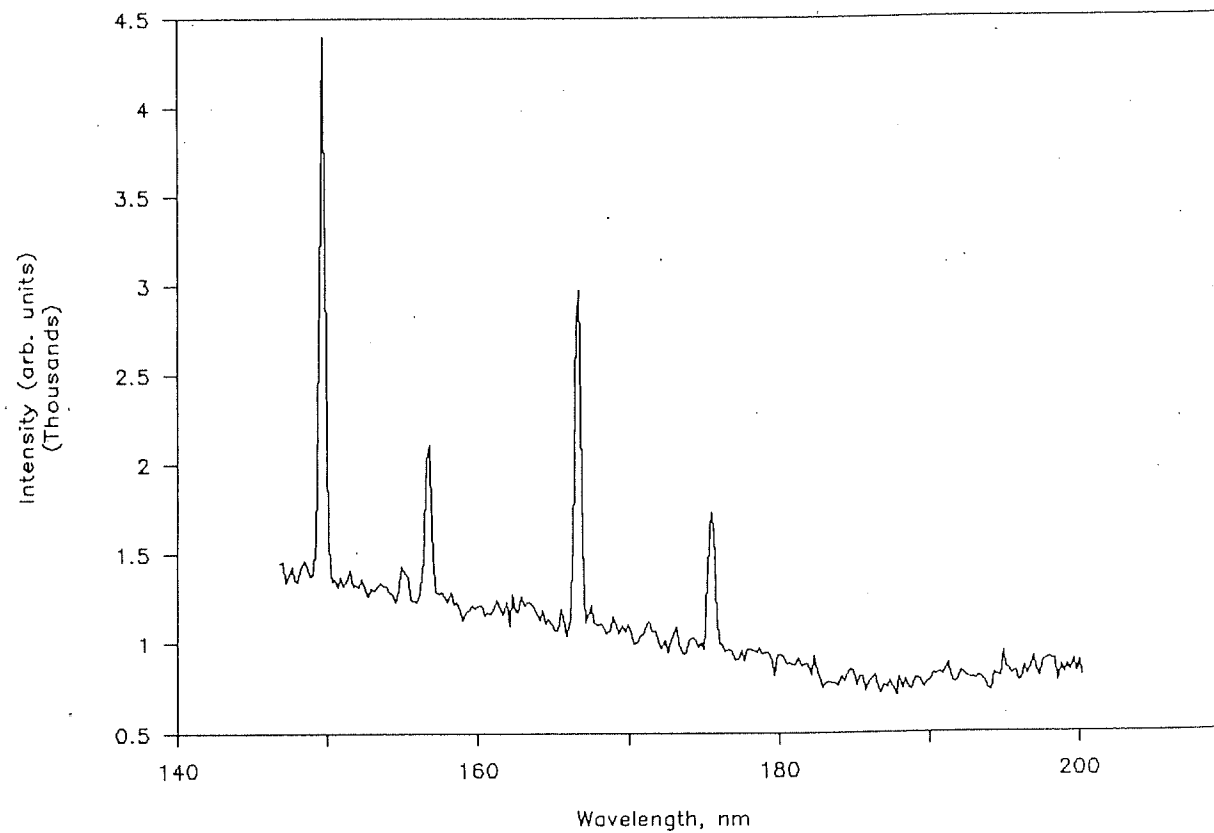
Figure 2.6 Argon mini-arc spectrum in 145-200 nm region.
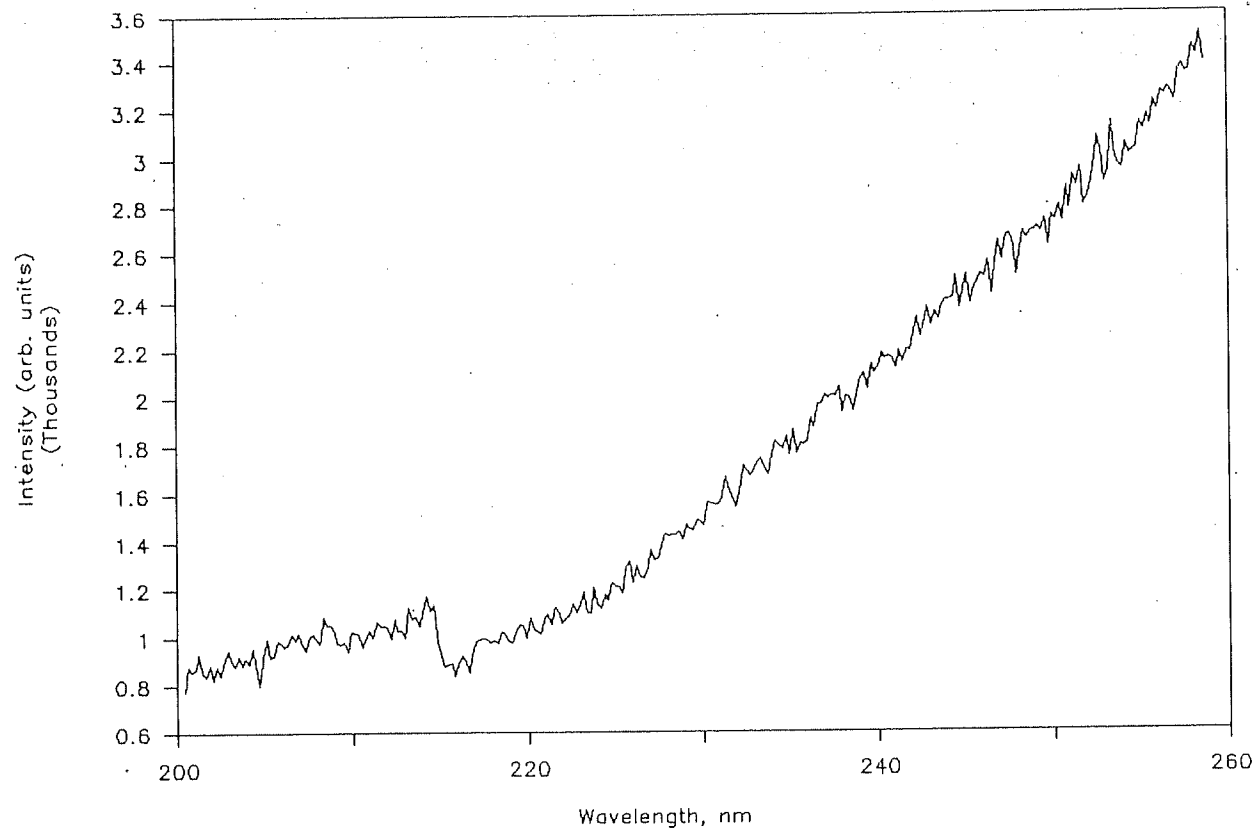
Figure 2.7 Argon mini-arc spectrum in 200-260 nm region.
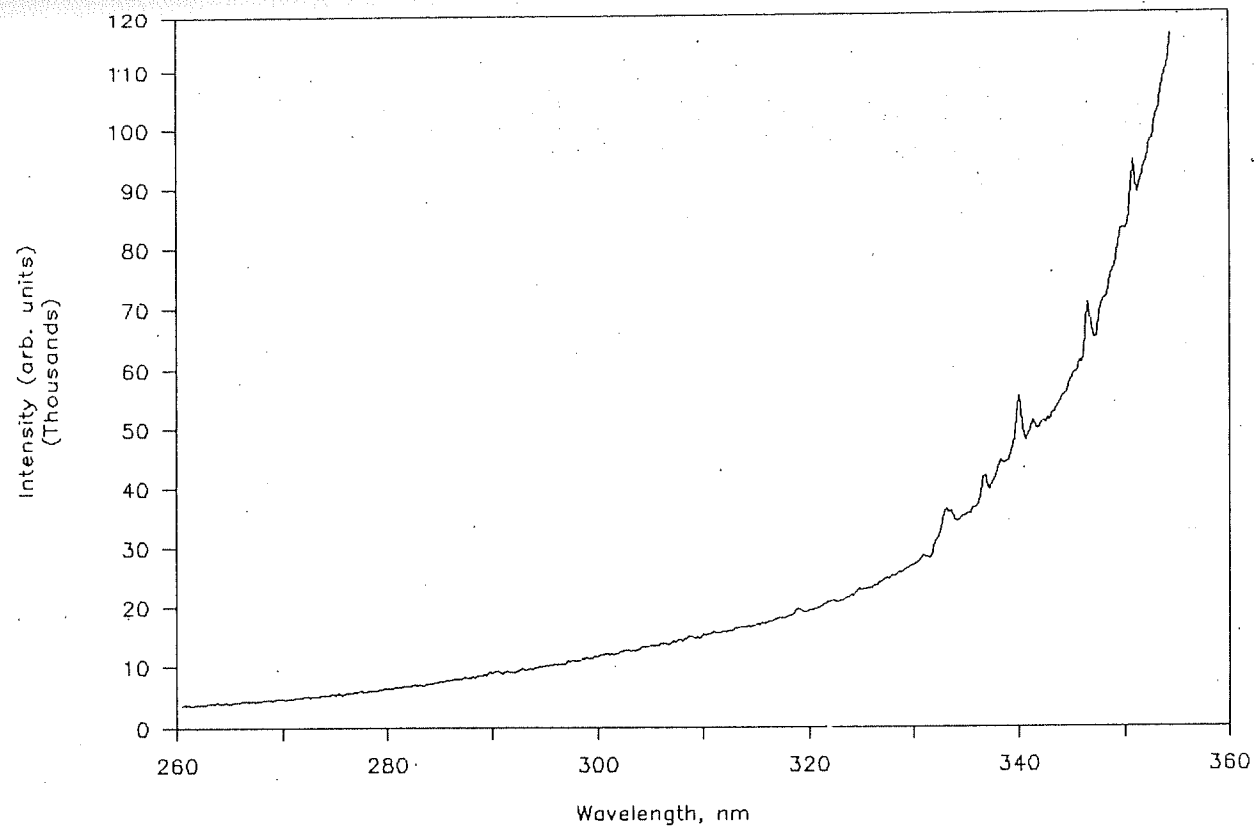
Figure 2.8 Argon mini-arc spectrum in 260-350 nm region.
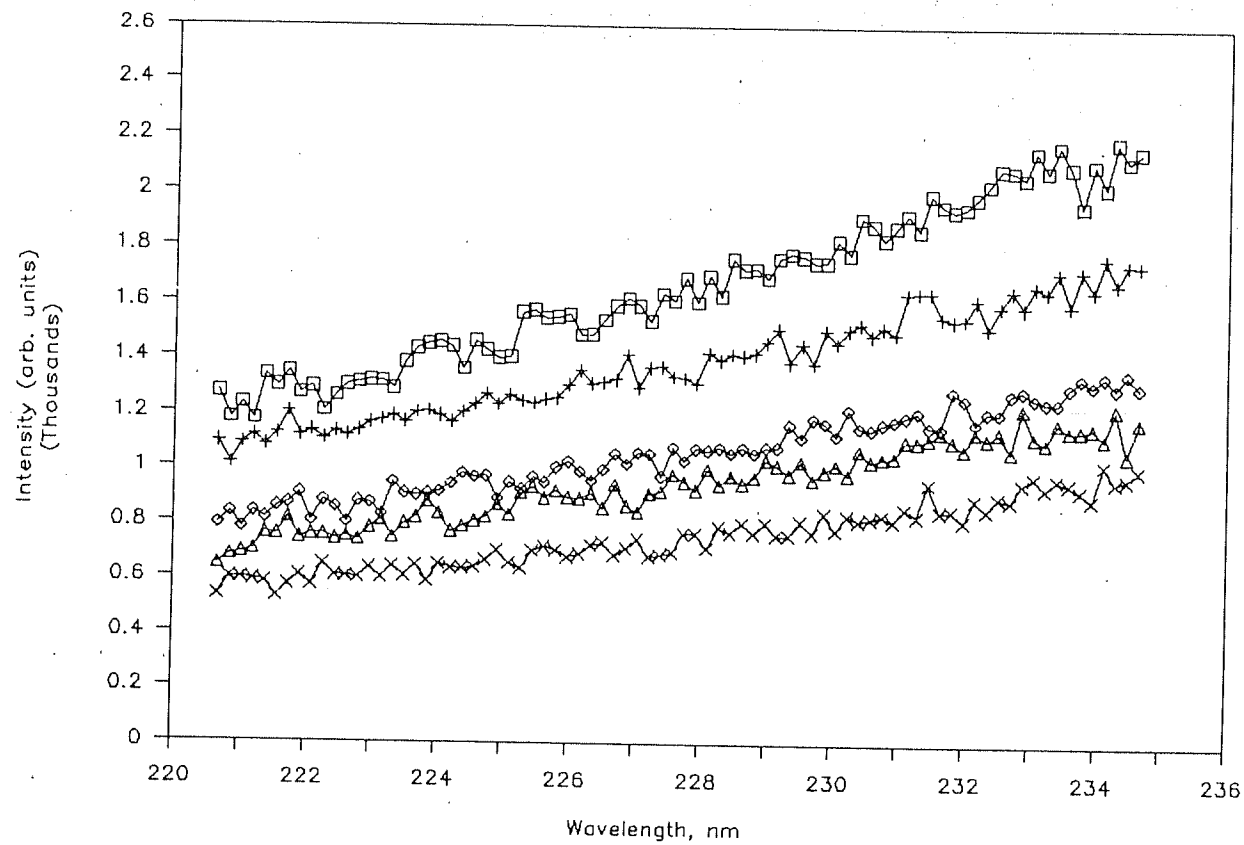
Figure 2.9 Argon mini-arc spectrum at 34, 38, 40 and 42 amps.

need to use light, attenuator. The light attenuator has been described in detail in Section (2.2.4).

As mentioned earlier, the gas purity necessary to maintain arc stability and reproducibility of the continuum emission is ensured by operating with a continuous flow of argon. Maintaining a high degree of argon purity (99.99%) within the arc chamber also minimizes the radiant power of atomic resonance lines in the spectrum which arise from small (ppm) concentration of oxygen, nitrogen, carbon and hydrogen. If commercial grade argon is used, the continuum intensity is reduced to some extent and an increase in the strength of the impurity resonance lines, is observed. Keeping in view of all these points, a research grade argon gas is used, through out the experimental studies.

2.2.4 Light attenuator

A wide spectral region 188 – 340 nm is covered in the present studies. The out put flux of the mini-arc source in the near UV region ($\approx$340nm) is more than 1000 times larger as compared to that in the shorter wavelength region. Having set the optimum values for gain and operating voltage of the photomultipliers, it was difficult to cover such a large photon flux. Reducing the arc current did not help much as the photomultipliers were saturated even at low arc currents (~ 34A). Hence the only option left was to reduce the photon flux near UV region by using a light attenuator after the M_gF_2 window, at the output end of mini-arc. The attenuator designed and fabricated in the laboratory, is made from the tungsten wire mesh having transmittance better than 90%. The tungsten wire mesh is folded a large number of times and the final product made circular in shape, is held between two thin copper rings by riveting. The attenuator made in this way had a transmittance of about 3%.

2.3   1-Meter Monochromator

A 1-meter vacuum ultra-violet monochromator has been used to disperse the continuum radiation produced by argon mini-arc light source. This is an asymmetric type of normal incidence, monochromator (Jovin - Yvon, France) which could be evacuated when required. The spectral holographic concave grating (Jovin-Yvon, France) used, had rulings of 1200 lines per mm and could be conveniently used in the spectral range from 115 to 340 nm in the first order. Wavelength selection is achieved by a sine drive which could be operated manually or by an electrically driven synchronous motor. The electric motor used in the monochromator offers various speeds ranging from 0.001nm/min to 10nm/min. The monochromator is evacuated to a base pressure of 10^{-6} Torr.

2.3.1   Resolution of the monochromator

In the absorption/fluorescence cross section measurements, the resolution i.e, the instrumental band width of the monochromator plays a vital role. The resolving power of an instrument is defined as the degree of separation between two closely spaced spectral lines. This can be understood by Rayleigh's criterion. If the diffraction pattern of two lines are considered then according to this criterion, the spectral lines would be resolved only when the minimum of the first peak falls on the maximum of the second. In the case of monochromator, employing concave grating as the dispersing element, the resolving power which is the ratio of λ and $\Delta\lambda$ depends upon the order number, the number of ruled lines of the grating and the focal length of the monochromator. In this case, $\Delta\lambda$ is the minimum wavelength separation which can be resolved by the monochromator at a wavelength λ of spectral lines. $\Delta\lambda$ is called the resolution or sometimes, instrumental band width of the monochromator.

This could also be defined in terms of full width at half maxima (FWHM) for a spectral line. At a slit width of about 50 microns each for both entrance and exit slits of the above monochromator, an average resolution of about 0.05 nm has been obtained for wavelengths ranging from 180 to 340 nm. This would give a resolving power of 5000 for the monochromator at a typical wavelength of 250 nm.

A resolution of 0.2 nm has been used through out the experiment. This corresponds to a slit width of 200 microns each for both entrance and exit slits. Such a beam width has been selected in the present work so as to accommodate very low fluorescence signals produced in a few spectral regions.

2.4 Beam Splitter

A beam splitter has been used between the exit slit of the monochromator and the absorption/fluorescence chamber to monitor the incident photon intensity during the experiment. Two types of beam splitters could be used in the experiment. These are shown in the Figs. (2.10a) and (2.10b).

The first type of beam splitter Fig. (2.10a) consist of a high transparency wire mesh mounted at an angle of 45^0 to the beam axis. More than 90% of the light is transmitted and the rest is reflected towards a light detector which includes a perspex light pipe coated at the front end with a scintillator and a RCA 6199 photomultiplier. Any of the two scintillators, sodium salicylate or p-terphenyle could be used to convert VUV and UV radiations into visible.

The second type of beam splitter tried in the present experiment, is simply a quartz plate (instead of wire mesh) mounted at an angle of 45^0 to the photon beam axis. More than 95% of the photon beam is transmitted through the quartz plate Fig. (2.10b). The rest is reflected to the
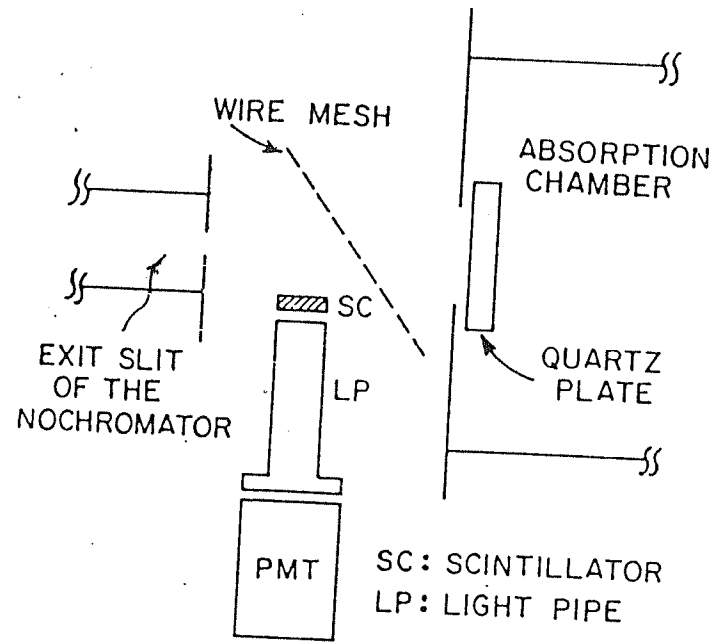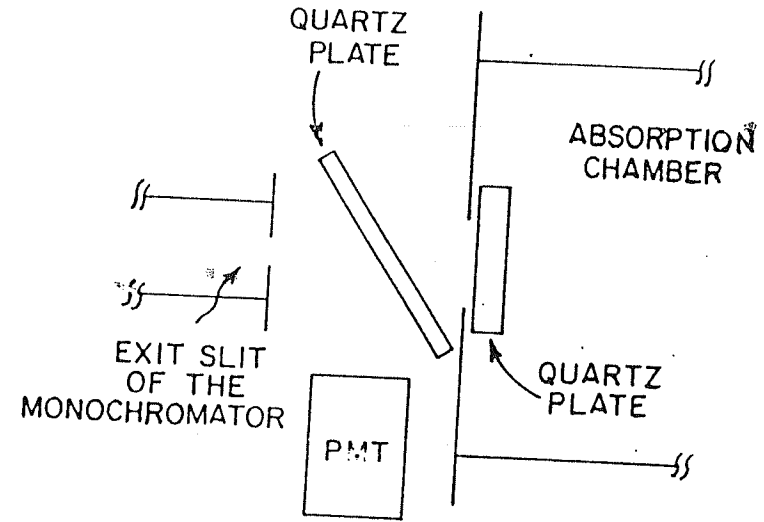
Figure 2.10 Two types of beam splitters.

photomultiplier, EMI 9558 QB, having a spectral response between 180-850 nm. This type of configuration has advantages in the experiment where measurements are carried out at wavelengths greater than 175 nm. No scintillator is used in this set-up and therefore, losses in light intensity due to quantum efficiency of the scintillator have been avoided. The use of light pipe is also not necessary in this case as the intensity of the light reflected from the quartz plate is sufficiently large. In comparison, the reflected light from the wire mesh used in the first type of beam splitter is extremely small.

In view of this, the second type of beam splitter has been used in the present experiment. The transmitted photon beam enters the absorption/fluorescence chamber through a quartz plate which isolates the beam splitter from the absorption chamber as far as vacuum is concerned. The beam splitter region is evacuated to a pressure better than 10^{-5} Torr through the exit slit of the monochromator.

2.5 Absorption/Fluorescence Chamber

The photon beam transmitted from the beam splitter enters a long chamber through a quartz plate where both absorption and fluorescence of molecules takes place. That is why this chamber has been named as absorption/fluorescence chamber. Figure (2.11) gives the top view of the absorption/fluorescence chamber.

The chamber has been designed and fabricated in the laboratory from non-magnetic stainless steel (no.304). All the necessary arrangements have been made to study absorption and fluorescence signals. The main structure of the chamber is made out of a cylindrical stainless steel pipe of diameter 15.8 cm and a length of 26 cms. The optical path length l, needed in the measurement of absorption cross section is 24.8
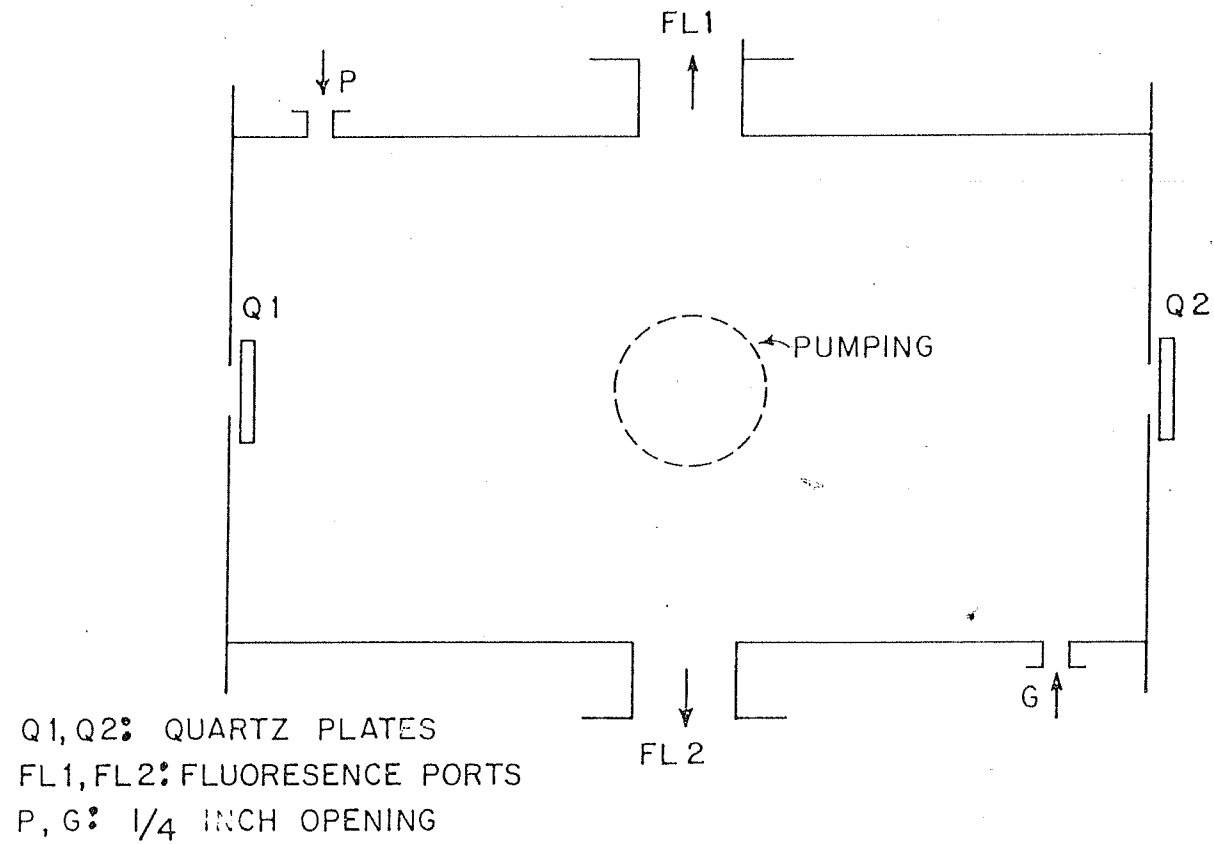
Figure 2.11 Top view of the absorption/fluorescence chamber.

Q1, Q2: QUARTZ PLATES
FL1, FL2: FLUORESENCE PORTS
P, G: 1/4 INCH OPENING

cms. Q1, Q2 are the quartz plates used, for the purpose of vacuum sealing at both ends of the chamber. FL1, FL2 are two ports of diameter $\simeq$ 5 cms perpendicular to the photon beam axis and are used for the measurement of fluorescence intensity from the molecules. The ends of the two ports are vacuum sealed, again by quartz plates. In the present experiment, only one port is being used for fluorescence measurements. The total fluorescence intensity is measured at a given photon wavelength with a thermoelectrically cooled photomultiplier EMI 9558 QB positioned behind one of the two ports. G and P are two 1/4 inch dia. openings for introducing the target gas and for the measurement of absolute gas pressure respectively. The absorption/fluorescence chamber was evacuated to a pressure of 10^{-6} Torr using pumping arrangements discussed in Section (2.6).

In fact, one could measure the transmitted intensity at the end of the absorption chamber. It was found that in this geometry, the transmitted intensity included the fluorescent component produced along the photon beam axis because of absorption of photons by target molecules. As a result, the absorption cross sections measured were found to be less in the spectral region where high fluorescence quantum yield from target gas was observed. To avoid this, another monochromator was used after the absorption chamber.

2.5.1 0.2-m Monochromator

The need and importance of another monochromator after the absorption chamber has already been discussed in the previous section (Section 2.5). The monochromator used is a 0.2 meter VUV monochromator from λ – Minuteman Laboratories Inc., USA. The instrument (model: 302-VM) has a single reflecting surface. An abberation corrected concave holographic grating produced by Jobin-Yvon having 1200 lines/mm rulings has been used in the monochromator.

The gratings of the two monochromators are co-rotated so as to allow photon beam of same wavelength to be transmitted. The 1-m monochromator decided the instrumental resolution and the new monochromator was used to avoid detection of the fluorescence emission produced at wavelengths higher than that for incident photon beam. A slit width of about 800 microns each was used for both entrance and exit slits of the 0.2-m monochromator so as to take care of wavelength mismatch, if any, between the two monochromators. A quartz plate was vacuum sealed at the exit slit of the new monochromator which was evacuated to a pressure of 10^{-3} to 10^{-4} Torr depending upon the spectral region where photoabsorption cross sections are measured. At wavelengths near 200 nm, a pressure of 10^{-4} Torr was used for the 0.2-m monochromator whereas at photon wavelengths larger than 280 nm, a pressure of 10^{-3} Torr was sufficient. The dispersed intensity from 0.2-m monochromator was measured by using an EMI 9558 QB photomultiplier.

2.6 Vacuum System and Related Instruments

In this section, the vacuum systems used to evacuate 1-m monochromator, absorption/fluorescence chamber, 0.2-m monochromator and the reference side of MKS Baratron capacitance manometer would be described in detail. The pressure measuring instruments: both for measuring relative and absolute pressures; gas handling systems and gas purification devices would also be discussed.

2.6.1 Vacuum systems

Various types of vacuum systems have been used in the present experiment depending upon the requirement. There were four sub-systems which had to be evacuated to different pressures. These include 1-m monochromator along with beam

splitter, absorption/fluorescence chamber, 0.2-m monochromator and the reference side of the MKS Baratron capacitance manometer. The 1-m monochromator and the beam splitter are evacuated to a pressure of 10^{-6} Torr using a combination of oil diffusion pump (500 lit/sec) and a rotary pump (750 lit/min). The beam splitter in this sub-system, is pumped through the exit slit of the monochromator. The absorption/fluorescence chamber, which is vacuum sealed on both sides by quartz plates, is evacuated to a pressure of 10^{-6} Torr by a combination of diffstak (MK2 series, 300 lit/sec) and rotary pump (E2M8, 200 lit/min) procured from Edwards, UK. The 0.2-m monochromator is also vacuum sealed on both sides by quartz plates. Sorption/rotary pump is used to get the desired pressure. Finally, the MKS Baratron capacitance manometer is used to make absolute pressure measurements of the target gas in the absorption/fluorescence chamber. To get the absolute pressure from differential manometer, the reference side of the MKS differential unit is evacuated to a pressure of better than 10^{-6} Torr using an oil diffusion pump (120 lit/sec) backed by a rotary pump (300 lit/min).

2.6.2 Pressure measurements

The pressure in the four sub-systems has been measured by using thermocouple gauges up to a pressure of 10^{-3} Torr and Penning gauges in the pressure range between 10^{-3} to 10^{-5} Torr. Both the gauge heads and measurement units of these gauges have been procured from IBP Torr Ltd. An ionization gauge (Veeco-RG 830, Veeco Inst., USA.) has been used to estimate the pressure ranging from 10^{-3} to better than 10^{-6} Torr.

A calibrated MKS Baratron differential capacitance manometer, with sensor and read-out unit was procured from MKS Instruments, USA, to make absolute pressure measurements

of the target gas in the absorption/fluorescence chamber. The sensor head, 310 MH-10 is a differential gauge and the reference side of the gauge had to be evacuated to a pressure better than 10^{-6} Torr. In the present experiment, the target gas pressure could be varied from 2×10^{-3} Torr to 5 Torr. Therefore, a reference pressure of 10^{-6} Torr was adequate to get absolute pressure within the accuracy quoted by the manufacturer. Fig.(2.12) shows the arrangement made for using MKS Baratron capacitance manometer in the system.

One of the largest sources of error is the temperature sensitivity of the sensor of the capacitance manometer. Changes in temperature will affect zero stability, full scale range (span) and linearity of the MKS unit. To minimize these effects the sensor head is maintained at a constant elevated temperature of 318^0K.

In Fig.(2.12), A and B are greaseless shut-off valves made of glass (Konetes, USA), SH is the sensor head of MKS Baratron capacitance Manometer. To start with, valve B is closed and A is opened then the null deflection is adjusted keeping the sensor head in the most sensitive pressure range. For pressure measurements, valve A is closed and the valve B is opened to have access to the absorption/fluorescence chamber where absolute pressure has to be measured.

2.6.3 Gas handling

Argon gas was used in the mini-arc source. SO_2 gas and CS_2 in vapour phase were used for absorption and fluorescence studies. The following discussion covers the source of supply, quality, handling and purification, if any, of these gases.
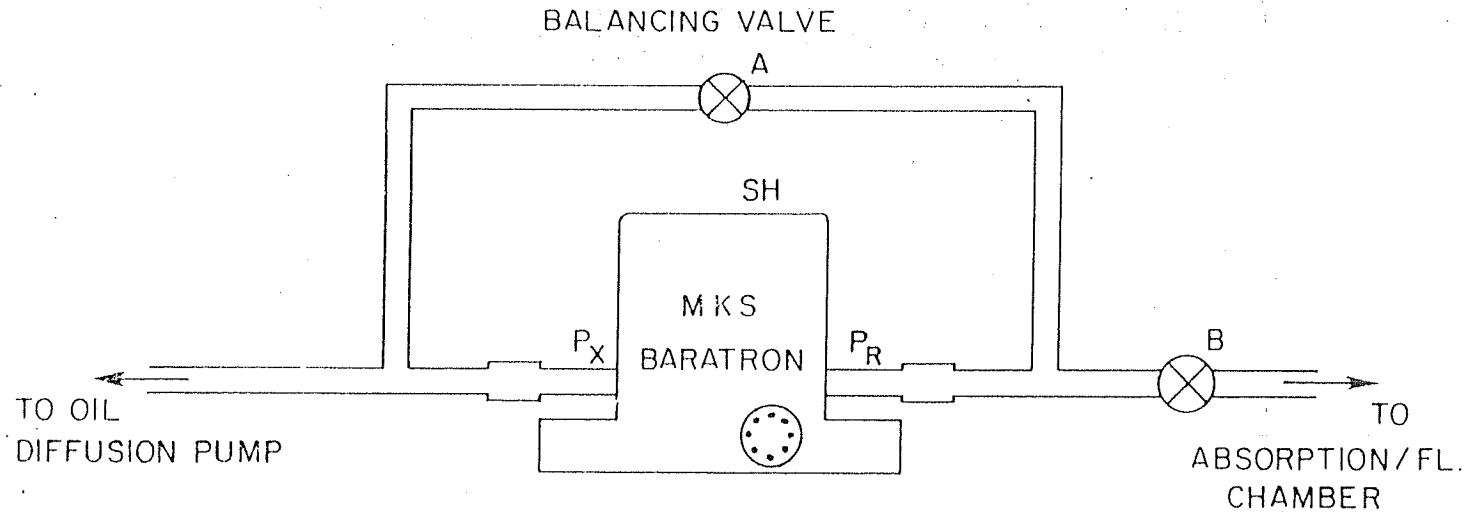
Figure 2.12 Connection for MKS Baratron for absolute pressure measurement.

Argon :

Argon gas was procured from Indian Oxygen Limited. A research grade IOLAR-II (99.99% pure) gas was used in the mini-arc light source without further purification. The gas line was of 1/4 inch refrigerator copper tubing connected through a ball type gas flow meter to the gas manifold which in turn supplies gas at three positions to the mini-arc light source.

SO_2 :

SO_2 gas was imported from L'Air Liquid, France. The research grade liquefied gas, was used without any further purification. The cylinder was supplied with a safety valve and a two stage gas regulator was connected to control the SO_2 flow. The gas line made of 1/4 inch dia.copper tubing was coupled to a needle valve (Granville-Phillips, USA) for the purpose of finer control.The other end of the needle valve was connected to the absorption/fluorescence chamber. Before introducing the SO_2 gas into the system, the gas line was thoroughly pumped to remove any kind of impurities.

CS_2 :

A research grade (99.9% pure) CS_2 liquid was used to extract the CS_2 vapour. The vapour extraction system is shown in Fig.(2.13).

F1,F2 are small glass flasks; V1, V2 are needle valves; and K1, K2 are glass shut-off valves. Opening of valve K1 leads the vapour to the experimental chamber whereas K2 is used to evacuate the residual gases in the gas line when K1 is closed. CS_2 liquid was filled in flask F1, the flask F2 was kept so that an unusual pressure build up could be avoided in the gas line.

F1

V1

F2

V2

K1

K2
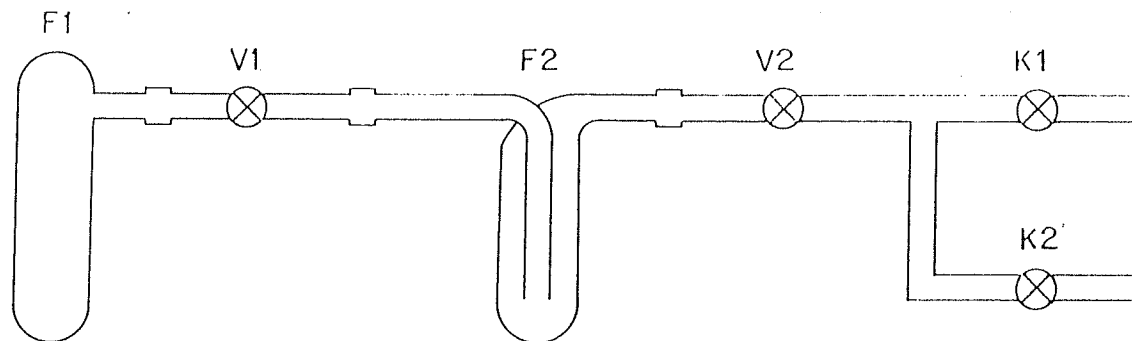
F1, F2 : GLASS FLASKS
V1, V2 : NEEDLE VALVES
K1, K2 ; SHUT OFFVALVES

Figure 2.13 CS_2 vapour extraction arrangement.

CS$_2$ liquid was frozen down to liquid nitrogen temperature (77^{0}K). CS$_2$ solidifies at 162^{0}K itself, and hence the gas line can be evacuated through K2 valve by a rotary pump. CS$_2$ settles down to liquid form again at room temperature having a vapour pressure of about 400 Torr. The CS$_2$ vapour was extracted into the system through K1 valve. The needle valves V1,V2 not only helped in separating the CS$_2$ liquid flask from the experimental system, but also in maintaining an excellent control over the flow rate.

The desired pressure of SO$_2$/CS$_2$ inside the absorption chamber is achieved by controlling the baffle valve opening of Edwards Diffstak pump and needle valve. Stability in the gas pressure inside absorption/fluorescence chamber was achieved by the coarse adjustment of baffling action and fine control of needle valve.

2.7 Light Intensity Measurements

To obtain absorption and fluorescence cross section for various molecules, the required quantities to be measured experimentally, are light intensities at various ports during the experiment and the absolute pressure of the target gas under study. The details about absolute pressure measurement have already been discussed in the previous section. The following section covers the description regarding the kind of detectors used in the experiment for light intensity measurements, pulse extraction from the output of the detectors used and other related topics. In case of absorption cross section measurements, light intensities at beam splitter and exit slit of 0.2-m monochromator were needed, whereas for fluorescence cross section, light signals at the beam splitter and fluorescence port were required.

2.7.1 Detectors

The measurement of photoabsorption cross section in the present experiment, covers the spectral region from 180 to 340 nm, whereas the fluorescence emission from the neutral molecules or ions extends upto a wavelength larger than 750 nm.

Below 800 nm, photomultipliers are extremely sensitive light detectors providing a current output proportional to the incident light intensity. The photomultipliers with various types of photocathodes used, have different spectral response and different quantum efficiency which varies with incident photon wavelength. A photomultiplier with a tri-alkali type of photocathode has a S-20 type of spectral response which extends from about 180 to 750 nm, if used with a quartz window. The (Cs) Na_2 K Sb tri-alkali photocathode used in some photomultipliers render a moderate level of background noise.

Photomultiplier tubes have an appreciable current even in total darkness. This "dark current" is temperature dependent, it decreases rapidly on cooling below room temperature, and is given by Richardson's equation.

$$n = AT^2 \ e^{-(\phi/KT)} \ cm^{-2} \ sec^{-1} \qquad \longrightarrow (2.1)$$

In this equation, n is the number of thermal electrons produced, A is the geometrical factor related to the photocathode dimensions, T is the absolute temperature in degrees Kelvin, ϕ is the work function of photocathode material and K is the Boltzman constant. In the case of S-20 photocathode, the work function is 1 ev. Hence one expects appreciable thermal current at room temperature.

It is evident from Eq.(2.1) that the thermal

contribution to the dark current becomes negligibly small below a certain critical temperature. For S-20 photocathode, negligible back ground reduction occurs below -30^0C. When the tube is cooled sufficiently to suppress the thermal component of the dark current, a fairly constant component, sets the noise limit. This non-thermal part of the dark current is due to several causes, including cosmic rays and radio active atoms in the tube.

In the present experiment, the photomultipliers used at various ports for light intensity measurements are Thorn EMI's 9558 QB. These photomultipliers have S-20 type of photocathode with spectral response extended in the ultraviolet region using quartz (fused silica) as the window. The spectral response curve of the photocathode, (S-20) as given by the manufacturers, is shown in Fig.(2.14).

The photomultiplier tube at the beam splitter port is thermoelectrically cooled down to -30^0C by the thermoelectric refrigerated chamber (Modle: TE 206-TSRF, Products for Research,USA). The photomultipliers used for measuring the transmitted intensity at the exit slit of the 0.2 meter monochromator and fluorescence intensity at the fluorescence port were cooled down to -30^0C by thermoelectrically cooled photomultiplier housing (Modle: FACT - 50 MK3, Thorn EMI,UK). It may be pointed out here that the absorption and fluorescence measurements were not made simultaneously.

In a photomultiplier, discrete electrical output pulses are generated at the anode for each photon striking the photocathode. The amplitude spectrum of output pulses comprises of peaks, arising due to a photon striking at the photocathode and also from the thermal release of electrons within the dynode structure. But the amplitude of pulses generated at various stages of the dynodes is much smaller than that of pulses due to a photon event. A useful improvement in output signal to noise performance is achieved
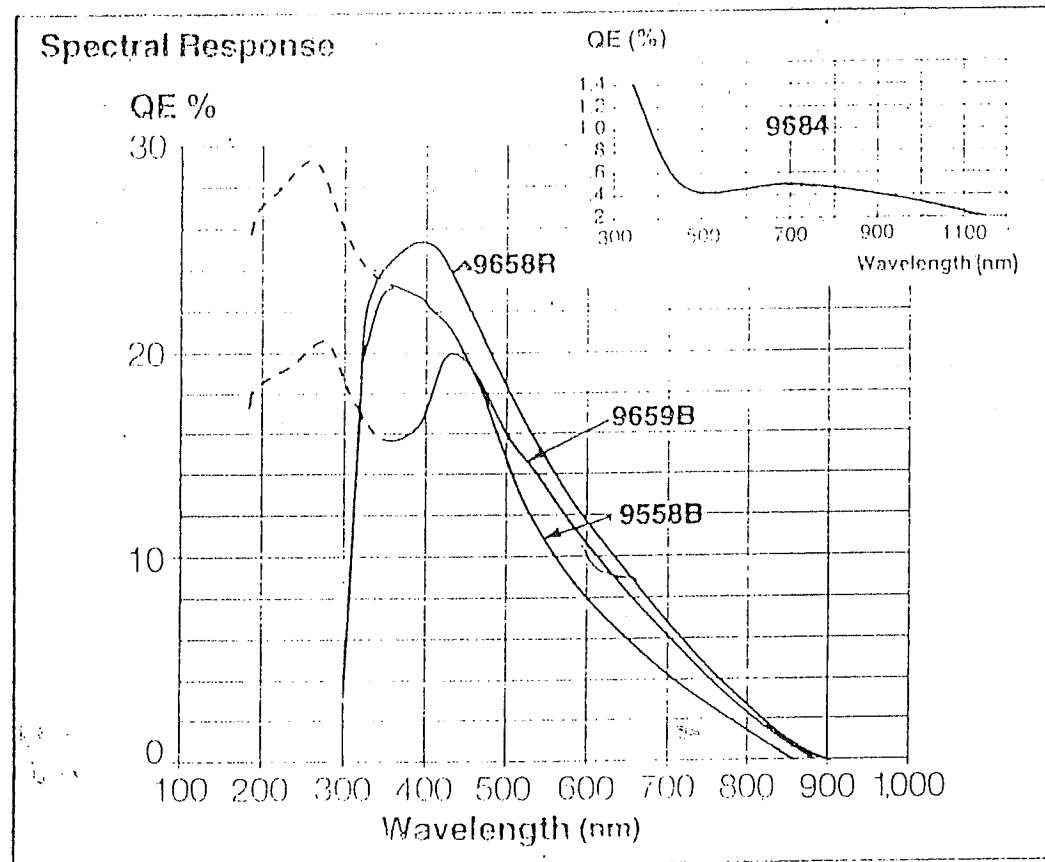
Figure 2.14 Spectral response of various photocathodes.

if these lower amplitude pulses are rejected from the data.

There are two ways in which a photomultiplier can be used. These are analog mode and photon counting mode. In analog mode, dark current will give a combined contribution of electron emission from the photocathode and dynodes together with electrical leakage within the tube. In photon counting mode, the contribution of electron emission from dynodes and electrical leakage can be avoided by using a pulse height discriminator. The threshold voltage of pulse height discriminator is chosen in a such a way that the signal to noise ratio is maximum.

For measuring light intensities in the present experiment, all photomultipliers were used in the counting mode. Except in one spectral region, where the fluorescence were appreciable (signal to noise ratio 10:1 for SO_2 at wavelengths 220 to 230 nm), the fluorescence signals in all other spectral region for both SO_2 and CS_2 were extremely small. The light intensity at beam splitter was about 5% of the incident flux. Also a considerable reduction in the transmitted intensity was observed at the exit slit of 0.2-m monochromator because of light losses in the dispersing unit. That is why all the photomultipliers were operated in the counting mode. In addition, cooling of the photocathodes for all the photomultipliers helped to have reduced dark current and large size photon pulses.

Optimization of signal to noise ratio was carried out for the photomultipliers used in the experiment. Figure(2.15) gives the plot of signal to noise ratio verses applied voltage . From the figure, it is clear that the signal to noise ratio remains stable in a certain range of applied voltage. Therefore, an applied voltage of 1220V for the photomultipliers used to carry out fluorescence/absorption studies and 1150 volts for the photomultiplier used at the beam splitter were fixed. A special mention would be made in
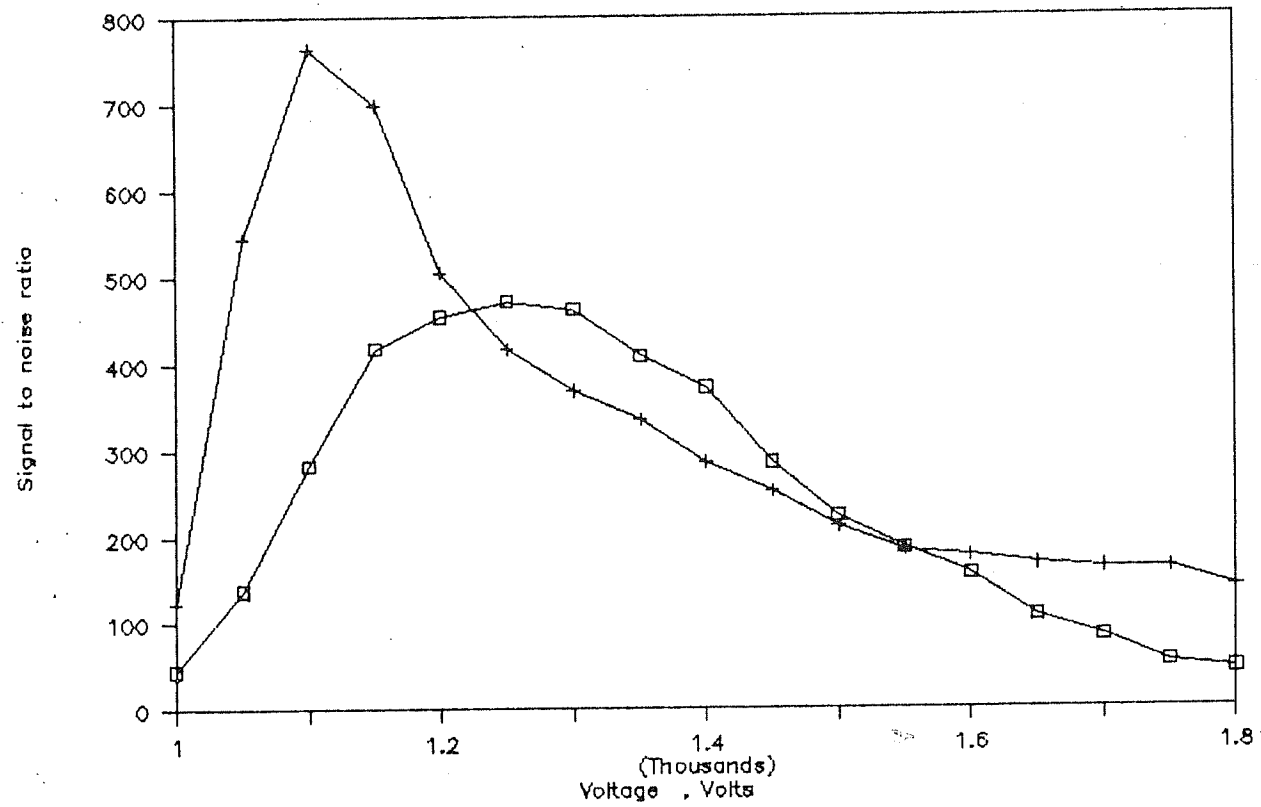
Figure 2.15 Optimization of signal to noise ratio of the photomultipliers.

the text if and when different voltages for the photomultipliers are used.

2.7.2 Data acquisition system

Data acquisition system includes pre-amplifier, amplifier, discriminator units for the photomultipliers and a microprocessor-controlled 1024 channel dual multi channel analyzer (MCA). The entire system was designed and built in our laboratory to suit our requirements, and the block diagram is shown in Fig.(2.16).

The anode output from both the photomultipliers was fed to a charge sensitive preamplifier having decay time constant of about 330 ns. Output of the preamplifiers, after sufficient amplification, using another amplifier, was fed to a variable threshold discriminator to cut off noise and obtain clean and uniform pulses. Photomultiplier voltage and the discriminator threshold level were optimally set in conjunction with each other to obtain maximum signal to noise ratio.

The MCA consists of two main units, namely the microcomputer and the interface. The interface unit comprises of two 20-bit counters; a timer and two 8-bit digital to analog (D/A) converters. The microcomputer was specially programmed so as to function as a dual MCA operating in scalar mode, having two sets of simultaneous data storage of 1024 channels, each with storage capacity of $2^{20}-1$ counts per channel. It used a video terminal as its console to accept commands and set data acquisition parameters. Various options for gate time were provided to store the data. The duration per channel was available from 0.1 sec to 100 sec. A dot matrix printer was connected to obtain hard copy of the raw data and its profile as well. The data could also be transferred on a communication link to a remote computer for
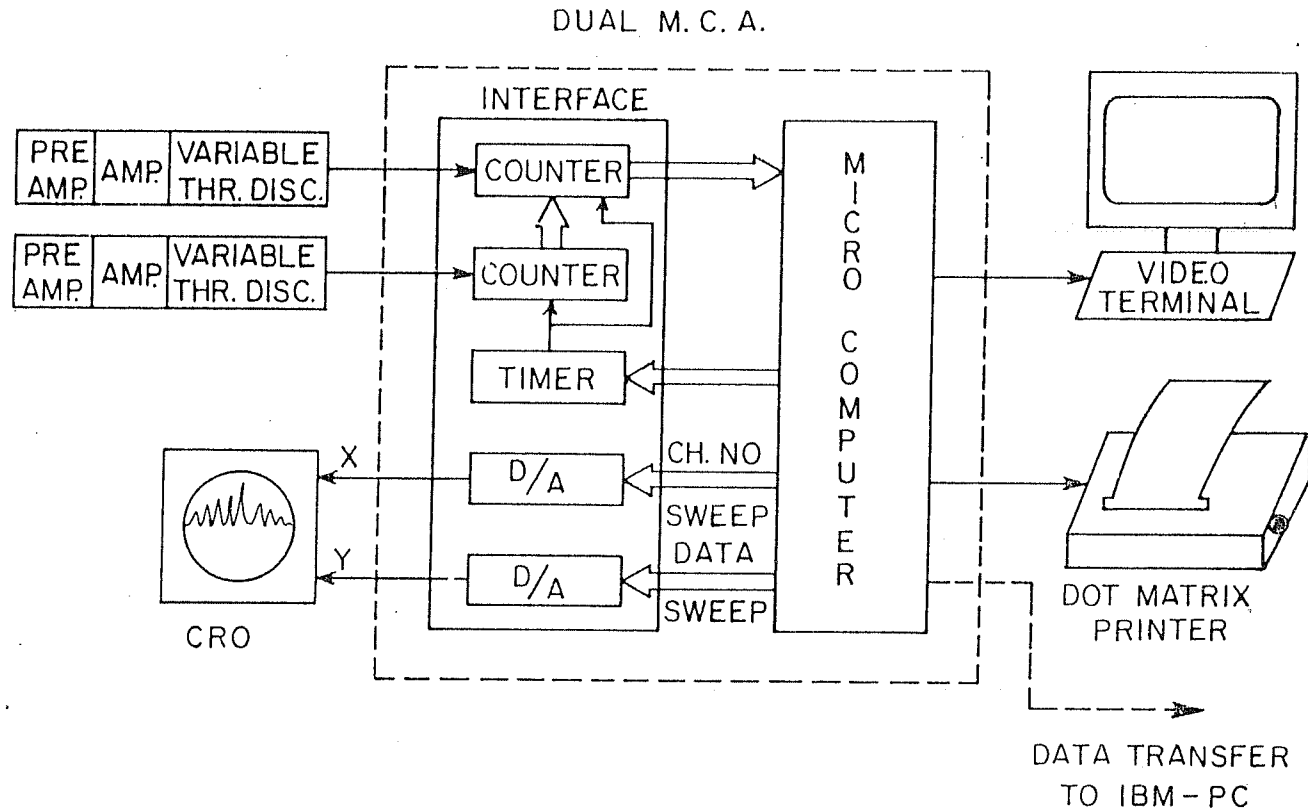
Figure 2.16 Block diagram of the data acquisition system.

off - line processing, long term storage and documentation.

Initially the acquisition parameters like time duration gate pulse, number of scans etc, are set into the MCA through the video terminal. Then, the computer triggers the timer to generate a gate pulse of width corresponding to a pre-selected value. During this interval of time, incoming pulses from photomultipliers are allowed to be counted in two separate counters. At the end of the gate pulse, two sets of the total counts data are retrieved by the computer and stored separately in the corresponding channel memory. Then the channel number is advanced, counters are reset, and a fresh trigger pulse is sent to the timer. A fast scan of each channels data along with its corresponding channel number is continuously fed to two D/A converters to produce X and Y sweep voltages for an external CRO which gives visual display of current status of the data profile.

On completion of full acquisition scan, the raw data can be printed on a dot matrix printer and a printed profile can also be obtained. Further processing of the raw data can be done by transferring it to a remote computer/IBM-PC through a communication link provided.

2.8 Operation of the Instrument

To start the experiment, all the pumping units were turned on. Power supplies for the photomultipliers and thermoelectrically cooled houses were switched on at least 5 to 6 hours prior to any spectral measurements to be carried out. This allows the temperature of the housings to be stabilized. Also the stability in dark current of the photomultiplier could be achieved. The system was evacuated until background pressure of 10^{-6} Torr was reached in 1-m monochromator, absorption/fluorescence chamber and reference

side of the MKS Baratron capacitance, manometer. Next the light source was started following the procedure out lined below.

Water circulation for the mini-arc light source was turned on. Required pressure ($\simeq$ 1 atm.) of the argon gas was maintained in the light source, with the help of ball type gas flow meter. The current regulated power supply was switched on. The arc was transferred form the cathode to the anode with the help of an auxiliary electrode, a tungsten rod. The current across the discharge was set to a high value ($\sim$ 42A) near 200nm whereas a current of 34A was maintained for the incident photon wavelengths larger than 280 nm.

Having decided the spectral range, the operating conditions for the argon mini-arc light source were finalized. The pressure of the target gas to be used in the absorption/fluorescence chamber had then to be decided for absorption and fluorescence measurements. The procedure for carrying out absorption and fluorescence studies has been discussed in detail in the following sub-section.

2.8.1 Absorption cross sections measurement

Two spectral scans were necessary to obtain absorption cross section of the target gas. First scan was taken without the target gas in the absorption/fluorescence chamber, whereas the second scan was carried out with the desired pressure of target gas in the chamber. When there was no gas in the absorption chamber, the two photomultipliers at the beam splitter port and at the exit slit of 0.2-m monochromator were used for the purpose of calibration of incident intensity. This part has been discussed in Chapter III in detail. The signals from two photomultipliers after proper amplification were fed to the dual 1024 MCA. The typical gate time used to store the incoming pulses from the

photomultipliers was 10 seconds per channel. The grating of the two monochromators were co-rotated at a speed of 1nm/min so that the wavelength coverage was 0.167 nm during each channel of the MCA. The synchronization between grating rotations of the two monochromators and the start of counting by MCA was insured to a high accuracy by using the same switch for all these operations. The scanning was stopped after covering the desired spectral range.

Same procedure was repeated after filling the absorption/fluorescence chamber with target gas. The required pressure of the gas was monitored by the MKS Baratron capacitance manometer. The intensities measured at beam splitter and at the exit slit of 0.2-m monochromator were stored for both with and without gas scans. This information was used to calculate the absorption cross section of target gas as a function of incident photon wavelength. Further discussion on the methodology of absorption cross section measurements has been covered in the next chapter.

2.8.2 Fluorescence cross section measurements

Here the aim was to study the fluorescence signals produced by the target gas perpendicular to or along the primary photon beam axis as a function of incident wavelength. For the measurement of fluorescence cross sections of SO_2, the fluorescence signals were collected by photomultiplier positioned perpendicular to the optic axis whereas for CS_2 vapour, the fluorescence studies were carried out in the direction along the photon beam axis. The reason for doing that has been discussed in detail in Chapter III. That is why, the 0.2-m monochromator at the end of the absorption/fluorescence chamber was not needed while carrying out fluorescence measurements. The operation of the instrument was similar to what has been described for absorption cross section measurements except the fluorescence

studies for CS_2 vapour. In case of SO_2, the photomultiplier housing which was used at the end of 0.2-m monochromator in absorption studies was shifted to the fluorescence port (FL1 in Fig. 2.10) perpendicular to the optic axis. Here, again two spectral scans were carried out. The one without gas was to measure the scattered signals arriving to the fluorescence port, if any, and the gas scan for the measurement of fluorescence signals.

For the measurement of fluorescence intensity in the direction along the photon beam axis as in the case of CS_2 vapour, a colour glass filter was used before the photomultiplier measuring fluorescence signals. The colour glass filter was chosen carefully such that it would not transmit the monochromatic incident photon wavelength from the argon mini-arc source, but would have high transmittance for fluorescence signals from the target molecules. The method to calculate fluorescence quantum yield in this configuration has been discussed in detail in Chapter 3.

2.9 Performance of the Instrument

The performance of the absorption/fluorescence spectrometer was studied in detail for various features like resolution, calibration of the photon wavelength scale etc. A quantitative analysis was also carried out to understand the effect of any change in absorption cross sections with a 0.2-m monochromator after the absorption chamber. All these features would be discussed one by one in the following sections.

2.9.1. Resolution

Instrumental resolution and resolving power of the 1m monochromator have already been discussed in Section (2.3.1).

Some more information about this aspect is in order here. Resolution of the system was measured using known intense atomic lines of mercury and carbon. For this purpose, quartz enveloped mercury lamp as well as argon mini-arc itself were used. The lamp was mounted on a flange situated at the entrance slit of the 1m monochromator. For 200 micron width of entrance and exit slit, full width at half maxima (FWHM) of atomic lines was found to be about 0.2 nm in the wavelength region 185 to 330 nm. Three mercury atomic lines at wavelengths 253.65, 284.77 and 326.41 nm and one carbon atomic line at 193.09 nm were chosen for measuring resolution of the system at 200 micron slit widths for both entrance and exit slit of the 1m monochromator.

Effect of mechanical vibrations on the resolution of the instrument was also studied. This was done at only one wavelength i.e, at CI 193.09 nm atomic line. It was found that the vibration due to mechanical pumps did not affect the resolution of the system.

2.9.2 Wavelength calibration of the spectra

Wavelength analysis of the absorption and fluorescence spectra of target gases was carried out using the 1-meter scanning monochromator. The scanning drive of the monochromator is coupled to a counter that displays the wavelength appearing at the exit slit, directly in angstrom units. The monochromator counter which displays the wavelength, was calibrated with known atomic lines for wavelength calibration in the spectral region from 185 to 330 nm. It was found that there was a constant difference between the two wavelength scales, one provided by the counter of the monochromator and other by standard atomic lines. This correction was used in the subsequent analysis of the photoabsorption and fluorescence spectra of the target gases.

2.9.3. Effect of using 0.2 monochromator

In the experiment for measuring absorption cross sections of target molecules, initially, the transmitted intensity was measured at the end of the absorption chamber. It was found that the absorption cross sections measured in this way were always smaller than those reported in the literature. Also, it was noticed that the absorption cross sections were always pressure dependent even though the pressure of the target gas used was well within the pressure limit allowed by Beer-Lambert law. Lower the pressure used, higher the value of absorption cross section was obtained. Taking typically the case of SO_2 at 204.0 nm incident photon wavelength, the value of absorption cross section at 80 mTorr was found to be 1.7 times that measured at 300 mTorr of target gas pressure. This discrepancy could be explained in terms of some additional light signals being detected by the photomultiplier measuring the transmitted intensity. It is obvious that the target molecules gets excited because of photoabsorption and re-emits as a fluorescence signal at wavelengths larger than the incident photon wavelength. This fluorescence emission would have a component along the direction of the photon beam axis. Therefore, the fluorescence would give an additional contribution to the transmitted signal with the result that the absorption cross section would become smaller in value. Higher the pressure of the target gas, higher would be the contribution due to fluorescence component along the beam axis and therefore smaller would be the absorption cross section. This fact was clearly observed in the present experiment as we were using SO_2 as the target gas which has a large fluorescence quantum efficiency.

To overcome this defect, a 0.2-m monochromator was used behind the absorption chamber and the transmitted intensity was measured at the exit slit of the monochromator. As

described before, this monochromator was evacuated to an appropriate pressure. By co-rotating the gratings of 1-m and 0.2-m monochromators, one could eliminate the possibility of fluorescence signals from being detected by the photomultiplier measuring the transmitted intensity. Using this system, the absorption cross section at many photon wavelengths were measured as a test case at large number of pressures varying from 80 to 300 mTorr. The cross section values at all pressures were found to be same within the stipulated experimental errors.

CHAPTER - 3

METHOD

To find the fluorescence quantum yield of a molecule at an incident wavelength, it is required to measure the total photoabsorption and fluorescence cross section. The fluorescence quantum yield can be obtained by taking the ratio of fluorescence to absorption cross section. In the present experiment, the fluorescence signals were measured perpendicular to, and along the optic axis for SO_2 and CS_2 gases respectively depending upon the strength of the emission from the photoexcited products. The absorption cross sections in the present experiment were measured absolutely, whereas, the fluorescence cross sections were measured in a relative way. These measurements were made absolute by normalizing our results at certain incident wavelength (228nm) where the fluorescence quantum yield for SO_2 gas is reported to be 100% (Hui and Rice, 1971).

3.1 Photoabsorption Cross Section Measurement

The total photoabsorption cross section, $\sigma_{T\lambda}$, for a given molecule could be measured using the Beer-Lambert law:

$$I_\lambda = I_{0\lambda} \exp(-\sigma_{T\lambda} \, nl) \longrightarrow (3.1)$$

where $I_{0\lambda}$ and I_λ are the fluxes incident on and transmitted through the gas, n is the concentration in particles per cubic centimeter and l is the path length in centimeters. In

the above equation, n is given by

$$n = n_o \times \frac{p}{760} \times \frac{273}{T} \qquad \longrightarrow (3.2)$$

where n_o is the Loschmidt's number, p is the absolute pressure in the absorption chamber measured in Torr and T is temperature of the gas in degrees Kelvin.

When there is no gas in the absorption chamber, the intensities I_{0NG}, I_{NG} measured at the beam splitter and at the end of absorption/fluorescence chamber are supposed to be same. But in actual practice, there is a difference in the two values because of quartz windows intercepting the photon beam, and the two photomultipliers, even though they are of the same type. This gives a calibration for the incident intensity. That is,

$$I_{NG} = D \, I_{0NG} \qquad \longrightarrow (3.3)$$

With gas inside the chamber, the beam splitter intensity (I_{0G}) is multiplied by this calibration factor to get $I_{0\lambda}$ of Eq. (3.1). Therefore, the intensity measured at the other end of absorption/fluorescence chamber, in this case, is given by

$$I_G = D \, I_{0G} \exp(-\sigma_{T\lambda} \, nl)$$

substituting the value for D from Eq. (3.3)

$$I_G = \frac{I_{NG}}{I_{0NG}} I_{0G} \exp(-\sigma_{T\lambda} nl) \qquad\qquad \longrightarrow (3.4)$$

This way, any change in intensity of the incident beam (I_{0G}) during the experiment can be taken care of. Thus, the absorption cross section at a given photon wavelength could be measured by knowing the intensities without and with the target gas molecules in the absorption chamber i.e., I_{0NG}, I_{0G} at the beam splitter and I_{NG}, I_G at the end of absorption chamber, n the number density of species under investigation and l the length of the absorbing column.

3.2 Total Fluorescence Cross Section Measurement

The measurement of fluorescence signals in the case of SO_2 gas were carried out in the direction perpendicular to the optic axis. This could be achieved as SO_2 is known to have larger fluorescence quantum yield. In comparison, the strength of the fluorescence signals was quite less in the case of CS_2. Hence the fluorescence signals of CS_2 were extracted along the optic axis by making appropriate arrangements.

3.2.1 Fluorescence signals measured perpendicular to the optic axis

The total fluorescence intensity measured perpendicular to the optic axis (Fig. 3.1) from the absorption/fluorescence chamber is given by

$$I_{f\lambda} = KF\gamma_{f\lambda} I_{0\lambda} \frac{\exp(-n\sigma_{T\lambda} l)[1-\exp(-n\sigma_{T\lambda}\Delta l)]}{1 + k\tau_r n} \qquad \longrightarrow (3.5)$$
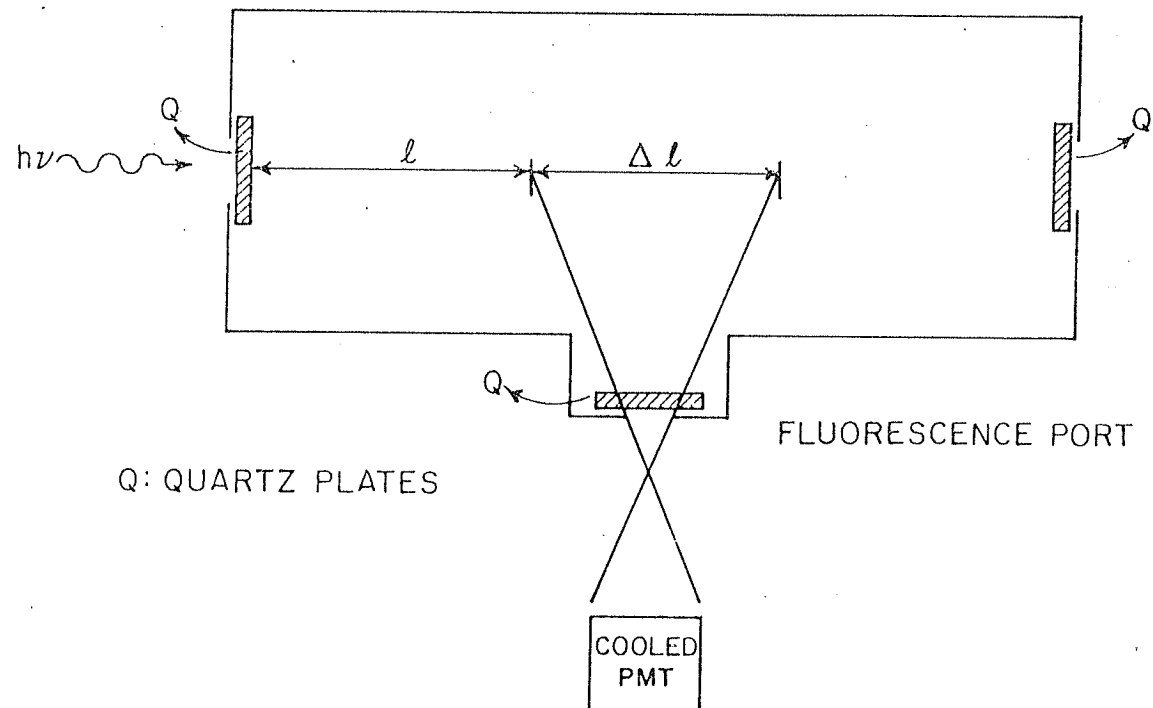
Figure 3.1 Measurement of fluorescence signals perpendicular to optic axis.

where K is the geometrical constant which depends upon the system, F is the photocathode quantum efficiency, $\gamma_{f\lambda}$ is the quantum yield for the production of fluorescence emission, l is the optical path length as shown in Fig. (3.1), Δl is the light path along the optic axis as viewed by the photomultiplier measuring fluorescence, k is the quenching rate constant of the product and τ_r is the radiative lifetime of the emitting state. For SO_2 gas , the approximate values for these parameters are given below

k, quenching rate constant of SO_2^* by SO_2

$$\sim \quad 10^{-12} cm^3/molecule/sec$$

τ_r, radiative lifetime (λ=220.6nm) $\sim$ 35 x 10^{-9} sec

n, number density of SO_2 (at 150 mT) $\sim$ 5 x 10^{15} molecules/cm^3

$\sigma_{T\lambda}$, absorption cross section (λ=228nm) $\sim$ 2.4 x 10^{-18} cm^2

l, optical path length (Fig. 3.1) less than 10 cm

The terms $k\tau_r n$, $n\sigma_{T\lambda} l$ and $n\sigma_{T\lambda} \Delta l$ are much smaller compared to one. Therefore, Eq. (3.5) can be simplified as

$$I_{f\lambda} = KF \; \gamma_{f\lambda} \; I_0 \left\{ [1-n\sigma_{T\lambda} l+H(O) + ---] [1-(1-n\sigma_{T\lambda} \Delta l+H(O) + ---)] \right\}$$

$$\longrightarrow (3.6)$$

(*Note: H(O) stands for higher order terms*)

$$= KF \, \gamma_{f\lambda} \, I_{0\lambda} \left\{ n\sigma_{T\lambda}\Delta l + n^2 \sigma_{T\lambda}^2 \, l \, \Delta l + H(0) + \text{-----} \right\}$$

$$\longrightarrow (3.7)$$

neglecting the higher order terms in Eq.(3.7) ;

and substituting $\gamma_{f\lambda} = \dfrac{\sigma_{f\lambda}}{\sigma_{T\lambda}}$, Eq.(3.7) becomes

$$I_{f\lambda} = KF\sigma_{f\lambda} \, I_{0\lambda} \, n \, \Delta l$$

or

$$\frac{I_{f\lambda}}{I_{0\lambda}} = KF\Delta l \, n \, \sigma_{f\lambda} \qquad\qquad \longrightarrow (3.8)$$

Slope of the graph between $I_{f\lambda}/I_{0\lambda}$ and n (pressure) gives $KF\Delta l \, \sigma_{f\lambda}$. The fluorescence quantum yield of SO_2 at 228 nm, is reported to be 100% by Hui and Rice (1971). Measuring the total absorption cross section at this wavelength the value for fluorescence cross section at 228 nm is obtained ($\sigma_{f\lambda} = \gamma_{f\lambda} \, \sigma_{T\lambda}$). Substituting the value of $\sigma_{f\lambda}$ in Eq.(3.8), the constant $KF\Delta l$ was determined. This way the relative fluorescence cross sections measured in the present experiment were made absolute having obtained the value for the constant $KF\Delta l$.

3.2.2 Fluorescence signals measured along the optic axis

In the case of CS_2, the strength of fluorescence signals was low and thus could not be detected perpendicular to the optic axis. Instead, the detection of weak fluorescence signals along the optic axis was possible, as large number of molecules contribute to fluorescence signals in this configuration. The experimental arrangement to measure fluorescence signals along the optic axis is given in Fig.(3.2). Q_1, Q_2 are quartz plates used for the purpose of vacuum sealing the absorption/fluorescence chamber, F is a colour glass filter (*Wratten-3*) having an appropriate band width to match the emission spectrum of target molecules and at the same time rejecting the incident radiation to be detected at the other end of absorption/fluorescence chamber.

To extract the fluorescence intensity from the target molecules alone is rather difficult in this configuration as the quartz plate seems to fluoresce at UV and VUV (incident) wavelengths. A method developed to calculate fluorescence cross sections, in this case, is given below.

When there is no gas in the fluorescence chamber, the fluorescence intensity from quartz plate Q_2 (Fig. 3.2) detected at the end of absorption/fluorescence chamber is given by

$$I_{f\lambda Q} = CK_1 \gamma_{f\lambda Q} I_{o\lambda} \qquad \longrightarrow (3.9)$$

where $I_{o\lambda}$ is the intensity of photon beam detected by beam splitter photomultiplier, C is a constant which depends upon the reflectance and transmission of the beam splitter and quartz plate (Q1), K_1 is a constant which takes care of geometry of the system and quantum efficiency of the photomultiplier and $\gamma_{f\lambda Q}$ is the fluorescence quantum yield

70
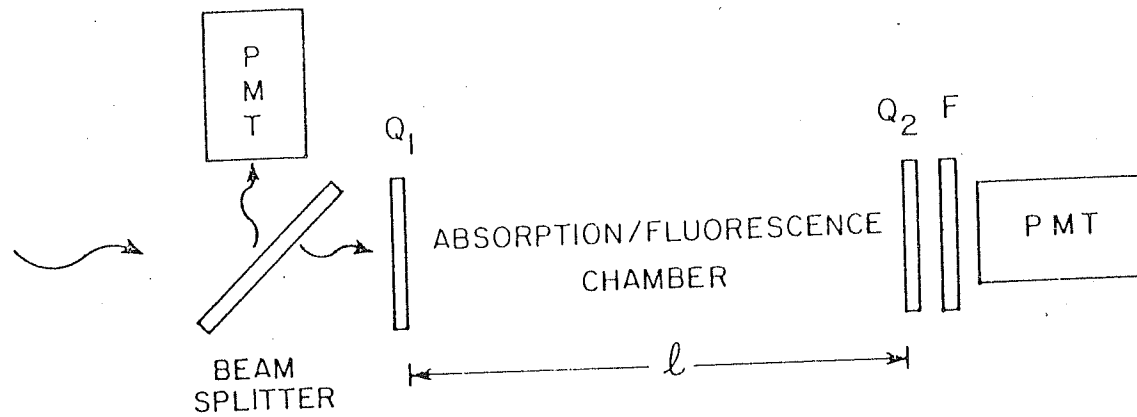
Figure 3.2 Measurement of fluorescence signals along the optic axis.

of the quartz plate (Q2). $I_{o\lambda}$ and $I_{f\lambda Q}$ can be measured from the beam splitter photomultiplier and the other photomultiplier positioned behind the colour glass filter. Therefore, at each wavelength, the value of $CK_1\gamma_{f\lambda Q}$ can be obtained.

With gas inside the chamber, the total fluorescent intensity would have contributions both from quartz plate Q_2 and the target gas molecules. With gas in, the intensity of photon beam incident on the front edge of the quartz plate Q_2 would be $CI_{o\lambda}\exp(-n\sigma_{T\lambda}l)$. Therefore, the fluorescent intensity because of quartz alone would be given by

$$I_{f\lambda Q} = CK_1\gamma_{f\lambda Q}I_{o\lambda}\exp(-n\sigma_{T\lambda}l) \quad\longrightarrow (3.10)$$

The fluorescence intensity because of gas alone would be given by

$$I_{f\lambda G} = KFC\gamma_{f\lambda G}I_{o\lambda}[1-\exp(-n\sigma_{T\lambda}l)] \quad\longrightarrow (3.11)$$

where K is the geometrical constant which depends upon the system, F is the photocathode quantum efficiency, $\gamma_{f\lambda G}$ is the quantum yield for the production of fluorescent emission from target gas molecules alone. The two constants K and K_1 are different as the geometry involved in the production of fluorescence for gas and quartz is different. The total fluorescence intensity at a given wavelength includes the fluorescence intensities because of quartz alone and also from the target gas molecules. This is given by

$$I_{f\lambda T} = CK_1\gamma_{f\lambda Q}I_{o\lambda}\exp(-n\sigma_{T\lambda}l) + KFC\gamma_{f\lambda G}I_{o\lambda}[1-\exp(-n\sigma_{T\lambda}l)]$$

$$\longrightarrow (3.12)$$

Again the value of 100% for the fluorescence quantum yield of SO_2 gas at 228 nm (Hui and Rice, 1971) was utilized for the purpose of normalizing our results. The experiment is repeated with SO_2 gas in this configuration. As already mentioned, the values $n\sigma_{T\lambda}l$, $k\tau_r n$ for SO_2 gas are negligibly small as compared to one. Therefore Eq.(3.12) can be simplified as

$$\frac{I_{f\lambda T}}{I_{0\lambda}} = CK_1\gamma_{f\lambda Q} \left[1 - n\sigma_{T\lambda}l + H(0) + ---\right] +$$

$$KFC\gamma_{f\lambda G} \left[1 - (1 - n\sigma_{T\lambda}l + H(0) + ---)\right]$$

$$= CK_1\gamma_{f\lambda Q} + \left[KFC\gamma_{f\lambda G} - CK_1\gamma_{f\lambda Q}\right] n \, \sigma_{T\lambda}l \longrightarrow (3.13)$$

The product $CK_1\gamma_{f\lambda Q}$ is known from Eq.(3.9). All other quantities like $I_{0\lambda}$, $I_{f\lambda T}$, n (pressure), l are known from the experiment and $\sigma_{T\lambda}$ has been measured in absorption studies. From the slope of the graph between $I_{f\lambda T}/I_{0\lambda}$ and n i.e. pressure, the value for KFC was determined from Eq.(3.13). Hence the absolute fluorescence cross sections for CS_2 could be obtained at a given wavelength using Eq.(3.12).

Thus, knowing the absolute total photoabsorption and fluorescence cross sections in the two geometrical configuration for SO_2 and CS_2 respectively, the fluorescence quantum yields could be obtained as a function of incident photon wavelength.

CHAPTER - 4

ERROR ANALYSIS

The errors in the experiments that measure photoabsorption, fluorescence cross sections and fluorescence quantum yield of molecules can conveniently be classified as follows: multiplicative, such as errors in pressure, temperature and absorption/fluorescence path length; additive, such as errors because of counting statistics and cross section shape errors caused by gas impurities and uncertainty in the incident photon energy. The complete description of these errors is given below in order to determine an estimate of the upper limit of actual error. The most probable estimate of the accuracy of the experiment is also given below for both SO_2 gas and CS_2 in vapour phase.

4.1 Pressure Measurement

The error in the pressure measurement could be attributed mainly to various parameters of the measuring instrument (MKS capacitance manometer), such as the instrumental calibration and drift in null reading etc. Since it is a differential gauge, the reference side has to be evacuated to pressures much better than 10^{-6} Torr. Hence, the order of vacuum of the reference side of the capacitance manometer may also contribute to the most probable estimate of the error, but in a small way.

The pressure of the target gas was measured absolutely

73

by MKS Baratron capacitance manometer (Model:310 BH-10). This manometer was capable of measuring pressure up to 10 Torr absolutely provided the reference side of the head was evacuated to a high degree of vacuum.

In the photoabsorption experiment the SO_2 gas was introduced in the pressure ranging from 200 to 350 mTorr, whereas, the vapour pressure of CS_2 varied from 2 mTorr to 5 Torr. The systematic errors provided by the manufacturer in various pressure ranges are given in Fig.(4.1). Since the capacity of the sensor head for the measurement of pressure is up to 10 Torr, the systematic error present in lower pressure ranges is more compare to that of high pressures (Fig. 4.1). Thus, the systematic errors at the two lowest pressures used in the measurement of cross section for SO_2 and CS_2 are $\pm0.1\%$ and $\pm1\%$, respectively, whereas for both the highest pressures the error is $\pm0.08\%$. As an upper limit to the actual error, the larger errors ±0.1 and $\pm1\%$ were chosen as the errors due to instrument calibration for SO_2 and CS_2 gases respectively and these values were used to estimate the most probable error in photoabsorption cross section measurement.

Similarly in the fluorescence studies the pressure ranges used for SO_2 and CS_2 respectively are 2-300 mTorr and 2-850mTorr. Again a maximum systematic error of $\pm1\%$ corresponding to lowest pressures used, was considered in the measurement of fluorescence cross sections for both the gases.

Zero adjustment in the MKS capacitance manometer was possible with the help of balancing valve as described in Section (2.6.2) $\left\{ \text{Fig.}(2.12) \right\}$. The null reading of the MKS Baratron capacitance manometer was noted before and after the experimental scan and no drift in the null reading was observed during this period. Therefore, error due to the drift in null reading of the manometer could be ignored.
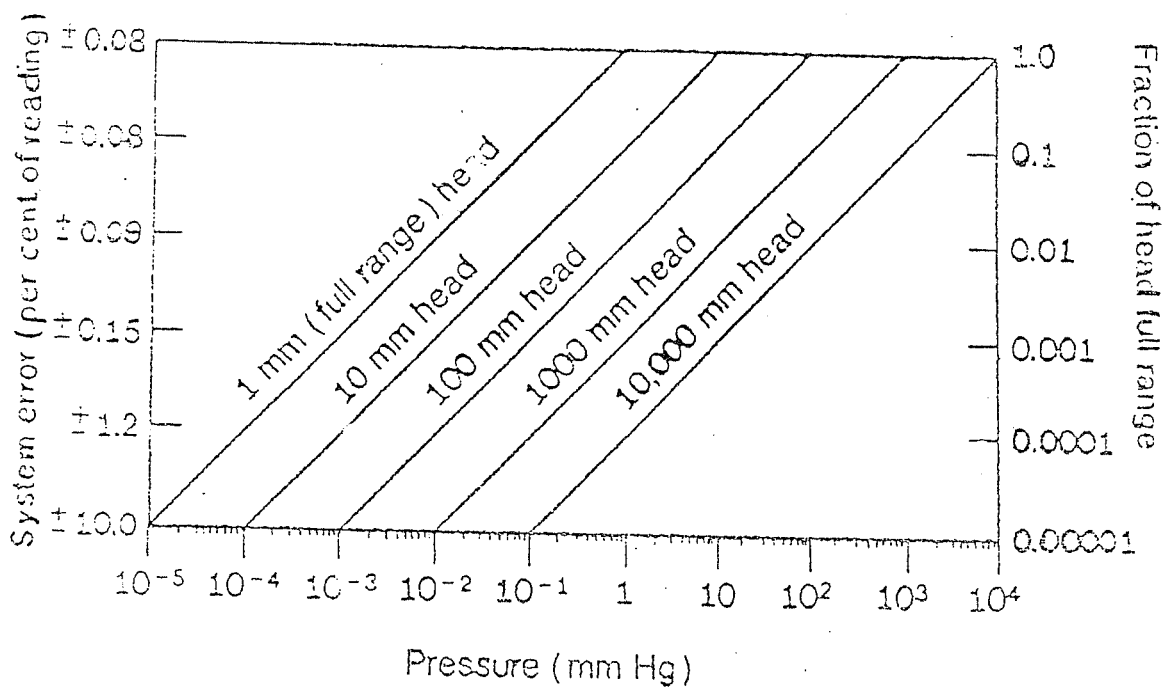
Figure 4.1 Systematical errors of MKS Baratron's absolute pressure measurements. (for different gauge heads).

The reference side of the MKS capacitance manometer was continuously evacuated to a pressure better than 10^{-6} Torr. Since the pressure measured using this gauge was always greater than 10^{-3} Torr, which was at least three orders of magnitude larger, the errors introduced because of reference side pressure were negligible.

4.2 Thermal Transpiration Effect

The material used for the sensor of the MKS Baratron capacitance manometer, is very sensitive to the thermal fluctuations. Therefore, it is operated at an elevated temperature (at 318K), while the temperature in the absorption/fluorescence chamber was around 300K. Thus we might expect the pressure in the absorption/fluorescence chamber to be slightly less than the pressure shown by the MKS unit head due to thermal transpiration effects. The thermal transpiration effects in the present work have been worked out on the lines suggested by Edmonds and Hobson (1965):

$$ P_{ch} = a \sqrt{\frac{T_{ch}}{T_m}} \ P_m \qquad\qquad \longrightarrow (4.1) $$

where P_{ch}, T_{ch} are the pressure and temperature in the absorption/fluorescence chamber, p_m is the pressure indicated by the MKS sensor, T_m is the temperature of the sensor head, and 'a' is a constant which depends on the geometry over which the temperature gradients occur. For an ideal aperture, $a \simeq 1$, but in practice, it may have a value slightly greater than unity. From Eq.(4.1), it is found that the pressure in the absorption/fluorescence chamber has to be raised by 2.9%.

This pressure correction has been incorporated in the present measurements and absorption and fluorescence cross sections have been calculated accordingly. The other error which occurred was due to inaccuracy in the measurement of temperature. This could be as high as ± 1 ^{0}C, which would introduce a maximum error of $\pm 0.4\%$.

4.3 Uncertainty in Optical Path Lengths

The absorption path length in the present experiment is the length between the quartz plates Q_1 and Q_2 inside the absorption chamber as shown in Fig.(2.11). This was measured as 24.8 $\pm$ 0.1cm, giving an error of $\pm 0.4\%$. In case of fluorescence experiment (for SO_2), Δl as defined in eqns.(3.5) and (3.8) has not been measured. Instead, the fluorescence cross sections have been normalized with some other experiment reported in literature at a certain incident photon wavelength. The maximum error in Δl has been estimated to be about $\pm 2\%$. One point to be noted here is that the the parameter Δl is used only in the case of fluorescence cross section measurement of SO_2, while the optical path length 'l' is used for absorption cross section measurements of both the gases, along with the fluorescence cross section measurement of CS_2.

4.4 Counting Statistics

Photon counting being a statistical process, follows Poissonian distribution. The uncertainty in 'n' number of counts is given by $\pm \sqrt{n}$. To reduce this uncertainty it is advisable to have a large number of counts. Therefore, care was taken to give a large integration time for the collection of photons. But, the strength of the fluorescence signals was so low that, even an integration time of 20 seconds per channel was not sufficient to obtain an appreciable number of

counts. The signals measured at the end of absorption chamber in the case of photoabsorption studies were also quite weak in certain spectral regions (λ_i < 200 nm). Therefore a major contribution to the total estimate of error for photoabsorption and fluorescence cross sections, was due to the counting statistics.

The counting statistics in case of absorption studies for SO_2 has introduced an error varying from ± 0.4 to $\pm 3\%$ depending upon the spectral region where the cross sections were measured, whereas for CS_2 vapour it varied from ± 0.2 to $\pm 4\%$. The larger errors of ± 3 and $\pm 4\%$ have been considered for SO_2 and CS_2 respectively for calculating the most probable estimate of accuracy. Similarly the counting statistics errors in the fluorescence studies were observed to be in the range ± 0.2 to $\pm 4.0\%$ and ± 0.1 to $\pm 5.0\%$ for SO_2 and CS_2 respectively depending upon the spectral region where cross sections are measured. Again, the larger errors of ± 4 and $\pm 5\%$ have been considered for SO_2 and CS_2 respectively.

4.5 Gas Impurity

The research grade SO_2 gas was procured from L'Air Liquide, France and was 99.95% pure. Carbon disulphide vapour was obtained from an analytical-grade liquid. The vapour (CS_2) was purified by fractional distillation before being introduced into the absorption/fluorescence chamber. Care was taken to maintain the purity of these gases. The gas handling system was completely made of metal, and was evacuated before the experiment. Therefore, the error due to the sample gas impurity was negligible.

4.6 Conclusion

The coherent sum of the errors discussed in this

chapter, acted as an estimate of the upper limit of the actual error. In the present experiment, it has been found to be ± 3.9, $\pm 5.8\%$ for absorption cross section measurement, and ± 7.4, $\pm 6.8\%$ for fluorescence cross section measurement for SO_2 and CS_2 respectively. The incoherent sum was obtained by adding the squares of all the errors and taking the square root of the total sum. The incoherent sum represented the most probable estimate of the accuracy of the experiment. In the present experiment, the most probable error was estimated to be ± 3.1, $\pm 4.2\%$ for absorption cross section measurements and ± 4.6, $\pm 5.1\%$ for fluorescence cross section measurements for the gases SO_2 and CS_2 respectively. The most probable error for fluorescence quantum yield turned out to be ± 5.5 and $\pm 6.6\%$ for SO_2 and CS_2 gases.

The error budget for the measurement of photoabsorption and fluorescence cross sections for SO_2 and CS_2 has been summarized in Table (4.1).

Table 4.1 Error budget in the measurement of photoabsorption and fluorescence cross sections for SO_2 and CS_2 at room temperature.

	Error in $\sigma_{T\lambda}$ measurement (%)		Error in $\sigma_{f\lambda}$ measurement (%)	
	SO_2	CS_2	SO_2	CS_2
Pressure	± 0.1	± 1.0	± 1.0	± 1.0
Temperature	± 0.4	± 0.4	± 0.4	± 0.4
Optical path length , l	± 0.4	± 0.4	$-$	± 0.4
'' Δl	$-$	$-$	± 2.0	$-$
Counting Statistics in Intensity	± 3.0	± 4.0	± 4.0	± 5.0
Coherent Sum	± 3.9	± 5.8	± 7.4	± 6.8
Incoherent Sum or total r.m.s. error	± 3.1	± 4.2	± 4.6	± 5.1

CHAPTER - 5

RESULTS AND DISCUSSIONS

The photoabsorption and fluorescence cross section measurements have been carried out in the two spectral regions: 188.5-231, 278.7-320 nm for SO_2 and 188.2-213, 287.5-339.5 nm for CS_2 respectively. As mentioned earlier, the fluorescence quantum yield of a molecule can be determined experimentally by measuring the photoabsorption and fluorescence cross section at an incident wavelength and taking the ratio of fluorescence to photoabsorption cross section. Both the gases, show prominant structures in the spectral regions mentioned above. The results obtained for both the gases are taken up separately for a detailed discussion.

5.1 Sulphur Dioxide

The ground state of SO_2 is $\tilde{X}$ $^1A_1$ with an O-S-O angle of 119.5°. The bond energy D_o(OS-O) is 5.65 ± 0.01 eV (Okabe, 1971). There are three main regions of absorption in the ultraviolet, namely, an extremely weak absorption in the 340 to 390 nm, a weak absorption in the 260 to 340 nm, and a strong absorption in the 180 to 235 nm region. The dissociation of SO_2 to SO + O starts below 219 nm. Above this wavelength, SO_2 exibits strong fluorescence.

5.1.1 SO_2 : Spectral region 188-231 nm

The photoabsorption cross sections as measured in the

present experiment are shown in Figs.(5.2) and (5.3). These cross sections have been measured at various SO_2 pressures ranging from 200 to 350 mTorr and the average cross sections are shown in Figs.(5.2) and (5.3). The photoabsorption, fluorescence cross section and the fluorescence quantum yield values along with the peak assignments in the spectral range 188.7-231.4 are given in Table (5.1). It was found that at a typical incident photon wavelength of 207.5 nm, the maximum pressure used in the experiment was well within the values of pressures where Beer-Lambert law was valid. The $\ln(I_{o\lambda}/I_\lambda)$ dependnce on pressure of the SO_2 gas has been shown in Fig.(5.1) at 207.5 nm.

Sulphur dioxide has a system of strong absorption bands beginning near 235 nm. Because the transition involves a large Franck-Condon shift, the 0-0 band is relatively weak and at ordinary temperatures does not stand out from the background. This appears to be the reason for the confused state of affairs surrounding the electronic assignment. Duchesne and Rosen (1947) grouped the bands into two systems, α_1 and α_2, considered to belong to two different electronic transitions. The possible assignment of these systems has been reported by Herzberg (1966). A contrary view, that the α_1 and α_2 bands form part of a single system of vibronic bands was developed by Coon et al (1967) and founded on the identification of the origin with the band at 234.8 nm. This system was identified with the transition $\tilde{C}\ ^1B_2 \leftarrow \tilde{X}\ ^1A_1$ following the ab initio calculations of Hillier and Saunders (1971). This was further confirmed by Brand and Srikameswaran (1972) and Brand et al (1976) after carrying out rotational analysis of a few bands of the 235.0 nm system.

Even though, there is very little question about the assignment of electronic transition of the *235.0 nm system*, the assignment of the different bands is not very easy. In the present experiment the same nomenclature has been followed for different bands as done by Okabe (1971). The
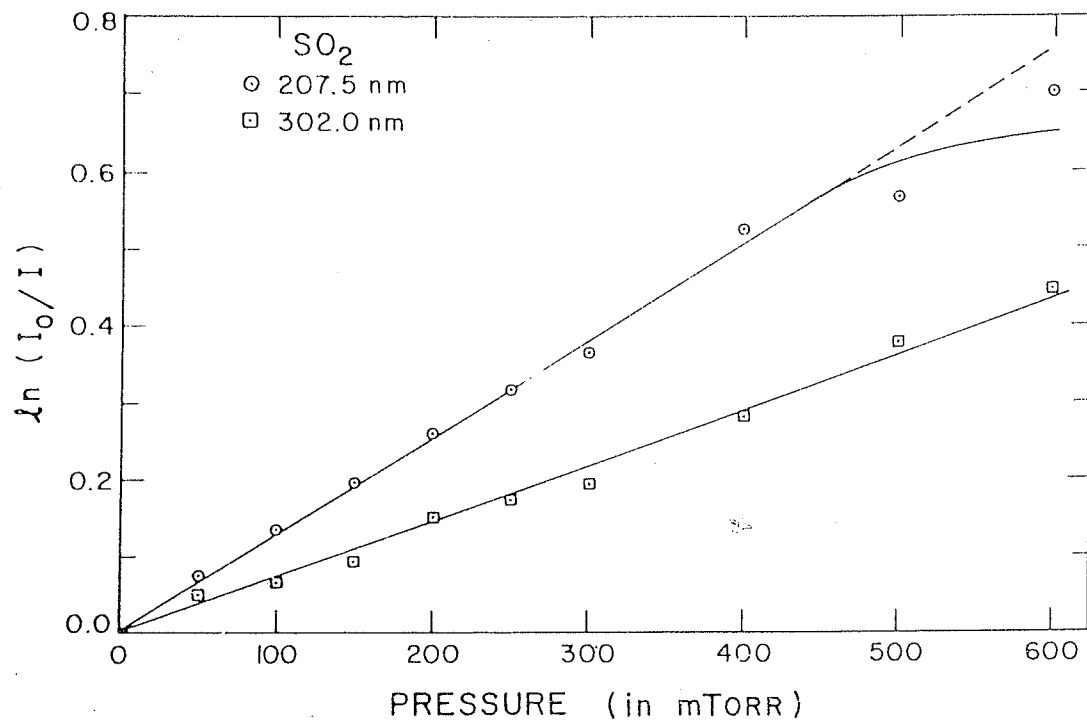
Figure 5.1 The $\ln(I_{0\lambda}/I_\lambda)$ dependence on SO_2 gas pressure at 207.5 and 302 nm.
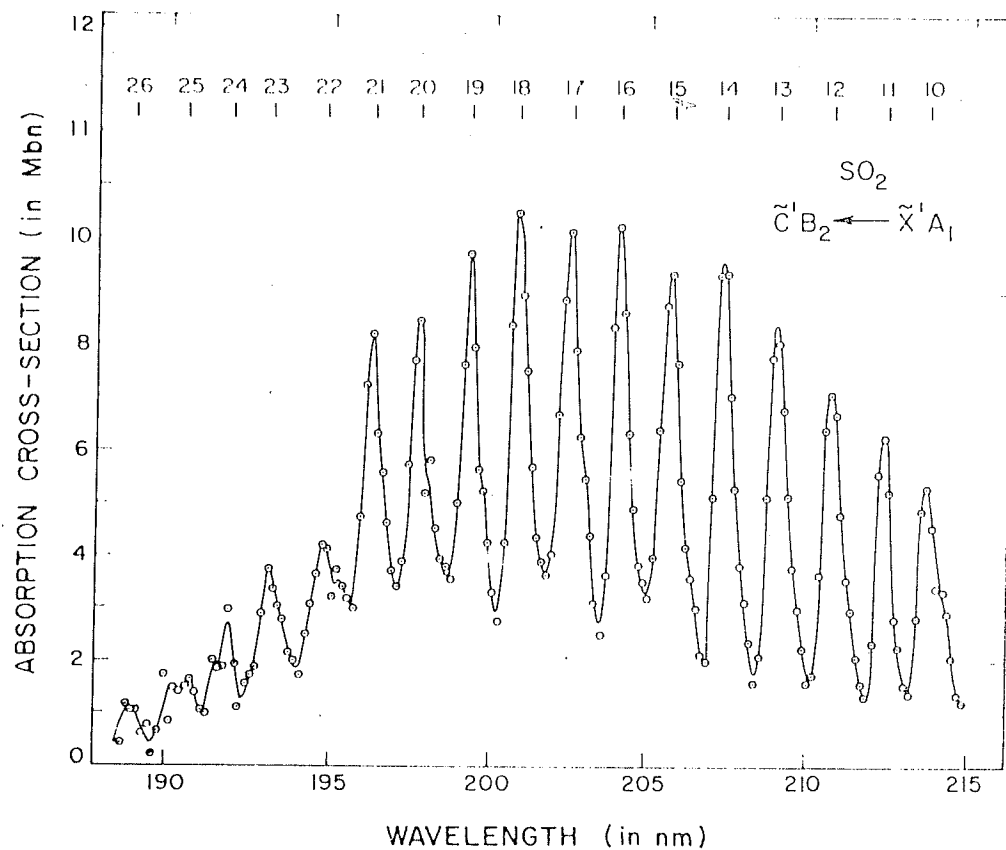
Figure 5.2 Photoabsorption cross sections for SO_2 in the spectral region 188.5-215 nm.
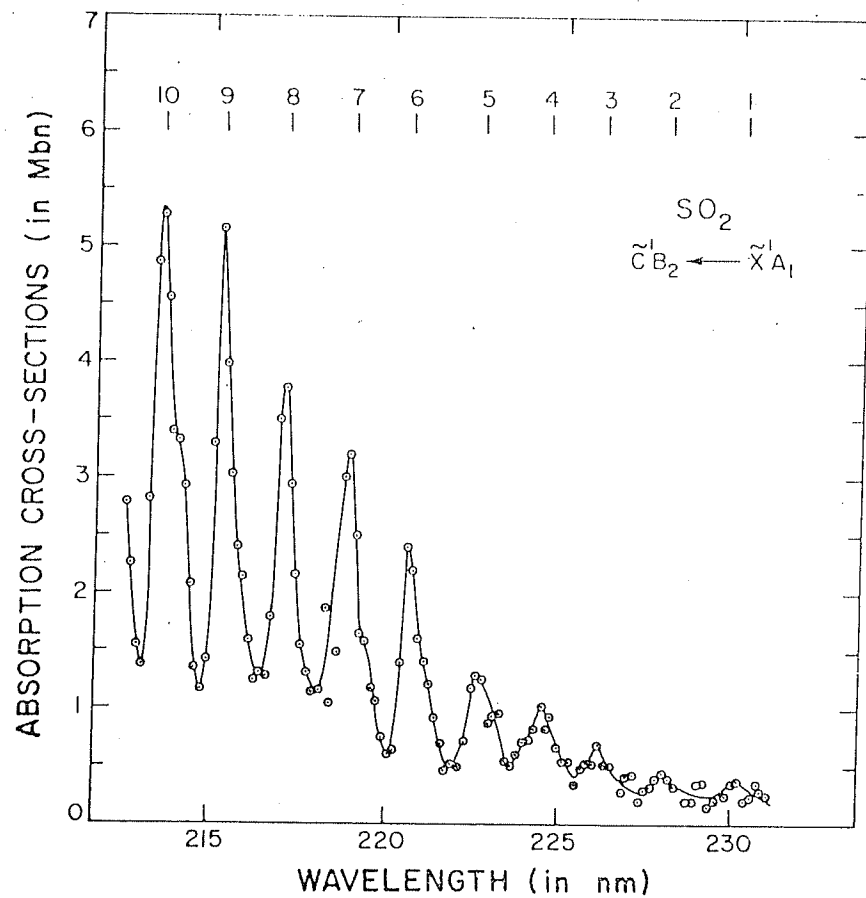
Figure 5.3 Photoabsorption cross sections for SO_2 in the spectral region 212.5-231 nm.

Table 5.1 Potoabsorption, fluorescence cross sections, and fluorescence quantum yields in 188.75-231.4 nm

PEAK ASSI. IF ANY No.	WAVE LENGTH IN nm	ABS. CROSS SEC. $\times 10^{-18}$ cm^2	FLR. CROSS SEC. $\times 10^{-20}$ cm^2	FLR. QUANT. YIELD %
26	188.75	1.17	–	–
	189.25	0.45	–	–
25	190.45	1.45	–	–
	191.12	1.02	–	–
	191.62	1.92	–	–
24	191.95	2.70	–	–
	192.37	1.25	–	–
23	193.00	3.76	–	–
	193.92	1.83	–	–
22	194.80	4.30	–	–
	195.30	3.55	–	–
	195.63	3.10	–	–
21	196.20	8.20	–	–
	197.03	3.45	–	–
20	197.70	8.44	–	–
	198.62	3.65	–	–
19	199.30	9.52	–	–
	200.22	2.95	–	–
18	200.80	10.47	1.31	0.1
	201.80	3.75	1.44	0.4
17	202.40	10.12	2.57	0.3
	203.40	2.50	2.65	1.1
16	204.00	10.22	2.22	0.2
	205.00	3.20	3.16	1.0
15	205.80	9.33	2.39	0.3
	206.90	1.97	2.91	1.5
14	207.30	9.55	2.19	0.2
	208.30	1.60	4.72	3.0
13	209.00	8.35	1.75	0.2
	210.08	1.58	5.45	3.4
12	210.70	7.07	1.15	0.2
	211.87	1.35	6.34	4.7
11	212.30	6.25	3.01	0.5
	213.13	1.38	4.19	3.0
10	213.50	5.27	5.45	1.0
	214.67	1.15	3.99	3.3
9	215.30	5.15	11.94	2.3
	216.47	1.32	11.35	8.6
8	217.00	3.78	17.53	4.6
	218.17	1.15	12.69	11.0
7	218.90	3.22	25.78	8.0
	220.07	0.60	12.95	21.6
6	220.57	2.39	58.68	24.6
	220.74	2.21	97.09	43.9
	220.90	1.62	75.78	46.8
	221.07	1.42	57.87	40.8
	221.24	1.22	49.31	40.4
	221.40	0.93	32.28	34.7

Table 5.1 continued..

PEAK ASSI. IF ANY No.	WAVE LENGTH IN nm	ABS. CROSS SEC. $\times 10^{-18}$ cm^2	FLR. CROSS SEC. $\times 10^{-20}$ cm^2	FLR. QUANT. YIELD %
	221.57	0.70	20.32	29.0
	221.74	0.47	9.89	21.0
	221.90	0.52	7.21	13.9
	222.07	0.50	9.39	18.8
	222.24	0.72	19.48	27.0
	222.40	1.17	51.41	43.9
5	222.57	1.30	79.85	61.9
	222.74	1.24	65.20	52.6
	222.90	0.86	58.55	68.1
	223.07	0.94	56.31	59.9
	223.24	0.96	46.30	48.2
	223.40	0.55	30.17	54.9
	223.57	0.51	17.31	33.9
	223.74	0.60	11.98	20.0
	223.90	0.71	17.72	25.0
	224.07	0.73	30.90	42.3
	224.24	0.83	38.78	46.7
4	224.40	1.02	54.25	53.2
	224.57	0.83	52.10	62.8
	224.74	0.94	45.87	48.8
	224.90	0.68	43.18	63.5
	225.07	0.55	36.71	66.7
	225.24	0.55	26.31	47.8
	225.40	0.36	18.22	50.6
	225.57	0.48	13.12	27.3
	225.74	0.53	15.60	29.4
	225.90	0.53	35.78	67.5
	226.07	0.69	46.32	67.1
3	226.16	0.60	49.23	82.1
	226.24	0.52	44.60	85.8
	226.40	0.51	42.08	82.5
	226.57	0.38	31.58	83.1
	226.74	0.28	22.45	80.2
	226.90	0.42	15.05	35.8
	227.07	0.43	14.58	33.9
	227.24	0.21	11.64	55.4
	227.40	0.29	11.12	38.3
	227.57	0.32	11.29	35.3
	227.74	0.39	18.52	47.5
	227.90	0.45	42.60	94.7
2	227.99	0.45	45.00	100.0
	228.24	0.32	30.14	99.2
	228.40	0.30	23.25	77.5
	228.57	0.20	19.11	91.0
	228.74	0.21	13.51	64.3
	228.90	0.36	12.22	33.9
	229.07	0.37	13.54	36.6
	229.24	0.16	10.81	67.6

Table 5.1   continued..

PEAK ASSI. IF ANY No.	WAVE LENGTH IN nm	ABS. CROSS SEC. $\times 10^{-18}$ cm^2	FLR. CROSS SEC. $\times 10^{-20}$ cm^2	FLR. QUANT. YIELD %
	229.40	0.20	7.19	36.0
	229.57	0.27	4.20	15.6
	229.74	0.25	9.04	36.2
	229.90	0.36	23.16	64.3
	230.07	0.38	27.40	72.1
1	230.24	0.21	19.93	94.9
	230.40	0.25	15.63	62.5
	230.57	0.36	12.33	34.3
	230.74	0.30	11.75	39.2
	230.90	0.26	9.73	37.4
	231.07	0.17	11.47	67.5
	231.24	0.21	9.96	47.4
	231.40	0.13	7.15	55.0

peaks in Figs.(5.2) and (5.3) have been numbered from 1 to 26 from 230.2 nm to lower wavelengths. It may be noted that the band 1 is by no means the origin of this band system.

The photoabsorption cross sections measured absolutely are shown in Figs.(5.2) and (5.3) for the spectral regions 188.5 to 215 nm and 212.5 to 231 nm respectively. The absorption cross sections vary from 1.17 Mbn to 4.30 Mbn from band 26 to band 22 (Fig. 5.2) followed by a sharp increase upto band 18. The cross sections from band 21 to 18 vary from 8.20 to 10.47 Mbn. The photoabsorption cross sections subsequently decrease slowly upto band 1 (Fig.5.3), where the cross section is as low as 0.38 Mbn. A comparison of photoabsorption cross section obtained in the present experiment at the peak of band 12 has been made in Table (5.2) with the values obtained by other researchers. Different experimental parameters used by the groups like instrumental bandwidth, type of light source, pressure range and temperature have been mentioned in the table. The cross section value reported by Freeman et al (1984) has been measured at much higher instrumental resolution of 0.002 nm and also at a lower temperature of 213 K. That is why their absorption cross section of 24.0 Mbn at the peak of band 12 is much higher and therefore a comparison is not really advisable. The cross sections measured by Wu and Judge (1981), Thompson et al (1963), Golomb et al (1962) and Warneck et al (1964) at 210.7 nm vary from ≈ 7 to 9 Mbn with instrumental resolution varying from 0.06 to 0.1 nm respectively. The cross section value measured in the present work is almost similar to that measured by Wu and Judge (1981) but is smaller by 6% when compared to the cross section reported by Thompson et al (1963): about 27% when compared with the values given by both Golomb et al (1962) and Warneck et al (1964). The present measurements discussed above have been carried out at the instrumental bandwidth of about 0.2 nm. As this spectral region has a band structure, the absorption cross sections at the peak of band 12 would

Table 5.2 Absorption cross section of SO_2 for band 12 (around 210.7 nm) of the $\tilde{C} - \tilde{X}$ transition as measured by various researchers.

Resolution (nm)	Light Source	Pressure (Torr)	Cell Length (cm)	Temperature (K)	$\sigma_{T\lambda}$ (Mbn)	Reference
0.2	Argon miniarc	0.20-0.35	24.8	$\simeq 300$	7.07	Present work (1990)
0.002	H_2 Discharge	0.03-40	27.0	213	24.0	Freeman et al (1984)
0.06	Synchrotron	0.01-40	11.51	294	$\simeq 7.0$	Wu and Judge (1981)
0.1	H_2 Discharge and Hg lines	2-10	12.4	$\simeq 300$	$\simeq 9.0$	Warneck et al (1964)
Not known	Not known	0.26-5	10.0	$\simeq 300$	$\simeq 7.5$	Thompson et al (1963)
0.1	H_2 Discharge	0.03-1	4.7	$\simeq 300$	$\simeq 9.0$	Golomb et al (1962)

strongly depend upon the instrumental resolution. In the present case, the instrumental resolution is poorer as compared to that reported by other groups and therefore, their cross sections should be larger than the values reported by them. It appears that in some experiments mentioned above, the transmitted intensity measured has a contribution due to the fluorescence emission from SO_2 emitted along the optic axis.

Fluorescence cross section measurement:

The fluorescence cross sections measured in the present experiment are shown in Fig.(5.4) from 200 to 232 nm. Only relative cross sections could be measured in our system. These cross sections were made absolute by normalising the results at the peak of band 2 (228 nm) where the fluorescence quantum efficiency of 100% has been reported by Hui and Rice (1972). Using this value of $\gamma_{f\lambda}$ along with the absorption cross section measured in the present experiment at this particular wavelength, the value of $\sigma_{f\lambda}$ is obtained. Measuring $I_{f\lambda}/I_{o\lambda}$ at various pressures of SO_2, one could obtain the constant $KF\Delta l$ as discussed in Sec.(3.2). Knowing this constant, the fluorescence cross sections were made absolute (Table 5.1).

The fluorescence signals below 200 nm could not be observed as these were almost merged in the dark current of the cooled photomultiplier. At wavelengths ranging from 200 to 210 nm, the fluorescence cross sections were less than 5×10^{-20} cm^2 but at longer wavelengths corresponding to peaks of bands 12 to 7, the cross sections varied from 6×10^{-20} to 2.5×10^{-19} cm^2 approximately. A large increase in fluorescence cross section at the peak of band 6 was observed but the cross sections decreased subsequently from 9.7×10^{-19} to 2.75×10^{-19} cm^2 for bands 6 to 1 respectively. It is interesting to note that the peak
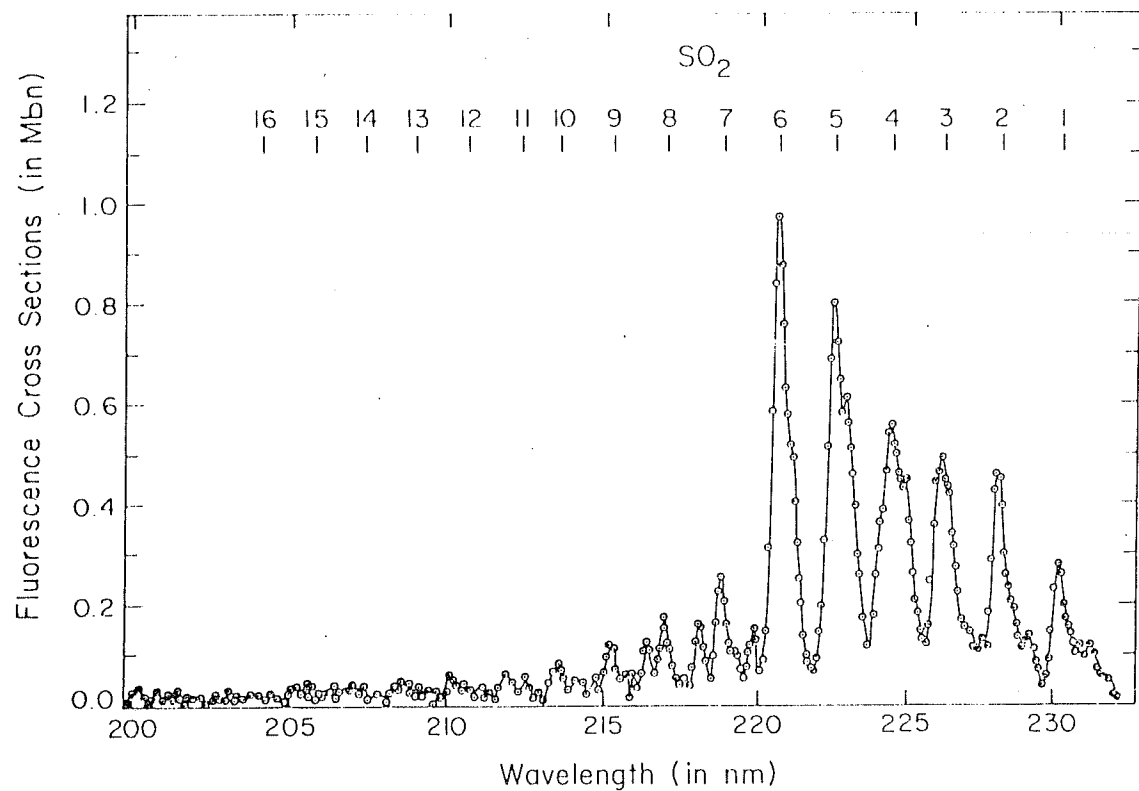
Figure 5.4 Fluorescence cross sections for SO_2 in the spectral region 200-232 nm.

intensity in the fluorescence spectrum increases from band 1 to 6 (Fig. 5.4) and then it suddenly falls, whereas absorption still continues to increase further after band 6 upto band 18 (Figs. 5.2 and 5.3). This indicates the occurrence of another process called predissociation. The threshold energy of incident photons responsible for this process as observed in the present experiment lies in the range between 218.9 and 220.6 nm. These values are almost similar to those obtained by Okabe (1971). It is not possible to compare the fluorescence cross sections obtained in the present experiment as, to the best of our knowledge, there are practically no other measurements available in the literature.

The fluorescence quantum yields as calculated from $\sigma_{T\lambda}$ and $\sigma_{f\lambda}$ values given in Table (5.1) are shown in Fig. (5.5) at photon wavelengths varying from 200 to 232 nm, and also listed in Table (5.1)

5.1.2 SO_2 Spectral region 278.7-320 nm

The photoabsorption cross sections as measured in the present experiment are shown in Figs. (5.6) and (5.7) in the spectral region from 278.7 to 320 nm. These cross sections have been measured at various SO_2 pressures ranging from 200 to 350 mTorr and the average cross sections have been obtained. It was found that at a typical incident photon wavelength of 302 nm, the maximum pressure used in the experiment was well within the values of pressures where the Beer-Lambert law was valid. The $\ln(I_{o\lambda}/I_\lambda)$ depedence on pressure of SO_2 has been shown in Fig. (5.1) for 302 nm wavelength.

The spectral region chosen for absorption measurements in the present experiment is part of the main absorption
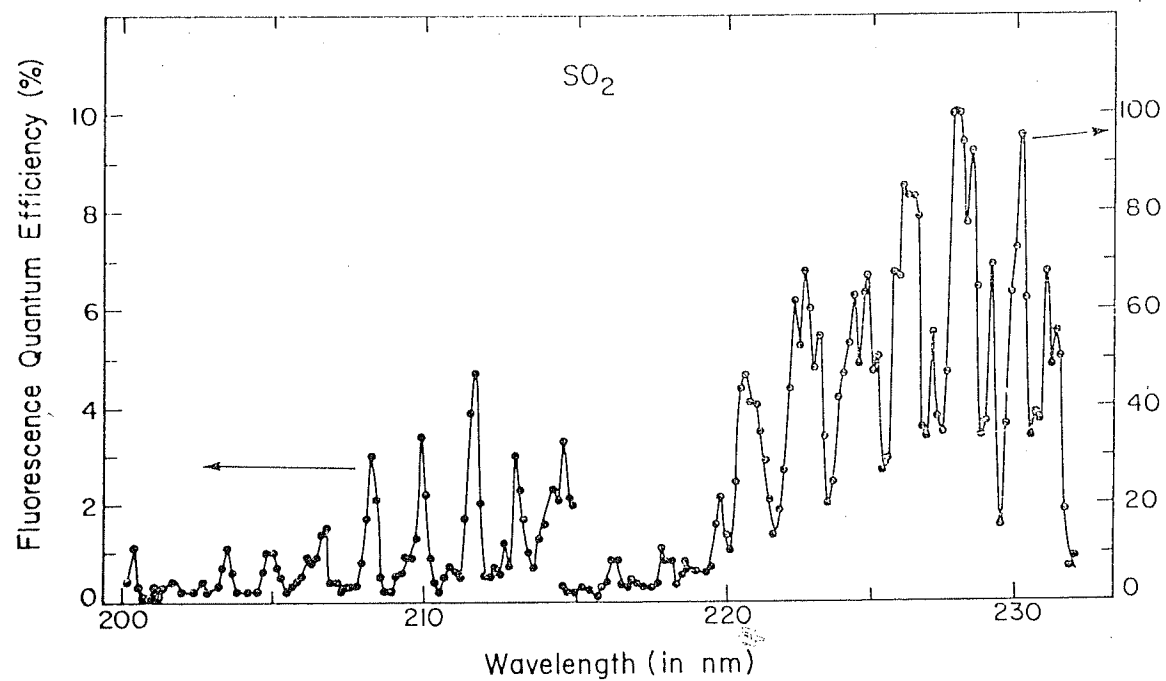
Figure 5.5 Fluorescence quantum yield for SO_2 in the spectral region 200-232 nm.
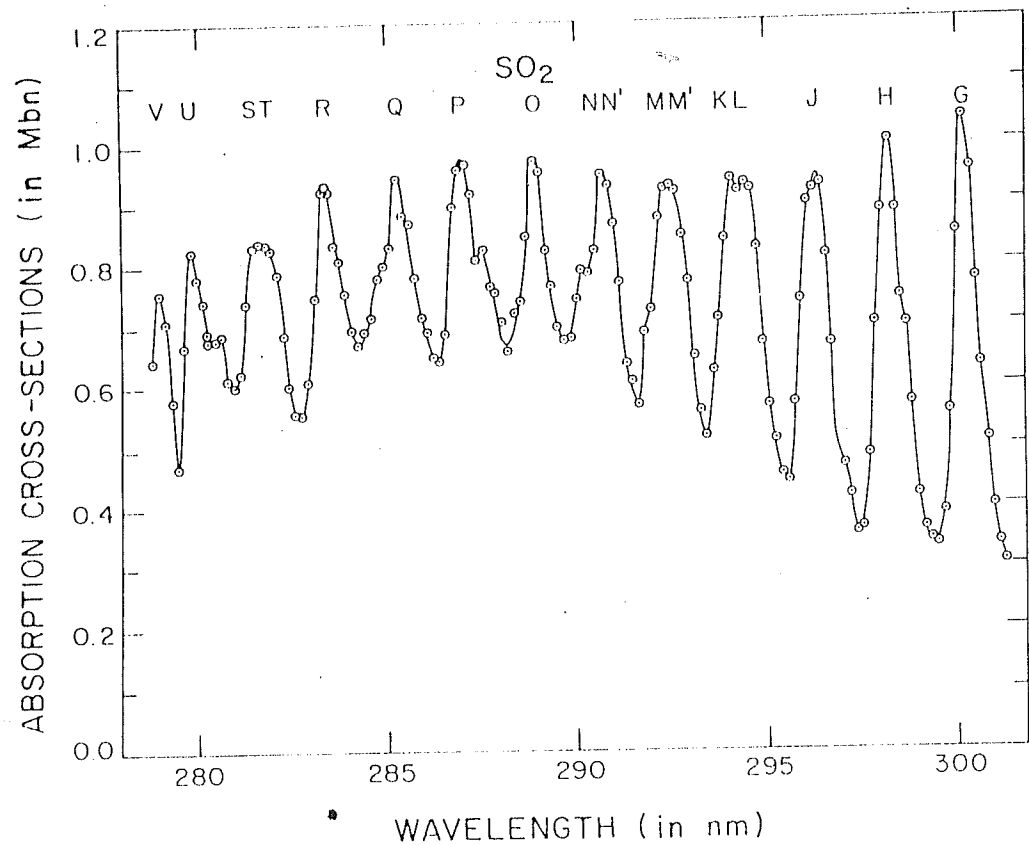
Figure   5.6   Photoabsorption   cross   sections   for SO_2 in   the spectral region 278.7-301.3 nm.
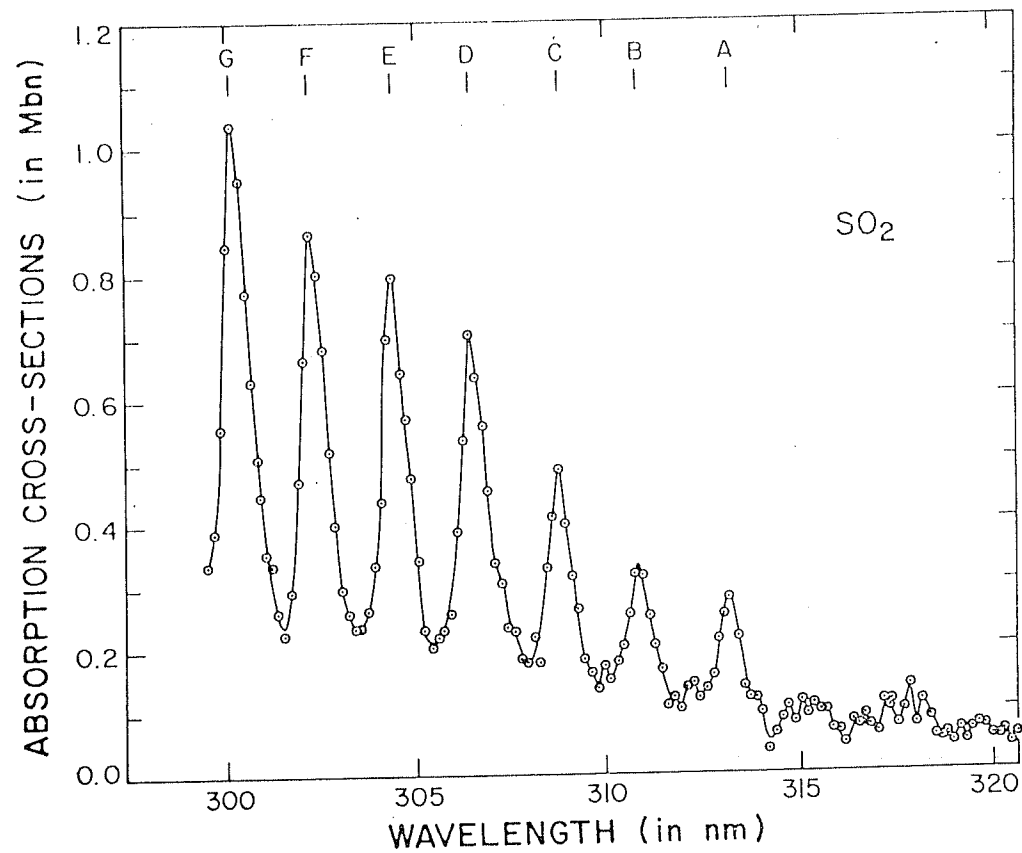
Figure 5.7 Photoabsorption cross sections for SO_2 in the spectral region 299.5-320 nm.

system of SO_2 which extends from 340 to 250 nm. It consists of discrete bands superimposed on an apparent continuum. Hamada and Merer (1975) established by rotational analysis that the discrete absorption is due to transitions $\tilde{A}\ ^1A_2 \leftarrow \tilde{X}\ ^1A_1$. The continuous absorption underlying the structured bands is attributed to the $\tilde{B}\ ^1B_1 \leftarrow \tilde{X}\ ^1A_1$ transition predicted by theory in this wavelength region (Hillier and Saunders, 1971). The most prominent bands in this region form a series extending to shorter wavelengths from 313 nm, labelled A, B, C,....by Clements (1935) who wrongly assigned the 'A' band (313 nm) as the electronic origin. The same labelling has been accepted by other researchers also. In the present experiment, the absorption peaks (Figs. 5.6 and 5.7) have also been assigned after Clements as A, B, C,.....U, V from about 313 nm to lower wavelengths. The photoabsorption, fluorescence cross section, and fluorescence quantum yield values in the spectral range 278.6-320.0 nm are given in Table (5.3). As discussed above, the band A is by no means the origin of this band system.

The absorption cross sections for SO_2 measured in the present experiment vary from 0.75 to about 0.94 Mbn at wavelengths corresponding to bands V to KL with a maximum of about 0.97 Mbn at band O. An increase in cross section has been observed between bands J and G but a sharp decrease in cross section values has been noticed subsequently from bands G to A (Figs. 5.6 and 5.7). Absorption cross section of 10.36×10^{-19} cm^2 has been measured at band G where as the cross section at band A is 2.79×10^{-19} cm^2. A few weak bands have also been observed at photon wavelengths between 314 and 320.6 nm. Some quantitative absorption data have been reported by few researchers like Thompson et al (1963), Wu (1981), Brassington (1981) and McGee and Burris (1987). A comparison of cross section values reported by Wu (1981), Brassington (1981) and McGee and Burris (1987) has been made in Table (5.4) with those meassured in the present work at peaks of some of the bands only. The data from Wu is

Table 5.3 Photoabsorption, fluorescence cross sections, and fluorescence quantum yields for SO_2 in 278.6-320 nm region

WAVE LENGTH	ABS. CROSS SEC.	FLR. CROSS SEC.	FLR. QUANT. YIELD	WAVE LENGTH	ABS. CROSS SEC.	FLR. CROSS SEC.	FLR. QUANT. YIELD
	$\times 10^{-19}$	$\times 10^{-20}$			$\times 10^{-19}$	$\times 10^{-20}$	
IN nm	cm^2	cm^2	%	IN nm	cm^2	cm^2	%
278.67	6.44	7.51	11.7	286.50	6.85	4.90	7.2
278.83	7.55	8.05	10.7	286.67	8.95	6.40	7.2
279.00	7.07	7.75	11.0	286.83	9.56	5.95	6.2
279.17	5.74	7.20	12.4	287.00	9.64	5.50	5.7
279.33	4.71	8.35	17.7	287.17	9.16	5.20	5.7
279.50	6.67	9.55	14.3	287.33	8.06	5.05	6.3
279.67	8.25	9.90	12.0	287.50	8.22	4.93	6.0
279.83	7.81	8.50	10.9	287.67	7.62	4.55	6.0
280.00	7.41	7.50	10.1	287.83	7.52	4.10	5.5
280.17	6.91	7.15	10.3	288.00	7.14	3.10	4.3
280.33	6.75	6.05	9.0	288.17	6.54	2.90	4.4
280.50	6.82	5.55	8.1	288.33	7.18	3.40	4.7
280.67	6.11	5.60	9.2	288.50	7.37	4.20	5.7
280.83	6.01	6.00	10.0	288.67	8.45	5.25	6.2
281.00	6.22	6.40	10.3	288.83	9.67	5.70	5.9
281.17	7.40	6.70	9.1	289.00	9.50	5.60	5.9
281.33	8.32	6.75	8.1	289.17	8.23	4.50	5.5
281.50	8.36	7.20	8.6	289.33	7.63	3.85	5.0
281.67	8.35	8.45	10.1	289.50	6.94	3.90	5.6
281.83	8.26	8.25	10.0	289.67	6.72	4.05	6.0
282.00	7.84	5.70	7.3	289.83	6.75	4.20	6.2
282.17	6.85	5.25	7.7	290.00	7.39	4.20	5.7
282.33	6.00	5.00	8.3	290.17	7.88	4.10	5.2
282.50	5.57	5.00	9.0	290.33	7.84	3.97	5.1
282.67	5.51	5.40	9.8	290.50	8.21	4.05	4.9
282.83	6.07	5.75	9.5	290.67	9.45	4.85	5.1
283.00	7.46	5.95	8.0	290.83	9.28	6.20	6.7
283.17	9.21	5.95	6.5	291.00	8.64	5.05	5.8
283.33	9.19	5.40	5.9	291.17	7.69	3.15	4.1
283.50	8.33	4.80	5.8	291.33	6.33	1.95	3.1
283.67	8.06	4.63	5.7	291.50	6.07	2.05	3.4
283.83	7.54	4.90	6.5	291.67	5.68	2.65	4.7
284.00	6.93	5.30	7.6	291.83	6.84	3.45	5.0
284.17	6.68	5.85	8.8	292.00	7.24	4.75	6.6
284.33	6.89	6.25	9.1	292.17	8.73	4.65	5.3
284.50	7.13	5.95	8.3	292.33	9.24	3.65	4.0
284.67	7.78	5.45	7.0	292.50	9.25	3.50	3.8
284.83	7.97	5.85	7.3	292.67	9.17	3.35	3.7
285.00	8.28	6.60	8.0	292.83	8.45	2.45	2.9
285.17	9.41	7.05	7.5	293.00	7.69	2.05	2.7
285.33	8.82	7.25	8.2	293.17	6.46	2.45	3.8
285.50	8.67	6.65	7.7	293.50	6.22	1.35	2.2
285.67	7.78	5.95	7.6	293.67	7.07	2.15	3.0
285.83	7.12	5.55	7.8	293.83	8.39	4.45	5.3
286.00	6.90	4.80	7.0	294.00	9.37	4.82	5.1
286.17	6.48	4.05	6.3	294.17	9.18	3.80	4.1
286.33	6.40	3.92	6.1	294.33	9.27	3.60	3.9

Table 5.3 continued...

WAVE LENGTH	ABS. CROSS SEC. $\times10^{-19}$	FLR. CROSS SEC. $\times10^{-20}$	FLR. QUANT. YIELD	WAVE LENGTH	ABS. CROSS SEC. $\times10^{-19}$	FLR. CROSS SEC. $\times10^{-20}$	FLR. QUANT. YIELD
IN nm	cm^2	cm^2	%	IN nm	cm^2	cm^2	%
294.50	9.19	3.70	4.0	302.50	7.99	3.90	4.9
294.67	8.24	3.55	4.3	302.67	6.78	4.35	6.4
294.83	6.68	3.20	4.8	302.83	5.18	4.70	9.1
295.00	5.66	2.65	4.7	303.00	4.01	4.95	12.3
295.17	5.12	2.45	4.8	303.17	2.95	4.30	14.6
295.33	4.54	0.90	2.0	303.33	2.58	3.10	12.0
295.50	4.41	0.65	1.5	303.50	2.32	2.30	9.9
295.67	5.69	1.05	1.8	303.67	2.36	2.15	9.1
295.83	7.38	2.15	2.9	303.83	2.59	2.55	9.8
296.00	8.98	2.90	3.2	304.00	3.32	3.00	9.0
296.17	9.20	3.52	3.8	304.17	4.38	3.15	7.2
296.33	9.28	2.90	3.1	304.33	6.98	3.10	4.4
296.50	8.13	1.85	2.3	304.50	7.96	2.30	2.9
296.67	6.66	1.20	1.8	304.67	6.42	2.10	3.3
296.83	3.51	1.00	2.8	304.83	5.71	1.90	3.3
297.00	4.71	1.07	2.3	305.00	4.76	1.10	2.3
297.17	4.18	1.00	2.4	305.17	3.39	1.05	3.1
297.33	3.57	0.70	2.0	305.33	2.31	1.50	6.5
297.50	3.62	0.70	1.9	305.50	2.02	2.00	9.9
297.67	4.84	1.10	2.3	305.67	2.19	1.95	8.9
297.83	6.98	1.70	2.4	305.83	2.31	1.87	8.1
298.00	8.85	2.30	2.6	306.00	2.57	1.85	7.2
298.17	9.98	2.50	2.5	306.17	3.89	1.95	5.0
298.33	8.85	2.50	2.8	306.33	5.38	2.65	4.9
298.50	7.43	2.30	3.1	306.50	7.05	2.55	3.6
298.67	6.97	1.75	2.5	306.67	6.34	1.60	2.5
298.83	5.71	1.42	2.5	306.83	5.57	1.35	2.4
299.00	4.18	1.37	3.3	307.00	4.53	1.70	3.8
299.17	3.60	1.35	3.8	307.17	3.37	2.25	6.7
299.33	3.42	1.15	3.4	307.33	3.05	2.60	8.5
299.50	3.35	1.10	3.3	307.50	2.35	2.10	8.9
299.67	3.88	2.95	7.6	307.67	2.29	1.90	8.3
299.83	5.56	3.23	5.8	307.83	1.89	1.95	10.6
300.00	8.46	2.75	3.3	308.00	1.80	2.25	12.5
300.17	10.36	2.30	2.2	308.17	2.10	2.50	12.5
300.33	9.51	2.20	2.3	308.33	2.40	2.80	11.7
300.50	7.71	2.35	3.0	308.50	3.28	3.05	9.3
300.67	6.29	2.50	4.0	308.67	4.09	3.40	8.3
300.83	5.09	2.50	4.9	308.83	4.87	3.65	9.4
301.00	4.48	2.40	5.4	309.00	3.97	3.60	9.1
301.17	3.52	2.05	5.8	309.17	3.14	3.30	10.5
301.33	3.36	1.70	5.1	309.33	2.63	2.95	11.2
301.50	2.59	1.55	6.0	309.50	1.82	2.92	16.0
301.67	2.23	1.45	6.5	309.67	1.62	2.90	17.9
301.83	2.91	2.10	7.2	309.83	1.36	2.60	19.1
302.00	4.71	2.85	6.1	310.00	1.71	1.50	8.8
302.17	6.66	3.05	4.6	310.17	1.53	1.35	8.8
302.33	8.66	3.35	3.9	310.33	1.75	1.65	9.4

Table 5.3 continued...

WAVE LENGTH	ABS. CROSS SEC. $\times 10^{-19}$	FLR. CROSS SEC. $\times 10^{-20}$	FLR. QUANT. YIELD	WAVE LENGTH	ABS. CROSS SEC. $\times 10^{-19}$	FLR. CROSS SEC. $\times 10^{-20}$	FLR. QUANT. YIELD
IN nm	cm^2	cm^2	%	IN nm	cm^2	cm^2	%
310.50	2.02	2.25	11.1	315.33	0.93	3.05	32.8
310.67	2.53	2.85	11.3	315.50	1.10	2.95	26.8
310.83	3.18	2.90	9.1	315.67	0.97	2.82	29.1
311.00	3.15	2.85	9.0	315.83	0.98	2.65	27.0
311.17	2.49	2.62	10.5	316.00	0.69	2.62	38.0
311.33	2.05	2.52	12.3	316.17	0.66	2.70	40.9
311.50	1.66	2.50	15.1	316.33	0.44	2.77	63.0
311.67	1.09	1.95	17.9	316.50	0.80	2.77	34.6
311.83	1.22	2.10	17.2	316.67	0.74	2.75	37.2
312.00	1.05	2.85	27.1	316.83	0.90	2.67	29.7
312.17	1.38	3.00	21.7	317.00	0.73	2.65	36.3
312.33	1.45	3.05	21.0	317.17	0.62	2.60	41.9
312.50	1.18	3.00	25.4	317.33	1.13	2.60	23.0
312.67	1.35	3.05	22.6	317.50	1.00	2.70	27.0
312.83	1.54	3.10	20.1	317.67	0.76	2.90	38.2
313.00	2.15	3.25	15.1	317.83	0.98	2.95	30.1
313.17	2.52	3.30	13.1	318.00	1.35	2.80	20.7
313.33	2.79	3.30	11.8	318.17	0.75	2.60	34.7
313.50	2.17	3.15	14.5	318.33	1.12	2.25	20.1
313.67	1.38	3.07	22.2	318.50	0.86	–	–
313.83	1.23	3.07	25.0	318.67	0.52	–	–
314.00	1.19	3.15	26.5	318.83	0.50	–	–
314.17	0.97	3.30	34.0	319.00	0.57	–	–
314.33	0.50	3.35	67.0	319.17	0.47	–	–
314.50	0.63	3.37	53.4	319.33	0.66	–	–
314.67	0.87	3.35	38.5	319.50	0.47	–	–
314.83	1.07	3.30	30.8	319.67	0.68	–	–
315.00	0.72	3.22	44.7	319.83	0.71	–	–
315.17	1.12	3.10	27.7	320.00	0.70	–	–

Table 5.4 Photoabsorption cross sections, $\sigma_{T\lambda}$, for SO_2 in 10^{-19} cm^2 at room Temperature.

Band Assignment	Present work	Wu (1981)	Brassington (1981)	McGee and Burris (1987)
A	2.79	2.56	2.68	2.719
B	3.30	3.34	3.91	3.833
C	4.87	4.44	5.90	5.630
D	7.05	5.29	7.38	7.169
E	7.96	6.77	10.00	7.925
F	8.66	7.49	9.85	9.327
G	10.36	9.18	13.00	11.50
H	9.98	-	11.00	-
J	9.40	-	11.25	-

unpublished and has been obtained between 300 and 338 nm at 0.06 nm resolution. Accurate measurements of the SO_2 cross sections between 290 and 317 nm have been made by Brassington using a frequency-doubled dye-laser source with a 0.05 nm instrumental bandwidth. Sulphur dioxide absorption cross sections have also been measured by McGee and Burris (1987) between 300 and 324 nm at an instrumental resolution of 0.03 nm. A close look at these observations reveals that the increasing trend in cross sections at peaks of the bands from A to G is similar in the four cases, but quantitatively the values of the cross sections are much different. The cross section values reported by Brassington (1981), McGee and Burris (1987) are, in general, higher than those reported in the present experiments. This is expected as the instrumental resolution used in the two experiments is much higher. Also the instrumental resolution used in the measurements by Wu (1981) is much higher than that used in the present work. In spite of this, the cross section values reported by Wu are much smaller, varying from 8% at band A to about 25% at band D.

Fluorescence cross section measurement:

The total fluorescence cross sections have been measured at low pressures of SO_2 in the spectral region 278.7 to 320 nm. It was indicated by Brus and McDonald (1974) that at least two states appear to be involved in fluorescence by light absorption in this spectral region. One state had short collision-free radiative lifetime (50 micro sec) which was independent of exciting wavelength whereas the life time of the other state varied from 80 to 530 micro sec depending upon the exciting wavelength. That is why it was necessary to measure the fluorescence cross sections at both low and high pressures of SO_2. But for practical difficulties, fluorescence cross section have been measured in the present experiment at low pressures only.

The total fluorescence cross sections as measured in the present experiment at low pressures of SO_2 are shown in Fig.(5.8). The cross sections have been measured at a few pressures between 4 and 10 mTorr and the average cross sections have been obtained, and the values in the spectral region 278.6-318.3 nm are listed in Table (5.3). The fluorescence quantum yields as obtained from total fluorescence and absorption cross sections have also been shown in Fig.(5.8) as a function of exciting wavelength. The quantum yields as obtained in the present experiment are much less than unity at all exciting photon wavelengths, in this spectral region, whereas quantum yield of unity has been reported by Mettee (1968).

5.2   Carbon Disulphide

The ground state of CS_2 is X $^1\Sigma_g^+$ (linear). The bond energy, D_0(SC-S), is 4.463 ± 0.014 eV, corresponding to the incident wavelength 277.8 ± 1.0 nm (Okabe, 1972). The absorption spectrum of CS_2 in the near ultraviolet consists of two distinct regions of absorption, one extending from 290 to 380 nm and the other of much stronger absorption extending from 185 to 230 nm. The results obtained in these spectral regions would be taken up separately for detailed discussion.

5.2.1 CS_2 : Spectral region 188 - 213 nm

The photoabsorption cross sections as measured in the present experiment are shown in Fig.(5.10). These cross sections have been measured at various CS_2 pressures ranging from 1 to 5 mTorr and the average cross sections are shown in Fig.(5.10). Table (5.5) lists the photoabsorption cross section values covering the spectral range 188.2-210.2 nm. It
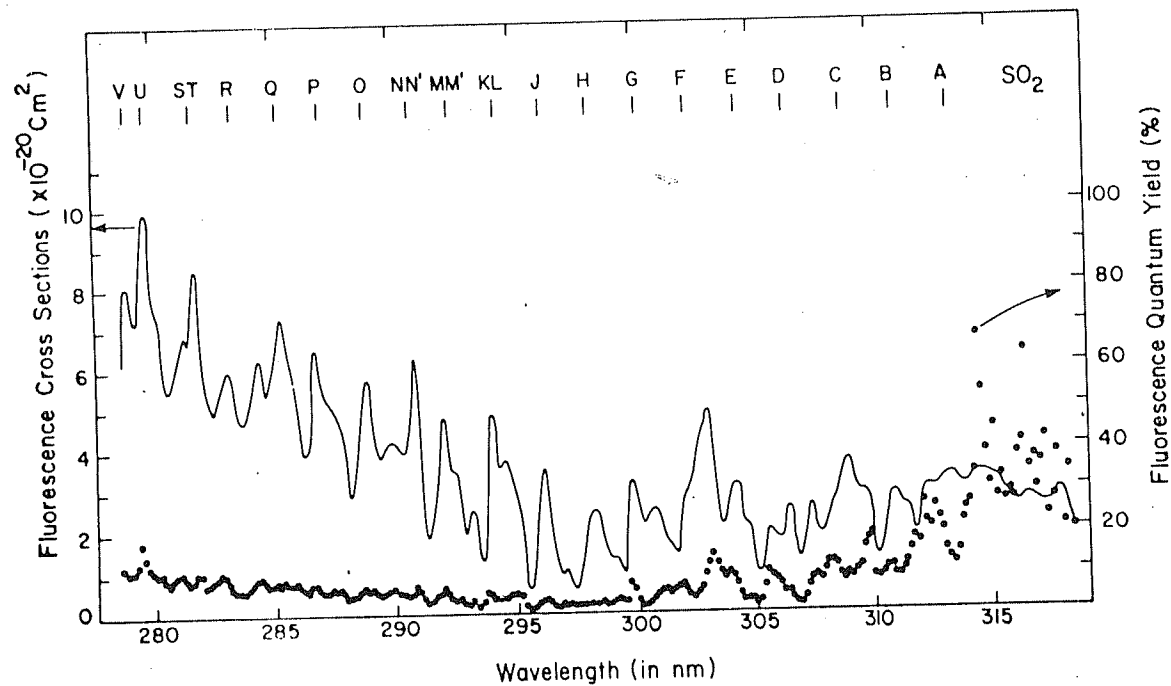
Figure 5.8 Fluorescence cross sections and fluorescence quantum yields for SO_2 in the spectral region 278.7-320.6 nm.
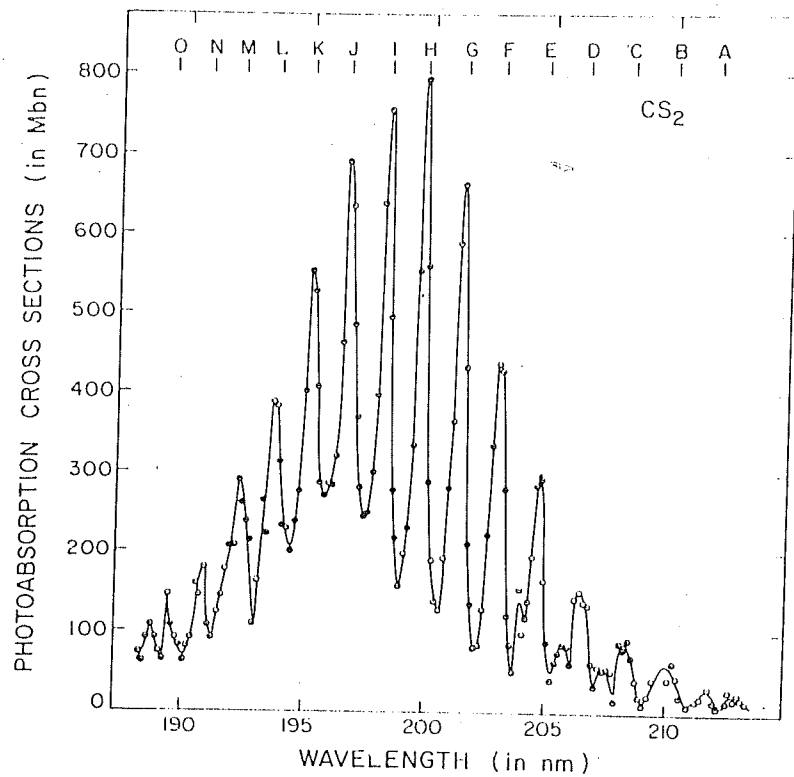
Figure 5.10 Photoabsorption cross sections for CS_2 in the spectral region 188.2-213 nm.

Table 5.5 Photoabsorption cross sections for CS_2
in 188.2-210.0 nm spectral region

WAVE LENGTH IN nm	ABS. CROSS SEC. $\times 10^{-18}$ cm^2	WAVE LENGTH IN nm	ABS. CROSS SEC. $\times 10^{-18}$ cm^2
188.25	73.2	196.58	690.4
188.42	61.2	196.75	634.1
188.58	90.9	196.92	485.7
188.92	107.3	197.08	370.1
189.08	74.6	197.25	280.8
189.25	64.3	197.42	244.7
189.42	144.1	197.58	249.3
189.58	107.9	197.75	299.5
189.75	91.4	197.92	397.6
189.92	82.6	198.08	638.5
190.08	63.6	198.25	755.7
190.25	81.4	198.42	494.8
190.42	91.2	198.58	278.7
190.58	158.9	198.75	217.3
190.75	144.5	198.92	157.5
190.92	178.6	199.08	198.0
191.08	106.7	199.25	231.5
191.25	92.3	199.42	333.3
191.42	123.2	199.58	554.3
191.58	143.6	199.75	794.0
191.75	177.0	199.92	559.5
191.92	207.7	200.08	288.1
192.08	207.8	200.25	189.8
192.25	290.1	200.42	138.8
192.42	262.3	200.58	126.6
192.58	238.7	200.75	192.9
192.75	215.5	200.92	283.4
192.92	109.8	201.08	366.3
193.08	163.3	201.25	588.8
193.25	265.5	201.42	663.3
193.42	223.2	201.58	432.2
193.58	387.1	201.75	210.2
193.75	382.8	201.92	135.6
193.92	313.3	202.08	79.8
194.08	233.0	202.25	83.1
194.25	229.1	202.42	128.2
194.42	200.8	202.58	223.2
194.58	238.4	202.75	334.2
194.75	277.8	202.92	436.0
194.92	402.3	203.08	427.9
195.08	551.4	203.25	279.7
195.25	528.8	203.42	121.3
195.42	407.7	203.58	85.4
195.58	287.7	203.75	51.1
195.75	271.4	203.92	154.0
195.92	286.3	204.08	98.0
196.08	285.0	204.25	140.4
196.25	320.1	204.42	193.5
196.42	462.7	204.58	286.5

Table 5.5 continued...

WAVE LENGTH	ABS. CROSS SEC. $\times 10^{-18}$	WAVE LENGTH	ABS. CROSS SEC. $\times 10^{-18}$
IN nm	cm^2	IN nm	cm^2
204.74	293.5	207.58	57.0
204.92	165.4	207.75	53.1
205.08	88.9	207.92	17.9
205.25	41.8	208.08	88.1
205.42	63.0	208.25	80.0
205.58	76.6	208.42	91.9
205.75	86.8	208.58	71.7
205.92	83.2	208.75	41.3
206.08	61.1	208.92	23.1
206.25	142.8	209.08	12.7
206.42	151.8	209.25	24.8
206.58	138.7	209.42	43.3
206.75	134.6	209.58	35.3
206.92	62.2	209.75	97.2
207.08	34.5	209.92	57.3
207.25	58.9	210.08	43.0
207.42	54.8	210.25	64.4

was found that at two typical incident photon wavelengths of 195.1 and 202.9 nm, the maximum pressure used in the experiment (i.e. 5 m Torr) was well within the values of pressures where Beer-Lambert law was valid. The $\ln(I_{o\lambda}/I_{\lambda})$ dependence on pressure of the CS_2 vapour has been shown in Fig. (5.9). For both the wavelengths, 195.1 and 202.9 nm, the Beer-Lambert law seems to break down at pressures larger than 5 mTorr.

Carbon disulphide has a very strong structured absorption in the range 185-230 nm. The band has been interpreted by Douglas and Zanon (1964) as a transition from X $^1\Sigma_g$ ground electronic state to a bent $^1B_2$ upper state with an equilibrium bond angle of $153°$ and a bond distance of 0.166 nm. This is about 0.011 nm more than in the ground state. The spectrum in this region is, however, not entirely understood. Also, due to the complex nature of the spectrum, the assignment of the different bands is not very easy. A new nomenclature is being given in the present work for different bands, and the peaks in Fig. (5.10) have been assigned from A to O from higher to lower wavelengths.

The photoabsorption cross sections in Fig. (5.10) show a sharp increase from band O to band H, varying from 144.1 to 794.0 Mbn. The cross sections subsequently decrease rapidly from band H to band A with values varying from 794.0 to 34.3 Mbn. Not much of quantitative work has been reported in this spectral region as the cross sections in this region are pressure dependent to a large extent and therefore, it becomes difficult to obtain absolute values of cross sections which are pressure independent over a range of pressures. However, comparison of cross section values measured in the present work and those reported by Molina et al (1981) has been made in Table (5.6) at peaks of some of the bands only. A close look at these observations reveals that the increasing trend in cross sections at peaks of the bands from M to H followed by decrease in values for bands from H to E

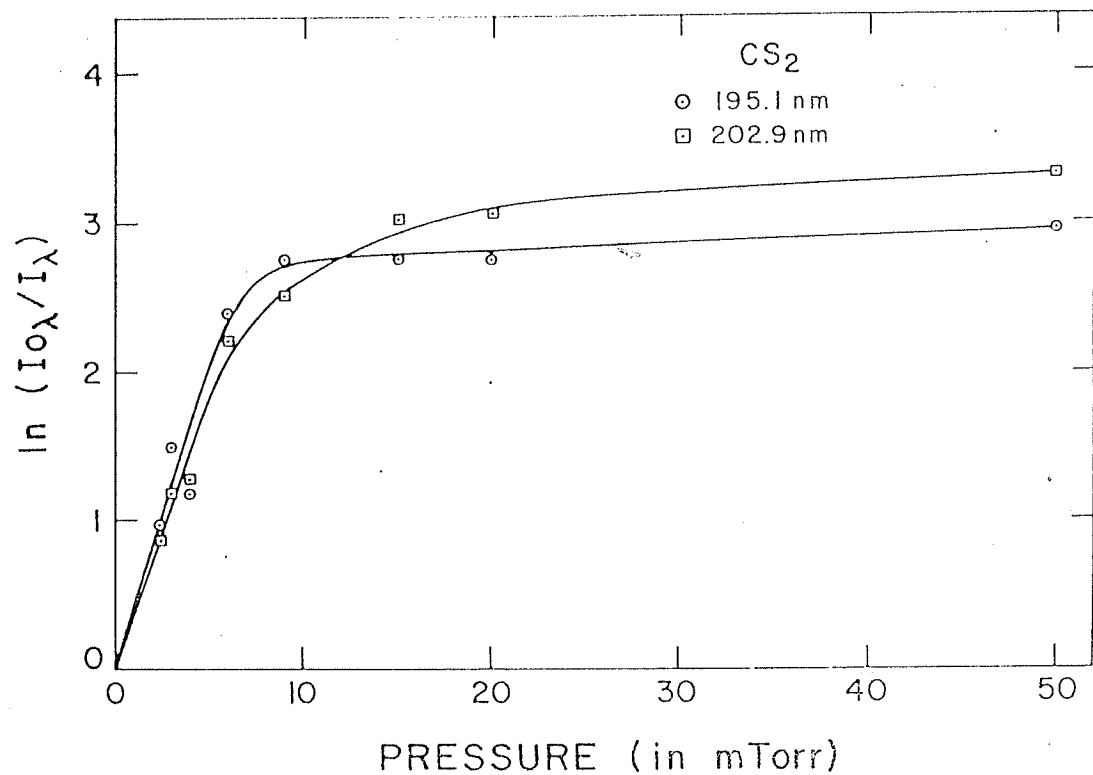Figure 5.9 The $\ln(I_{0\lambda}/I_\lambda)$ dependence on CS_2 gas pressure at 195.1 and 202.9 nm.

Table 5.6 Photoabsorption cross sections for CS_2 in Mbns at peaks of a few bands in 188-213 nm spectral region.

Band Assignment	Present work	Molina et al (1981)
M	290.1	179
K	551.4	393
J	690.4	485
H	794.0	532
G	663.3	437
F	436.0	278
E	293.5	181

is similar in two cases, but quantitatively, the values of the cross sections are much different. The cross section values reported by Molina et al (1981) are, in general, 30 to 40% less as compared to those reported in the present work. In both the experiments, an instrumental bandwidth of 0.2 nm has been used for the measurement of photoabsorption cross sections. This large discrepancy in the two measurements is perhaps due to larger pressures used for the target gas by Molina et al (1981) in their experiment. It is known that in this spectral region, the photoabsorption cross sections are pressure dependent to a large extent. It appears that the cross sections reported by Molina et al were not measured over a range of those pressures where the results were pressure independent.

Studies on the pressure dependence of photoabsorption cross sections for CS_2 have been carried out in detail in the present experiment. The cross sections have been measured at large number of pressures i.e., at 6, 9, 12, 15, 20, 50 and 100 m Torr but for clarity, cross section values measured at 9, 12, 15, 20 and 50 mTorr pressure are shown in Fig.(5.11) along with the average values of cross sections obtained at a few pressures less than 5 mTorr. At 50 mTorr, the peak intensities of the bands from L to F decrease by about 84 to 71% with the maximum decrease of about 90% at J, I and H bands. The peak intensities of the bands M to O decrease slowly and an attenuation of 71% for band M, 75% for N and 62% for band O has been observed. The bands E, D and C at 50 mTorr pressure are attenuated by about 71%, 46% and 28% respectively.

An attempt has been made to explain the pressure dependence of photoabsorption cross sections for CS_2 in this spectral region. It was reported by Callear (1963) that vibrationally excited CS is produced directly by the photochemical dissociation of CS_2:
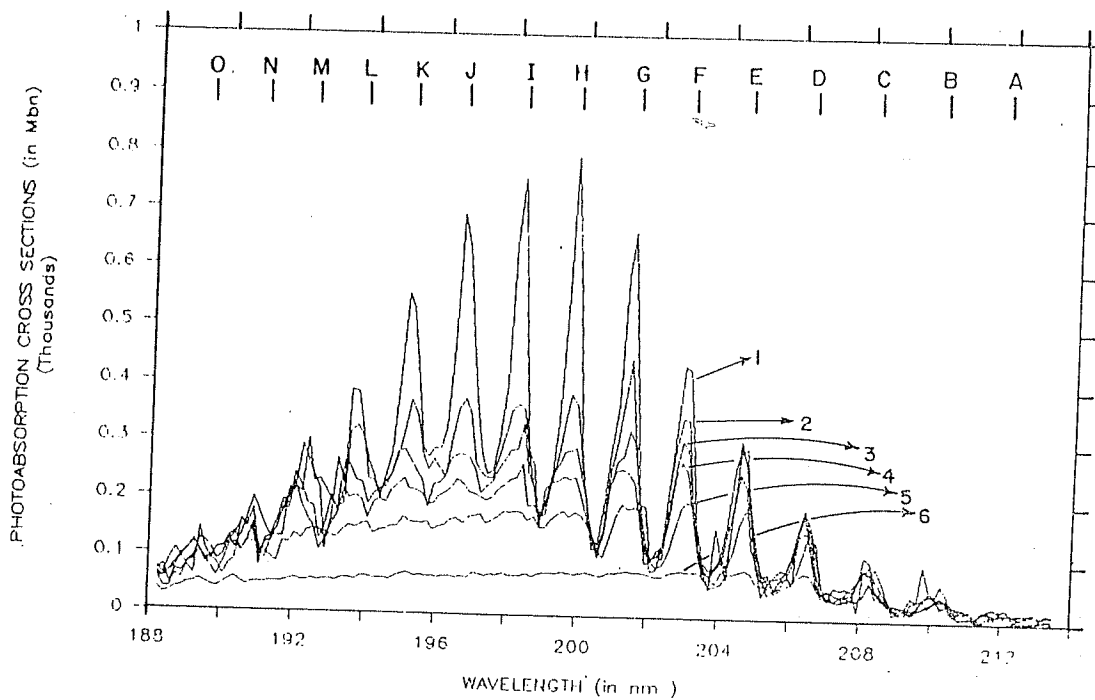
Figure 5.11 Photoabsorption cross sections for CS_2 (in 188.2-213 nm region) at different pressures. (9, 12, 15, 20 and 50 mTorr)

$$CS_2 + h\upsilon \longrightarrow CS\ (X\ ^1\Sigma^+,\ \upsilon = m)\ +\ S(\ ^3P) \qquad \underline{\hspace{1cm}}\ (5.1)$$
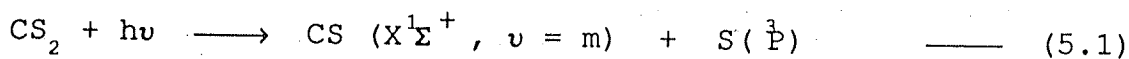
It was suggested that initially, at least three quarters of the molecules are distributed in levels with $\upsilon > 2$. The reaction (5.1) is apparently due to predissociation from the $^1B_2$ state of CS_2 in violation of the spin conservation rules because of the presence of heavy sulphur atoms. It was also reported by Callear (1963) that the decay of the vibrationally excited CS may partly be due to CS_2 itself but may largely occur by multiple quantum transitions induced by interaction with transient species, e.g.

$$CS\ (X\ ^1\Sigma^+,\ \upsilon = m)\ +\ S\ \longrightarrow\ CS\ (X\ ^1\Sigma^+,\ \upsilon = n)\ +\ S^*$$

$$\underline{\hspace{1cm}}\ (5.2)$$
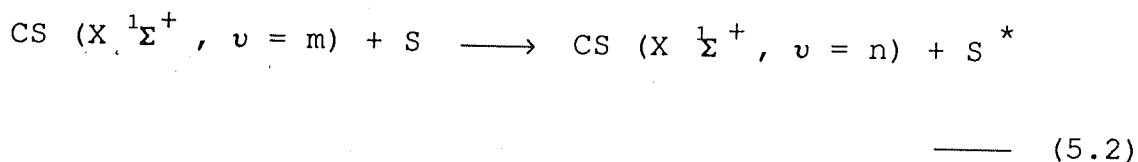
It was also pointed out that the atomic sulphur would decay by polymerisation rather than by reaction with CS_2. In view of this, it is clear that in the spectral region 188-213 nm, the CS radical is being produced in larger quantities in the higher vibrational states along with sulphur atoms. In addition to the slow radiative decay of CS from higher to lower vibrational states, there is a faster and predominant decay mechanism of CS ($\upsilon = m$) by vibrational relaxation due to interaction with sulphur atoms. From reaction (5.1), it is clear that more and more CS and sulphur atoms are produced at higher pressures of CS_2 vapour. The photoabsorption cross sections for both CS, S and polymerised S_2 are much smaller in this spectral region as compared to those reported for CS_2.

Fluorescence cross section measurement:

According to reaction (5.1), CS and S are both produced in the ground states. Therefore, the fluorescence emission is not possible. But it is known that energetically, sulphur atoms could be produced in ^1D state also. The threshold wavelength for the production of $S(^1S)$ from CS_2 was found to be 172.0 nm using the value of 65 KCal for the heat of formation of CS (Okabe, 1972). However, in a recent measurement, Hubin-Franskin et al (1976) reported a value of 34 K Cal for the heat of formation for the CS radical which correspond to the value of 211.0 nm for the threshold wavelength for $S(^1S)$ production. This shows that in this spectral region (188-211 nm), sulphur atoms are produced in ^3P, ^1D and ^1S state and therefore fluorescence at 772.7 nm corresponding to $^1S \rightarrow \ ^1D$ transition could be observed provided ^1S is deactivated collisionally by adding argon at a pressure larger than 100 Torr. An attempt has been made in the present work to measure total fluorescence cross sections as well as fluorescence quantum yields at a few wavelengths corresponding to the peaks of a few absorption bands in the spectral region 188-213 nm. A similar attempt has previously been made by Black et al (1977) at only five wavelengths between 190 and 210 nm. The relative fluorescence cross sections at different photon wavelengths were obtained using the method discussed in Section (3.2.2). These cross sections were made absolute by normalising the results with SO_2 at 228 nm where the fluorescence quantum efficiency of 100% has been reported by Hui and Rice (1972). A similar experiment was performed at 228 nm with SO_2. Using γ_{fAG} as 100% at this wavelength and the absorption cross section value of 0.45 Mbn (Ahmed and Kumar, 1990) and measuring $I_{fT\lambda}$ and $I_{O\lambda}$ at various pressures of SO_2, one could obtain the value of the product of constants KFC as given in equation (3.13) of Chapter 3. Knowing this constant, the fluorescence cross sections were made absolute. The fluorescence cross sections as well as fluorescence quantum yields as measured at peaks of some of

the vibrational bands are given in Table (5.7). The fluorescence quantum yield as obtained in the present experiment varies from about 30% to 19% at higher to lower photon wavelengths. As compared to the results in the present work, the fluorescence quantum yield values reported by Black et al (1977) vary from 5 to 10% at wavelengths between 190 and 210 nm respectively.

5.2.2 CS$_2$: Spectral region 287.5 - 339.5 nm

The photoabsorption cross sections as measured in the present experiment in the spectral range 287.5-339.5 nm are shown in Figs.(5.13) and (5.14). These cross sections have been measured at various CS$_2$ pressures ranging from 1 to 5 Torr and the average cross sections are shown in Figs.(5.13) and (5.14). The photoabsorption cross section values in this spectral region are listed in Table (5.8). It was found that at two typical incident photon wavelengths of 321 and 328 nm, the maximum pressure used in the experiment (i.e. 5 Torr) was well within the values of pressures where Beer-Lambert law was valid. The $\ln(I_{0\lambda}/I_{\lambda})$ dependence on pressure of CS$_2$ vapour has been shown in Fig.(5.12).

Although the gas phase absorption spectrum of CS$_2$ in this spectral region has been studied extensively and the general features are now understood quite well, much of the detail is still lacking because the spectrum contains regions of extraordinary complexity. This absorption system assigned by Kleman (1963) as *V system* extends from 1V band at 332.2 nm to 48 V band at 295.3 nm. The band extends to approximately 290 nm but no band assignment has been given by Kleman (1963) at wavelengths shorter than 295.3 nm. It has been established conclusively from the vibrational and rotational structure analysis of V system (Jungen et al, 1973) that the absorption features of this system correspond to the $^1B_2(^1\Delta_u) \leftarrow {}^1\Sigma_g^+$ transition. The absorption spectrum shown in
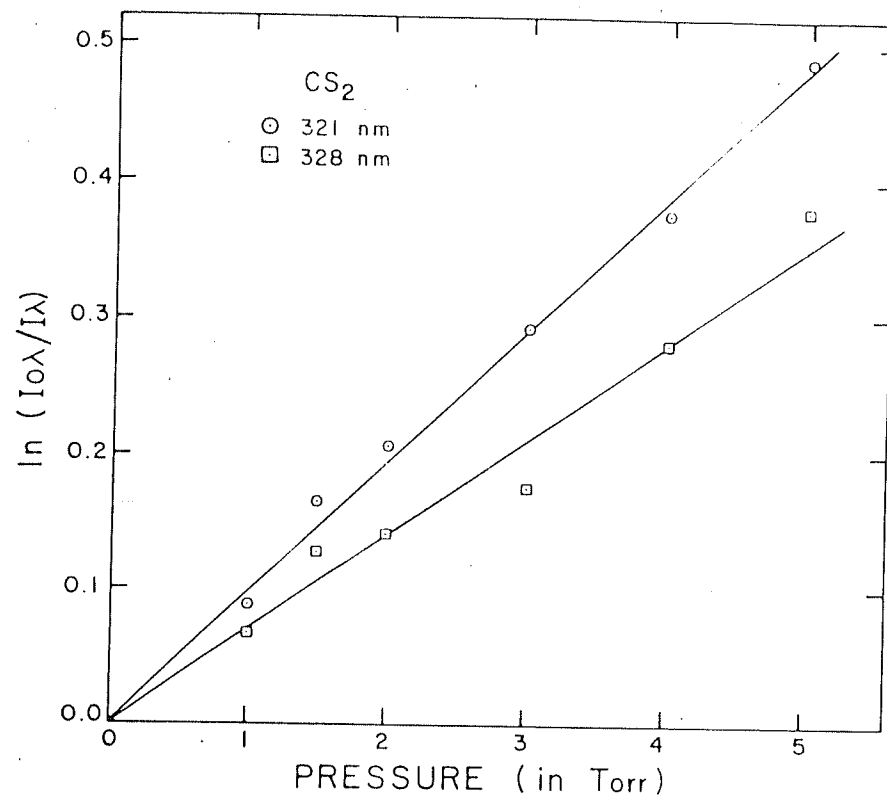
Figure 5.12 The $\ln(I_{o\lambda}/I_{\lambda})$ dependence on CS_2 gas pressure at 321 and 328 nm.
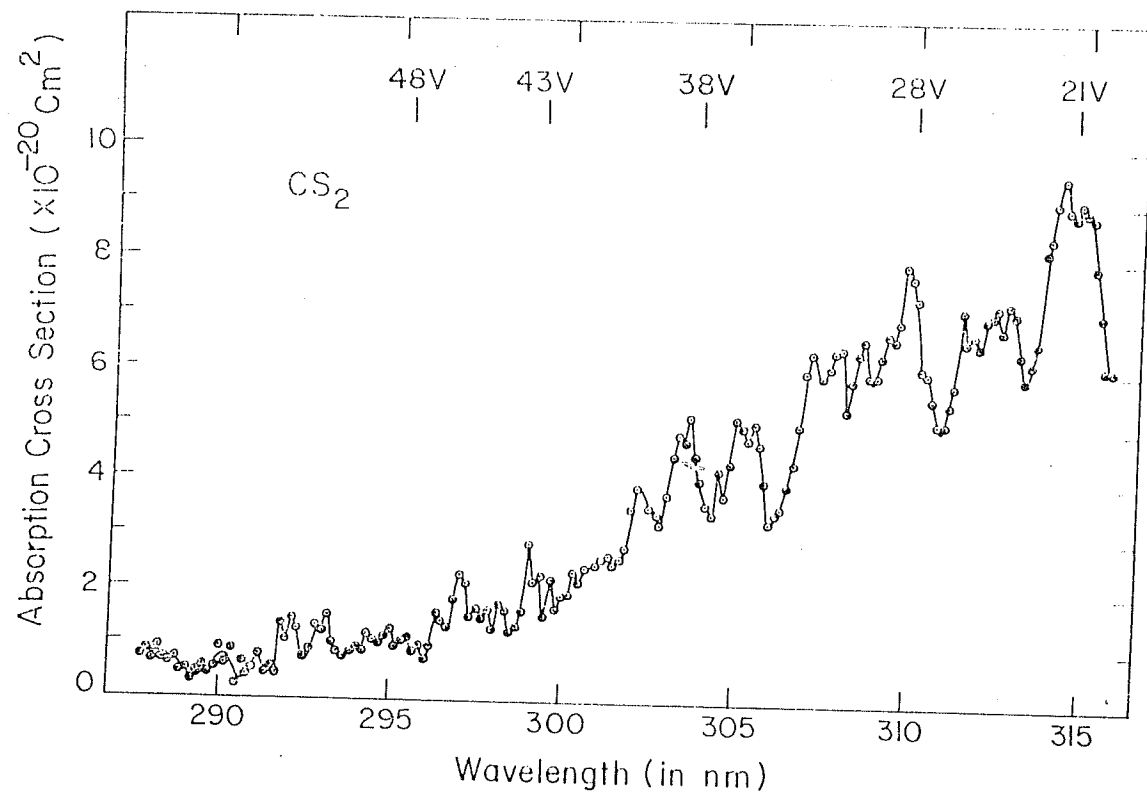
Figure 5.13 Photoabsorption cross section for CS_2 in the spectral region 287.5-315.7 nm.
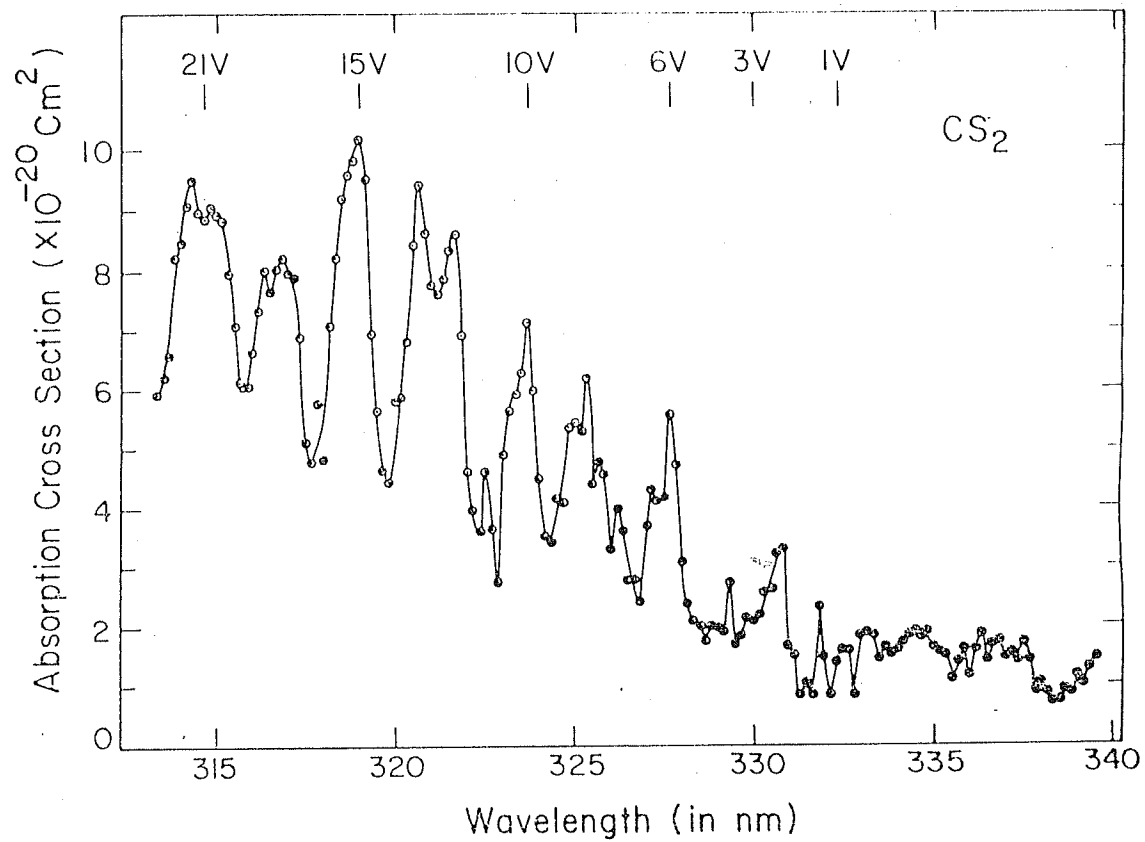
Figure 5.14 Photoabsorption cross section for CS_2 in the spectral region 313.3-339.5 nm.

Table 5.7 Fluorescence cross sections and fluorescence quantum yields for CS_2 at peaks of some of the bands. Also given are photoabsorption cross section at those wavelengths.

Wavelength in nm	$\sigma_{T\lambda}$ in Mbns	$\sigma_{f\lambda}$ in Mbns	$\gamma_{f\lambda}$ %
189.42	144.1	43.4	30.1
190.92	178.6	54.1	30.3
192.26	290.1	84.4	29.1
193.59	387.1	100.3	25.9
195.10	551.4	146.7	26.6
196.60	690.4	171.2	24.8
198.27	755.7	182.1	24.1
199.77	794.0	184.2	23.2
201.44	663.3	149.9	22.6
202.94	436.0	92.0	21.1
204.78	293.5	57.8	19.7
206.46	151.8	31.0	20.4
208.46	91.9	17.6	19.1

Table 5.8 Photoabsorption cross sections for CS_2
in the spectral region 287.6-339.4 nm

PEAK ASS. IF ANY	WAVE LEN. IN nm	ABS. CROSS SEC. ($\times 10^{-20}$) cm^2	PEAK ASS.	WAVE LEN. IN nm	ABS. CROSS SEC. ($\times 10^{-20}$) cm^2	PEAK ASS.	WAVE LEN. IN nm	ABS. CROSS SEC. ($\times 10^{-20}$) cm^2	PEAK ASS.	WAVE LEN. IN nm	ABS. CROSS SEC. ($\times 10^{-20}$) cm^2
	287.6	0.74		295.8	0.97		303.9	4.05		312.1	7.01
	287.8	0.82		295.9	0.74		304.1	3.57		312.3	7.04
	287.9	0.67		296.1	0.96		304.3	3.39		312.4	7.21
	288.1	0.88		296.3	1.53		304.4	4.20		312.6	6.81
	288.3	0.68		296.4	1.39		304.6	3.73		312.8	7.26
	288.4	0.64		296.6	1.31		304.8	4.35		312.9	7.10
	288.6	0.68		296.8	1.79		304.9	5.12		313.1	6.37
	288.8	0.46		296.9	2.25		305.1	5.01		313.3	5.93
	288.9	0.49		297.1	2.10		305.3	4.78		313.4	6.21
	289.1	0.31		297.3	1.49		305.4	5.07		313.6	6.58
	289.3	0.44		297.4	1.63		305.6	4.71		313.8	8.21
	289.4	0.54		297.6	1.46		305.8	4.00		313.9	8.46
	289.6	0.42		297.8	1.60		305.9	3.28		314.1	9.08
	289.8	0.53		297.9	1.26		306.1	3.43		314.3	9.49
	289.9	0.88		298.1	1.69		306.3	3.52		314.4	8.97
	290.1	0.58		298.3	1.63		306.4	3.96	21V	314.6	8.85
	290.3	0.86		298.4	1.22		306.6	4.36		314.8	9.05
	290.4	0.24		298.6	1.32		306.8	5.05		314.9	8.94
	290.6	0.62		298.8	1.60		306.9	5.99		315.1	8.81
	290.8	0.41		298.9	2.84		307.1	6.35		315.3	7.96
	290.9	0.52		299.1	2.16		307.3	5.99		315.4	7.07
	291.1	0.75		299.3	2.24		307.4	5.92		315.6	6.12
	291.3	0.45		299.4	1.52		307.6	6.09		315.8	6.10
	291.4	0.55		299.6	2.20		307.8	6.38		315.9	6.62
	291.6	0.43		299.8	1.64		307.9	6.44		316.1	7.32
	291.8	1.36		299.9	1.90		308.1	5.32		316.3	8.00
	291.9	1.08		300.1	1.92		308.3	5.88		316.4	7.64
	292.1	1.44		300.3	2.32		308.4	6.36		316.6	8.04
	292.3	1.25		300.4	2.14		308.6	6.59		316.8	8.19
	292.4	0.75		300.6	2.40		308.8	5.92		316.9	7.95
	292.6	0.87		300.8	2.42		308.9	5.95		317.1	7.90
	292.8	1.31		300.9	2.45		309.1	6.29		317.3	6.89
	292.9	1.20		301.1	2.59		309.3	6.70		317.4	5.13
	293.1	1.50		301.3	2.62		309.4	6.63		317.6	4.76
	293.3	0.99		301.4	2.45		309.6	6.92		317.8	5.76
	293.4	0.86		301.6	2.57		309.8	7.93		317.9	4.82
	293.6	0.75		301.8	2.77	29V	309.9	7.73		318.1	7.08
	293.8	0.82		301.9	3.49		310.1	7.33		318.3	8.20
	293.9	0.89		302.1	3.88		310.3	6.07		318.4	9.17
	294.1	0.87		302.3	3.83		310.4	6.00		318.6	9.58
	294.3	1.16		302.4	3.52		310.6	5.52		318.8	9.82
	294.4	1.07		302.6	3.43		310.8	5.12	15V	318.9	10.16
	294.6	1.02		302.8	3.23		310.9	5.12		319.1	9.50
	294.8	1.10		302.9	3.70		311.1	5.46		319.3	6.93
	294.9	1.24		303.1	4.47		311.3	5.79		319.4	5.64
	295.1	0.93		303.3	4.86		311.4	7.16		319.6	4.64
48V	295.3	1.06		303.4	4.74		311.6	6.59		319.8	4.44
	295.4	1.10		303.6	5.17		311.8	6.72		319.9	5.81
	295.6	0.86	38V	303.8	4.45		311.9	6.50		320.1	5.88

Table 5.8 continued...

PEAK ASS. IF ANY	WAVE LEN. IN nm	ABS. CROSS SEC. $(x10^{-20})$ cm^2	PEAK ASS.	WAVE LEN. IN nm	ABS. CROSS SEC. $(x10^{-20})$ cm^2	PEAK ASS.	WAVE LEN. IN nm	ABS. CROSS SEC. $(x10^{-20})$ cm^2
	320.3	6.81		327.1	4.31		333.9	1.60
	320.4	8.43		327.3	4.14		334.1	1.73
	320.6	9.40		327.4	4.17		334.3	1.84
	320.8	8.63	6V	327.6	5.55		334.4	1.89
	320.9	7.77		327.8	4.73		334.6	1.81
	321.1	7.63		327.9	3.08		334.8	1.90
	321.3	7.86		328.1	2.37		334.9	1.63
	321.4	8.35		328.3	2.07		335.1	1.55
	321.6	8.60		328.4	2.01		335.3	1.51
	321.8	6.92		328.6	1.77		335.4	1.11
	321.9	4.61		328.8	2.00		335.6	1.39
	322.1	3.98		328.9	1.97		335.8	1.60
	322.3	3.61		329.1	1.91		335.9	1.17
	322.4	4.61		329.3	2.72		336.1	1.60
	322.6	3.64		329.4	1.69		336.3	1.86
	322.8	2.76		329.6	1.85		336.4	1.43
	322.9	4.93	3V	329.8	2.14		336.6	1.69
	323.1	5.62		329.9	2.08		336.8	1.71
	323.3	5.93		330.1	2.19		336.9	1.46
	323.4	6.30		330.3	2.57		337.1	1.53
10V	323.6	7.12		330.4	2.62		337.3	1.43
	323.8	5.98		330.6	3.22		337.4	1.71
	323.9	4.49		330.8	3.27		337.6	1.43
	324.1	3.53		330.9	1.65		337.8	0.87
	324.3	3.42		331.1	1.52		337.9	1.01
	324.4	4.17		331.3	0.84		338.1	0.86
	324.6	4.15		331.4	1.02		338.3	0.74
	324.8	5.37		331.6	0.84		338.4	0.72
	324.9	5.46		331.8	2.31		338.6	0.90
	325.1	5.27		331.9	1.50		338.8	0.87
	325.3	6.18		332.1	0.84		338.9	1.18
	325.4	4.43		332.3	1.39		339.1	1.01
	325.6	4.79		332.4	1.58		339.3	1.27
	325.8	4.58		332.6	1.59		339.4	1.45
	325.9	3.30		332.8	0.82			
	326.1	4.00		332.9	1.84			
	326.3	3.62		333.1	1.86			
	326.4	2.78		333.3	1.84			
	326.6	2.81		333.4	1.43			
	326.8	2.41		333.6	1.64			
	326.9	3.70		333.8	1.54			

Fig.(5.14) in the spectral region 334.0-339.5 nm which forms part of a bigger system extending up to 350.0 nm, corresponds to $^1A_2(^1\Delta_u) \leftarrow ^1\Sigma_g^+$ transition. In the present experiment same nomenclature has been followed for different bands as done by Kleman (1963). The peaks in Fig.(5.13) and (5.14) have been numbered from 1V to 48V which correspond to photon wavelengths from 332.2 nm to shorter wavelengths.

The photoabsorption cross sections measured absolutely are shown in Figs.(5.13) and (5.14) for the spectral regions 287.5 to 315.7 nm and 313.3 to 339.5 nm respectively. The absorption cross section values, in general, are less than 1.50×10^{-20} cm^2 in the spectral region from 287.5 to 296.0 nm. The peak of the vibrational band 48V has a cross section value of 1.06×10^{-20} cm^2 in this region. At wavelengths larger than 296.0 nm, the band peaks show an increase in cross section up to the vibrational band V15 which corresponds to a photon wavelength of 318.9 cm. At the peak of V15, the absorption cross section as measured in the present work is 10.16×10^{-20} cm^2. Subsequently at larger wavelengths, decrease in cross section values has been observed. The typical values at the peaks of vibrational bands 10V and 6V are 7.12×10^{-20} and 5.55×10^{-20} cm^2 respectively. A comparison of photoabsorption cross sections obtained in the present experiment at the peak of a few vibrational bands of the V-system has been made in Table (5.9) with the values obtained by Wu and Judge (1981). The cross sections reported by them have been obtained between 319 and 330 nm at a instrumental bandwidth of 0.06 nm. A close look at these observations reveals that the decreasing trend in cross sections at the peaks of the bands from 13 V to 6 V as measured in the present experiment is missing in the data reported by Wu and Judge. Also, the values of the cross sections in the two cases are much different. The present cross section values are smaller by 15 to 40% at 13 V to 6 V bands as compared to those reported by Wu and Judge (1981). This is expected as the monochromator

Table 5.9 Photoabsorption cross sections, $\sigma_{T\lambda}$, for CS_2 in $10^{-20} cm^2$ at room temperature.

Band Assignment	Photon Wavelength in nm	$\sigma_{T\lambda}$ in 10^{-20} Cm^2	
		Present work	Wu and Judge (1981)
13 V	320.6	9.40	11.0
12 V	321.5	8.60	11.6
10 V	323.6	7.12	9.8
9 V	325.3	6.18	7.9
6 V	327.6	5.55	9.2

resolution used in the two cases is 0.2 and 0.06 nm respectively. A comparison on a large scale is not possible as the quantitative data on the photoabsorption cross sections for CS_2 are scarce.

Fluorescence cross section measurement:

The total fluorescence cross sections have been measured at a few pressures of CS_2 vapour from 10 m Torr to 850 m Torr around the peaks of some of the vibrational bands of the V-system at incident photon wavelengths between 300 to 320 nm. The method for measuring the relative fluorescence cross sections has been given in Section (3.2.2). The fluorescence cross sections along with fluorescence quantum yields obtained from the measured $\sigma_{T\lambda}$ and $\sigma_{f\lambda}$ are given in Table (5.10) at two typical pressures of 20 and 850 m Torr for the target gas.

The fluorescence of CS_2 excited by radiation in the 320 nm region has been studied by Heicklen (1963). From the absorption coefficient, he calculated the lifetime of the excited state to be 3×10^{-6} sec whereas a lifetime of about 15×10^{-6} sec was reported by Douglas (1966) in the same spectral region. This transition, therefore, has an anomalously long life and could be explained as due to extensive mixing with longer-lived states (Douglas, 1966). In other words, the molecule goes back and forth between two excited states, spending more of its time in the state with higher density of levels. Since it can not radiate while in the state with the high density of levels, the radiative lifetime is increased. More recent measurements at 337 nm using a laser showed a definite biexponential decay with lifetimes of 2.9×10^{-6} and 17×10^{-6} sec (Brus, 1971). At 337 nm, the normal bands of V system cannot be excited. But

Jungen et al (1973) found that, at room temperature, hot bands of the V system extend upto 340.0 nm and mask the other weaker bands. Thus the two lifetimes reported by Brus (1971) are due to the excitation of a hot band of the V system and an underlying triplet. In the present experiment, the fluorescence measurements have been carried out at incident photon wavelengths between 300 and 320 nm. This means that the fluorescence is due to the excitation of a few bands of V system only, with anomalously long radiative lifetime for the excited state as reported by Douglas (1966).

The fluorescence quantum yields as measured in the present experiment at different photon wavelengths have been found to be different for different pressures of CS_2 vapour. As a matter of fact, the yields are highest at low pressures and decrease with increase in pressure in a non-trivial way. Such a decrease cannot be explained in terms of normal quenching of molecules in the excited state by CS_2 itself. That is why a correction factor due to quenching by CS_2 has not been introduced in equation (3.12) which is used for obtaining fluorescence cross sections and fluorescence quantum yields. A more complex process seems to occur in this case. This process may involve vibrational relaxation of the upper excited state prior to quenching as reported by Lambert and Kimbell (1973). In view of this, the fluorescence quantum yields as measured in the present experiment (Table 5.10) have been given at two pressure of CS_2 vapour. The quantum yields vary from 7.3 to 1.2% and 0.9 to 0.2% at 20 and 850 m Torr of CS_2 pressure respectively at a few photon wavelengths from 302.09 to 318.92 nm. To the best of our knowledge, there are no other quantitative measurements for both fluorescence cross sections and fluorescence quantum yields reported in literature in this spectral region. Therefore, a direct comparison is not possible.

Table 5.10 Fluorescence cross sections and fluorescence quantum yields for CS_2 at peaks of some of the vibrational bands of V-system.Both $\sigma_{f\lambda}$ and $\gamma_{f\lambda}$ are given at 20 mTorr and 850 mTorr of target gas pressure. Also given are photoabsorption Cross Sections at these wavelengths.

Wavelength in nm	$\sigma_{T\lambda}$ in $10^{-20}cm^2$	At 20 mTorr		At 850 mTorr	
		$\sigma_{f\lambda}$ in $10^{-21}cm^2$	$\gamma_{f\lambda}$ %	$\sigma_{f\lambda}$ in $10^{-21}cm^2$	$\gamma_{f\lambda}$ %
302.09	3.88	2.85	7.3	0.33	0.9
303.59	5.17	4.11	7.9	0.36	0.7
304.92	5.12	3.47	6.8	0.34	0.7
307.09	6.35	3.84	6.0	0.29	0.5
308.59	6.59	0.80	1.2	0.25	0.4
309.76	7.93	1.34	1.7	0.28	0.4
311.42	7.16	2.23	3.1	0.27	0.4
312.76	7.26	1.36	1.9	0.24	0.3
314.26	9.49	0.64	0.7	0.25	0.3
316.76	8.19	1.02	1.2	0.22	0.3
318.92	10.16	1.22	1.2	0.21	0.2

e

ne

ong

Table 5.10 Fluorescence cross sections and fluorescence quantum yields for CS_2 at peaks of some of the vibrational bands of V-system. Both $\sigma_{f\lambda}$ and $\gamma_{f\lambda}$ are given at 20 mTorr and 850 mTorr of target gas pressure. Also given are photoabsorption Cross Sections at these wavelengths.

Wavelength in nm	$\sigma_{T\lambda}$ in $10^{-20}cm^2$	At 20 mTorr		At 850 mTorr	
		$\sigma_{f\lambda}$ in $10^{-21}cm^2$	$\gamma_{f\lambda}$ %	$\sigma_{f\lambda}$ in $10^{-21}cm^2$	$\gamma_{f\lambda}$ %
302.09	3.88	2.85	7.3	0.33	0.9
303.59	5.17	4.11	7.9	0.36	0.7
304.92	5.12	3.47	6.8	0.34	0.7
307.09	6.35	3.84	6.0	0.29	0.5
308.59	6.59	0.80	1.2	0.25	0.4
309.76	7.93	1.34	1.7	0.28	0.4
311.42	7.16	2.23	3.1	0.27	0.4
312.76	7.26	1.36	1.9	0.24	0.3
314.26	9.49	0.64	0.7	0.25	0.3
316.76	8.19	1.02	1.2	0.22	0.3
318.92	10.16	1.22	1.2	0.21	0.2

CHAPTER - 6

IONIC FLUORESCENCE

The fluorescence spectra of CS_2 and SO_2 have been studied at three incident wavelengths of 121.6, 73.6-74.4, and 58.4 nm and relative production cross sections for different product states have been measured. A new experimental set-up has been designed and fabricated in the laboratory to carry out these studies.

6.1 Experimental Set-Up

The experimental set-up for studying the fluorescence from molecular ions and other photofragmented species is shown in Fig.(6.1). It consists of a microwave discharge light source, fluorescence chamber, differential pumping assembly between the light source and the fluorescence chamber, a 0.2 meter monochromator positioned perpendicular to the optic axis, appropriate optics to focus the fluorescence emission at the entrance slit of the monochromator, thermoelectrically cooled photomultiplier and a fast data acquisition system. The details regarding the various subsystems as well as the performance of the whole system are given below.

The resonant emission lines HeI (58.4 nm), NeI (73.6-74.4 nm), and HI (121.6 nm) are produced by microwave discharge of helium, neon, and hydrogen respectively. The flow tube in the light source is a 6 mm dia, 20 cm long
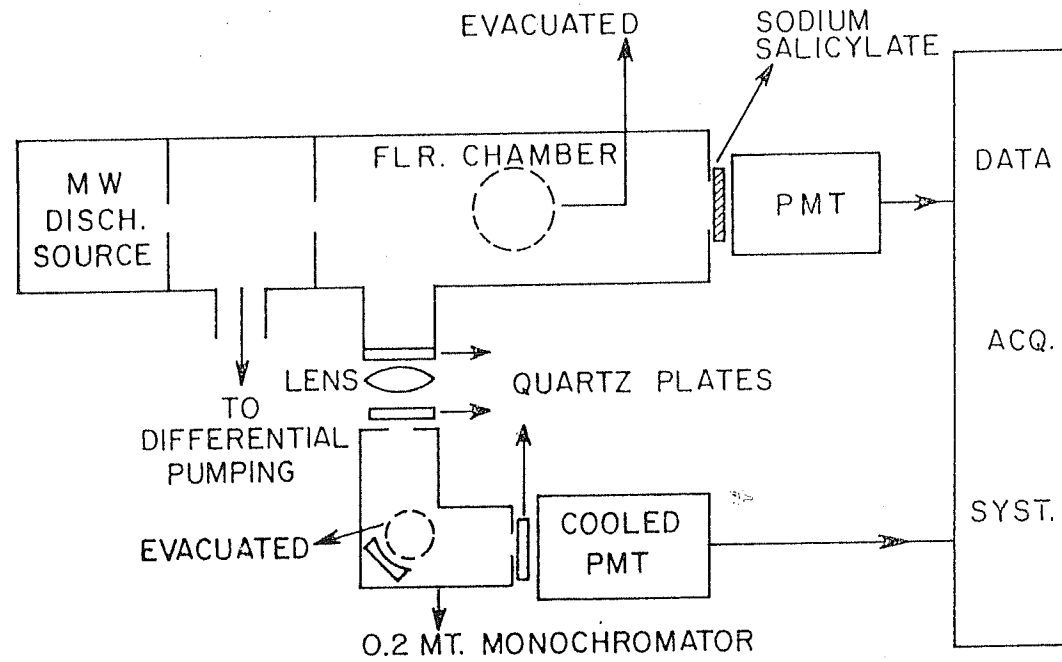
Figure 6.1 Schematic of the experimental arrangement.

quartz tube. The light source was energized by means of microwave generator (Kiva, Opthos Instruments MD, model MPG-4) with an average output power of 100 Watts at the frequency of 2.45 GHz. The microwave power was transmitted to the Evenson cavity, through a co-axial cable. The other end of the flow tube was connected to the differential pumping assembly and the discharge products were fast removed by a roots pump (Leybold Hearaus; pumping speed 40 litres/sec) backed by a mechanical pump (Hind Highvac.; pumping speed 750 litres/min).

The other end of the differential pumping assembly was connected to the fluorescence chamber. The vacuum ultraviolet radiation was allowed to pass to the chamber through a 2 mm wide, 2.5 cm long slit. The fluorescence chamber, 6.5 cm dia and 40 cm long and made of stainless steel was evacuated to a pressure of better than 10^{-5} Torr. The intensity of the resonant lines was monitored at the end of the chamber by using a combination of vacuum ultraviolet scintillator, sodium salicylate in this case and a photomultiplier of S-11 spectral response. This could be possible only when the target gas was not there in the chamber. A 0.2 meter monochromator (Minuteman Inc., USA) was positioned perpendicular to the optic axis to disperse the fluorescence emitted because of interaction of vacuum ultraviolet radiation with target molecules. The fluorescent radiation from the chamber passed through a quartz plate vacuum sealed to the chamber and a quartz lens whose focal length was chosen to match the f-number of the 0.2 meter monochromator. This optical system helped to focus the fluorescent radiation at the entrance slit of the monochromator. This monochromator covered the spectral range from 200 to 700 nm and had to be evacuated along with focussing assembly for studying the fluorescence in the ultraviolet region. The monochromator was vacuum sealed with two quartz plates at both the entrance and exit slit ends. The dispersed fluorescent radiation intensity was measured using a thermoelectrically cooled

photomultiplier of EMI 9558 QB type positioned behind the exit slit of the 0.2 meter monochromator. In this system, total fluorescence intensity could also be measured by removing the quartz lens and monochromator system and replacing this by a thermoelectrically cooled photomultiplier. In both the cases, the photomultipliers were operated in the counting mode and after proper amplification the signals were stored in a home-made microprocessor controlled 1024 channel dual multichannel analyzer operated in the multiscaling mode. The data stored for each run was transferred to IBM compatible personal computer for data analysis.

Sulphur dioxide used in the experiment was procured from L'Air Liquide, France and was used without further purification. Carbon disulphide vapour was obtained from an analytical-grade liquid and the vapour was purified by fractional distillation before being introduced into the fluorescence chamber. The pressure in the chamber was measured absolutely using a MKS Baratron Capacitance manometer (head 310 MH-10). This was a differential manometer and the pressure was made absolute by evacuating the reference side to a pressure of about 10^{-6} Torr.

The resolution of the system was measured with known intense lines of mercury (Hg). It was found that the monochromator resolution at the slit width of 150 microns each for both entrance and exit slits was 0.48 and 0.8 nm at 253.7 and 404.6 nm respectively. This resolution was used for studying the CS_2^+ fluorescence spectrum of B $^2\Sigma_u^+ \rightarrow$ X $^2\Pi_g$ system at 73.6-74.4 and 58.4 nm. For studying the fluorescence of all other systems for both SO_2 and CS_2, a monochromator resolution of 0.7 and 1.3 nm was used at 253.7 and 404.6 nm respectively which corresponded to the slit width of 400 microns each for entrance and exit slits.

6.2 Results and Discussion

Total and dispersed fluorescence intensities were measured for both SO_2 and CS_2 at three incident photon wavelengths 58.4, 73.6-74.4, and 121.6 nm. The first two resonant emissions are energetic enough to photoionize, photodissociate and/or dissociatively photoionize both target molecules, SO_2 and CS_2 but the photons at 121.6 nm do not posses sufficient energy to photoionize the target gas but could photodissociate these molecules. Therefore, the total and dispersed fluorescence spectrum at this wavelength would have contribution only from the excited parent neutral molecules or photofragmented species, whereas at 58.4 and 73.6-74.4 nm, the total and dispersed fluorescence would have components from neutral and dissociated species, ionized molecules and dissociatively ionized fragments. The results obtained for both sulphur dioxide and carbon disulphide would be taken up separately for detailed discussion.

6.2.1 Carbon Disulphide

Total fluorescence intensities measured at various pressures of CS_2 vapour ranging from 0 to 80 mTorr is shown in Fig.(6.2) at three incident photon wavelengths, 121.6, 73.6-74.4, and 58.4 nm. The fluorescence intensity measurement is relative but the pressure of the target gas has been measured absolutely. The total fluorescence intensity at the three incident photon wavelengths increases at low pressure and reaches a maximum at around 70 to 80, 15 and 20 to 25 mTorr for 121.6, 73.6-74.4 and 58.4 nm photon wavelengths respectively. These maximum pressures for CS_2 have been used to study the dispersed fluorescence at these three photon wavelengths. Also, from Fig.(6.2), it is clear that the maximum fluorescence quantum yield of CS_2 at 121.6
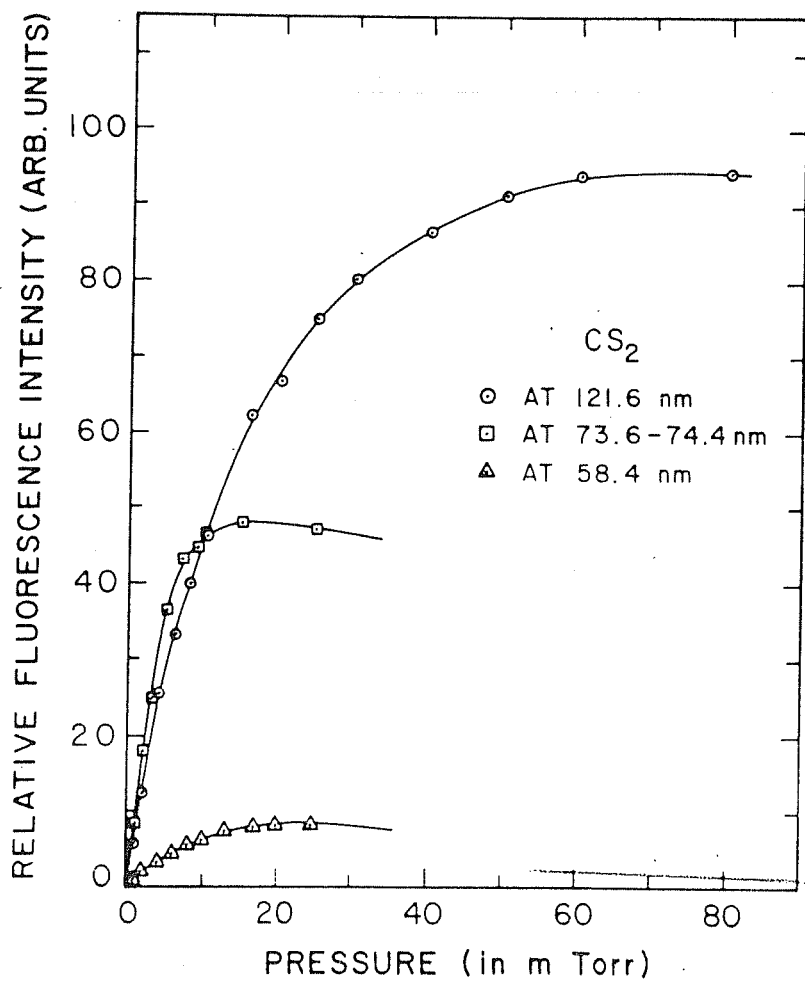
Figure 6.2 Total fluorescence for CS_2 as a function of pressure of the target gas at three incident photon wavelengths.

nm is about 1.97 and 11.1 times larger than that at 73.6-74.4 and 58.4 nm respectively.

6.2.1.1 CS(A $^1\Pi \to$ X $^1\Sigma^+$) system

The dispersed fluorescence for CS_2 at 121.6 nm as measured in the present experiment is shown in Fig.(6.3) in the spectral region 226 to 525 nm. Four broad peaks between 240 to 290 nm are seen in the spectrum whereas no fluorescence could be measured at other wavelengths between 226 to 240 and 290 to 525 nm. This fluorescence spectrum could not be attributed to CS_2^+ or CS^+ as it is energetically impossible to photoionize the target gas molecules at 121.6 nm. Therefore, the spectrum could only be from the parent neutral molecules or photofragmented species. The fluorescent spectrum in Fig.(6.3) has been carefully studied and has been identified to be due to CS(A $^1\Pi \to$ X $^1\Sigma^+$) transition. The assignment of the peaks have been made on the basis of data given by Pearse and Gaydon (1965). In the spectrum reported in the present experiment, all the vibrational bands could not be resolved. The first broad band is mainly due to (1,0) transition but has a contribution from (2,1) and (2,0) bands also. The second broad band has main contribution from (0,0) band but other vibrational bands like (1,1) and (2,2) also contribute significantly. The third broad band can be attributed to bands (0,1), (1,2) and (2,3) whereas the bands (0,2), (1,3) and (2,4) form the fourth broad band. The areas under these broad bands have been measured and relative production cross sections have been calculated. The production cross section for the most intense band, in this case the second broad band, is chosen to be 1.00 and the relative cross sections for other bands are obtained accordingly. At the incident photon wavelength of 121.6 nm, the relative production cross section for CS(A $^1\Pi \to$ X $^1\Sigma^+$) system in the four broad emission bands as obtained in the present experiment, have been found to be 0.36, 1.00, 0.36

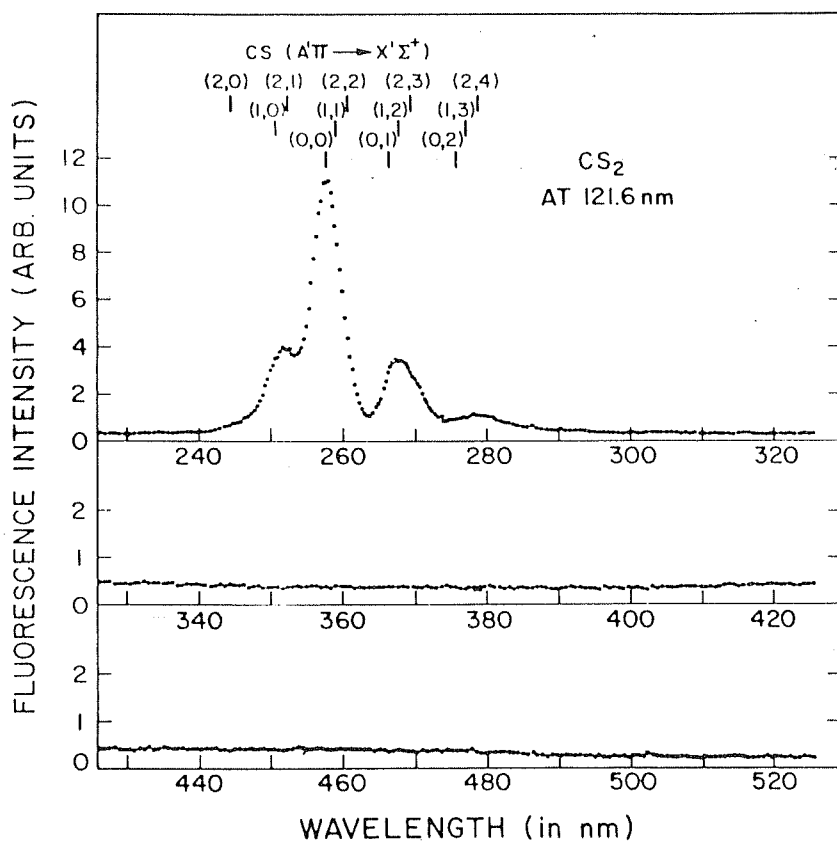Figure 6.3 The fluorescence spectrum of CS(A $^1\Pi \rightarrow$ X $^1\Sigma^+$) system observed when CS_2 is photoexcited at an incident photon wavelength of 121.6 nm.

and 0.11 respectively. A comparison of cross sections at other incident photon wavelengths (73.6-74.4 and 58.4 nm) is not possible as no bands corresponding to the above CS system were observed in the dispersed fluorescence spectra at these wavelengths.

6.2.1.2 $CS_2^+(B\ ^2\Sigma_u^+ \rightarrow X\ ^2\Pi_g)$ system.

The $B\ ^2\Sigma_u^+ \rightarrow X\ ^2\Pi_g$ fluorescence spectra produced by irradiation of photons at wavelengths 73.6-74.4 and 58.4 nm are shown in Fig.(6.4a) and (6.4b). The fluorescence emissions cover the spectral range from 276 to 295 nm. The bands shown in Fig.(6.4a) and (6.4b) have been assigned as per nomenclature used by Callomon (1958). The corresponding transition for each band has been given in Table (6.1). As has been mentioned previously, the fluorescence spectra have been obtained at the monochromator resolution of 0.48 and 0.8 nm at 253.7 and 404.6 nm respectively. Even though this resolution is sufficiently large for this type of experiment, some of the bands, have not been resolved. Band α does not appear in the fluorescence spectrum obtained at the incident photon wavelength 73.6-74.4 but it appears in the spectrum at incident wavelength 58.4 nm even though it is partially resolved. The band w, which in fact is a combination of three bands assigned as v, w and x is not resolved in the two spectra. The bands f and y are nicely resolved in Fig.(6.4b) whereas they appear as a single broad band in Fig.(6.4a). A few new bands below 270 nm and above 292 nm could be seen in Fig.(6.4a). No attempt has been made to identify these bands. The relative production cross section for all these bands of the $CS_2^+(B\ ^2\Sigma_u^+ \rightarrow X\ ^2\Pi_g)$ system produced by photons at incident wavelengths of 73.6-74.4 and 58.4 nm have been obtained and are given in Table (6.1). Also given in the table are the relative production cross sections of all these bands reported by Lee et al (1975) at incident wavelengths 55.5-82.7 nm. It is clear that the relative production cross
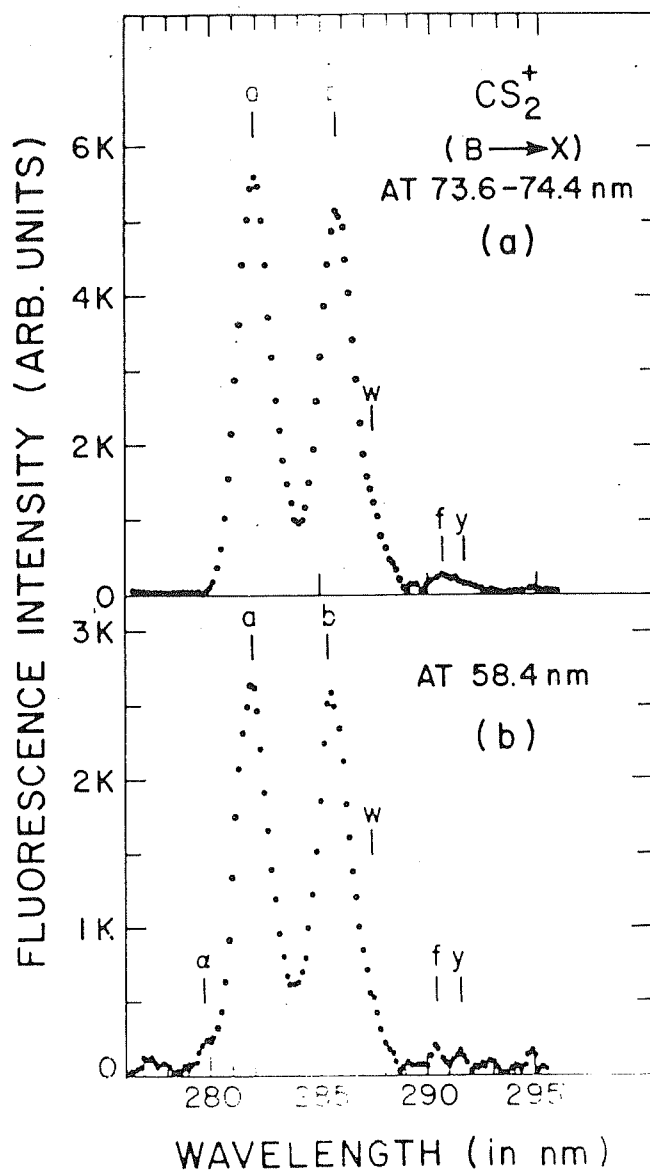
Figure 6.4 The fluorescence spectra of $CS_2^+(B\ ^2\Sigma_u^+\ \rightarrow\ X\ ^2\Pi_g)$ system when excited at an incident photon wavelengths of (a) 73.6-74.4 nm and (b) 58.4 nm.

Table 6.1. The band head positions and assignment as given by Callomon (1958) and the relative production cross sections for various bands of CS_2^+ (B $^2\Sigma_u^+ \rightarrow$ X $^2\Pi_g$) system produced by photons at a few incident wavelengths.

Band Head		Transition	Relative Production cross sections		
		B $^2\Sigma_u^+ \rightarrow$ X $^2\Pi_g$ (Ω)	Present Work at incident wavelength		Lee et al (1975) at incident wavelength
λ in nm	Assignment		73.6-74.4 nm	58.4 nm	55.5-82.7 nm
279.80	α	(020)→(020)(3/2)	-	0.09	-
282.00	a	(000)→(000)(3/2)	1.00	1.00	1.00
285.55	b	(000)→(000)(1/2)	0.92	0.98	0.86
287.35	v		not resolved	not resolved	0.06
287.40	w				
287.65	x				
290.80	f	(000)→(100)(1/2)	0.04	0.12	0.02
291.35	y		0.03	0.12	0.02

sections reported in the present experiment for the bands b, f and y are much larger at incident wavelength of 58.4 nm as compared to those at 73.6-74.4 nm. The average values of relative production cross sections for these bands reported by Lee et al (1975) at incident photon wavelengths ranging from 55.5 to 82.7 nm are, in general, smaller than values reported in the present work.

6.2.1.3 $CS_2^+(A\ ^2\Pi_u \rightarrow X\ ^2\Pi_g)$

The fluorescence spectrum in the wavelength region 437-555 nm produced by the interaction of vacuum ultraviolet photons of wavelengths 73.6-74.4 and 58.4 nm with CS_2 vapour is shown in Fig.(6.5a) and (6.5b). The present spectrum has been identified as the $CS_2^+(A\ ^2\Pi_u \rightarrow X\ ^2\Pi_g)$ system by Weissler et al (1971). The assignment of the different vibrational bands as obtained in the present experiment have been made using the wavelength data given by Weissler et al.

It is known that the states A $^2\Pi_u$ and X $^2\Pi_g$ are both doubly degenerate having spin-orbit splitting corresponding to Ω = 1/2 and 3/2. From the analysis of the $CS_2^+(B\ ^2\Sigma_u^+ \rightarrow X\ ^2\Pi_g)$ system, Callomon (1958) has determined that the vibrational levels of X $^2\Pi_{g,1/2}$ (000) and X $^2\Pi_{g,3/2}$ (000) are inverted, with a splitting of 440.71 cm^{-1}. On the other hand, the splitting in the vibrational levels of CS_2^+ (A $^2\Pi_u$) state is not yet known. In the present fluorescence spectrum (Fig. 6.5), no vibrational transition corresponding to spin-orbit split components of A $^2\Pi_u$ state of CS_2^+ could be observed. It appears that the spin-orbit splitting for this state is quite small. A similar inference has been drawn by Lee et al (1975) from their fluorescence measurements and Brundle and Turner (1969) from their photoelectron spectroscopic studies of the molecular ion.

The fluorescence spectra of CS_2 at helium and neon

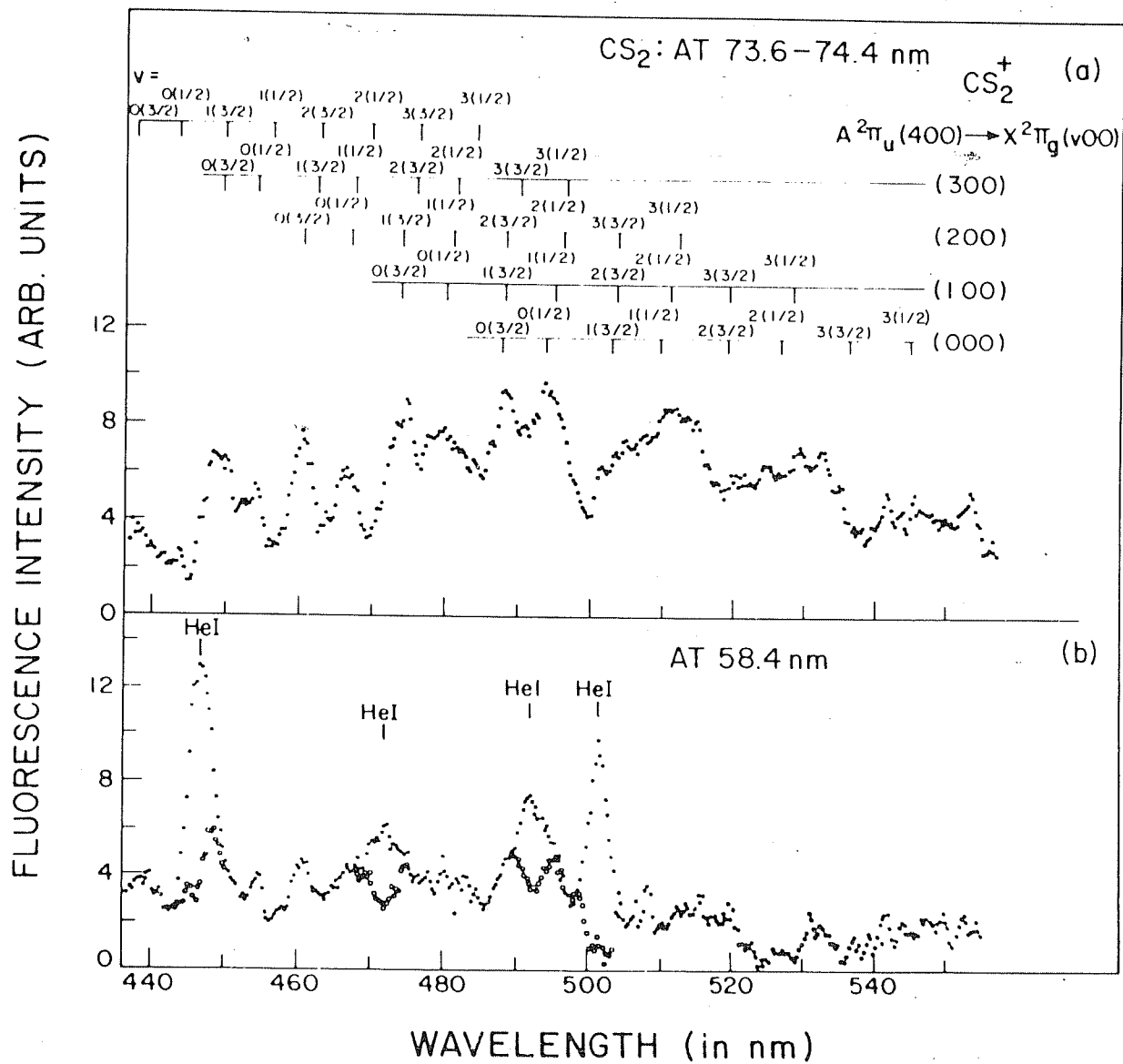Figure 6.5 The fluorescence spectra of $CS_2^+(A\ ^2\Pi_u \rightarrow X\ ^2\Pi_g)$ system when excited at an incident photon wavelength of (a) 73.6-74.4 nm and (b) 58.4 nm.

resonant lines in the vacuum ultraviolet region shows the occurrence of the helium lines in the visible region scattered from the fluorescence chamber as well as from the target gas. This is possible as the energy selection of the incident photons has not been carried out using any type of dispersing element. This has helped in preventing any loss of the intensity of 73.6-74.4 and 58.4 nm lines. But it has allowed the other emission lines of neutral helium to get scattered in the fluorescence chamber and enter the monochromator used for dispersing the fluorescence emissions. This effect is predominant in case of helium lines in the ultraviolet and visible regions but is negligibly small in case of neon lines. These scattered helium lines have been reproduced in another experiment under similar experimental conditions but without the target gas. This scattered line spectrum has been subtracted from the fluorescence spectrum of CS_2 at 58.4 nm as shown in Fig.(6.5b). The fluorescence spectrum after proper subtraction of scattered radiation is shown by open circles.

The relative production cross sections for the various emission wavelengths produced by incident photon wavelengths (73.6-74.4 and 58.4 nm) are given in Table (6.2) for the $CS_2^+(A\ ^2\Pi_u \rightarrow X\ ^2\Pi_g)$ system. Each emission wavelength region includes more than one vibrational bands. The transition for these bands are also given in the table. The relative production cross sections obtained in the present experiment at two incident photon wavelengths are compared with the data reported by Lee et al (1975) obtained at an incident photon wavelength of 92.3 nm. The emission wavelength regions in the two experiments are not exactly the same as the resolution in the two experiments are different. The measurements reported by Lee et al have been carried out at better resolution; therefore the emission wavelength regions in their case are extended on both sides. Also the relative production cross sections for the fifth emission wavelength region has been fixed at 1.00 and cross sections for other regions have been

Table 6.2 The relative production cross sections for CS_2^+ $(A\ ^2\Pi_u \to X^2\Pi_g)$ system in various emission wavelength regions. Also given are the transitions in different wavelength regions.

Emission wavelength region in nm	Transition $CS_2^+:A^2\Pi_u \to X^2\Pi_g\ (\Omega)$	Relative production cross sections		
		Present work		Lee et al (1975)
		At 58.4 nm	At 73.6-74.4nm	At 92.3 nm
445.0-451.3	(300)→(000)(3/2) (400)→(100)(3/2)	1.29	0.63	0.43
451.3-456.3	(300)→(000)(1/2)	0.74	0.48	0.43
456.3-463.0	(200)→(000)(3/2) (300)→(100)(3/2)	1.08	0.75	0.63
463.0-470.0	(200)→(000)(1/2) (300)→(100)(1/2)	1.12	0.68	0.75
470.0-476.7	(100)→(000)(3/2) (200)→(100)(3/2)	1.00	1.00	1.00
476.7-485.5	(100)→(000)(1/2) (200)→(100)(1/2) (300)→(200)(1/2)	1.42	1.33	0.93
485.5-492.0	(000)→(000)(3/2) (100)→(100)(3/2) (200)→(200)(3/2) (300)→(300)(3/2)	1.11	1.18	1.07
492.0-500.0	(000)→(000)(1/2) (100)→(100)(1/2) (200)→(200)(1/2) (300)→(300)(1/2)	1.23	1.35	1.41
500.0-519.0	(000)→(100)(3/2) (100)→(200)(3/2) (200)→(300)(3/2) (000)→(100)(1/2) (100)→(200)(1/2) (200)→(300)(1/2)	1.73	2.92	2.46

Table 6.2 continued...

Emission wavelength region in nm	Transition $CS_2^+ : A^2\Pi_u \rightarrow X^2\Pi_g$ (Ω)	Relative production cross sections		
		Present work		Lee et al (1975)
		At 58.4 nm	At 73.6-74.4nm	At 92.3 nm
519.0-538.0	$(000)\rightarrow(200)(3/2)$ $(100)\rightarrow(300)(3/2)$ $(000)\rightarrow(200)(1/2)$ $(100)\rightarrow(300)(1/2)$ $(000)\rightarrow(300)(3/2)$	1.04	2.47	3.02
538.0-555.0	$(000)\rightarrow(300)(1/2)$ and others	1.35	1.60	2.32

calculated accordingly. This has been done in spite of the fact that the area under this region is not the maximum. This is because for the similar wavelength region, the relative production cross section has been fixed at 1.00 by Lee et al (1975); therefore the comparison becomes simpler.

A direct comparison of the relative production cross sections measured in the present work with those reported by Lee et al (1975) is not exactly possible as both these measurements have been carried out at different incident photon wavelengths. It is clear from Table (6.2) that for a given emission wavelength region, the relative cross sections are different at three incident photon wavelengths. In the last few emission wavelength regions, the relative production cross sections appear to increase as the incident photon wavelength increases. It has been shown by Dibeler and Walker (1967) in their ion mass spectrometric studies that at wavelengths shorter than 80 nm, the dissociative ionization processes $CS_2 + h\nu \longrightarrow S^+ + CS + e$ and $CS^+ + S + e$ have appreciable efficiencies. Since these dissociative ionization processes will reduce the production of CS_2^+ ions, the cross sections for the production of fluorescence from excited CS_2^+ ions may be expected to decrease at shorter incident photon wavelength.

6.2.2 Sulphur Dioxide

Total fluorescence intensity measured at various pressures of sulphur dioxide gas from 0 to 60 mTorr is shown in Fig.(6.6), at three incident photon wavelengths, 121.6, 73.6-74.4, and 58.4 nm. The total fluorescence intensity at the three incident wavelengths increases at low pressures and reaches a maximum at around 30 mTorr for all the three wavelengths. This maximum pressure for SO_2 has been used to study the dispersed fluorescence at different incident wavelengths. Also, from Fig.(6.6), it is clear that the
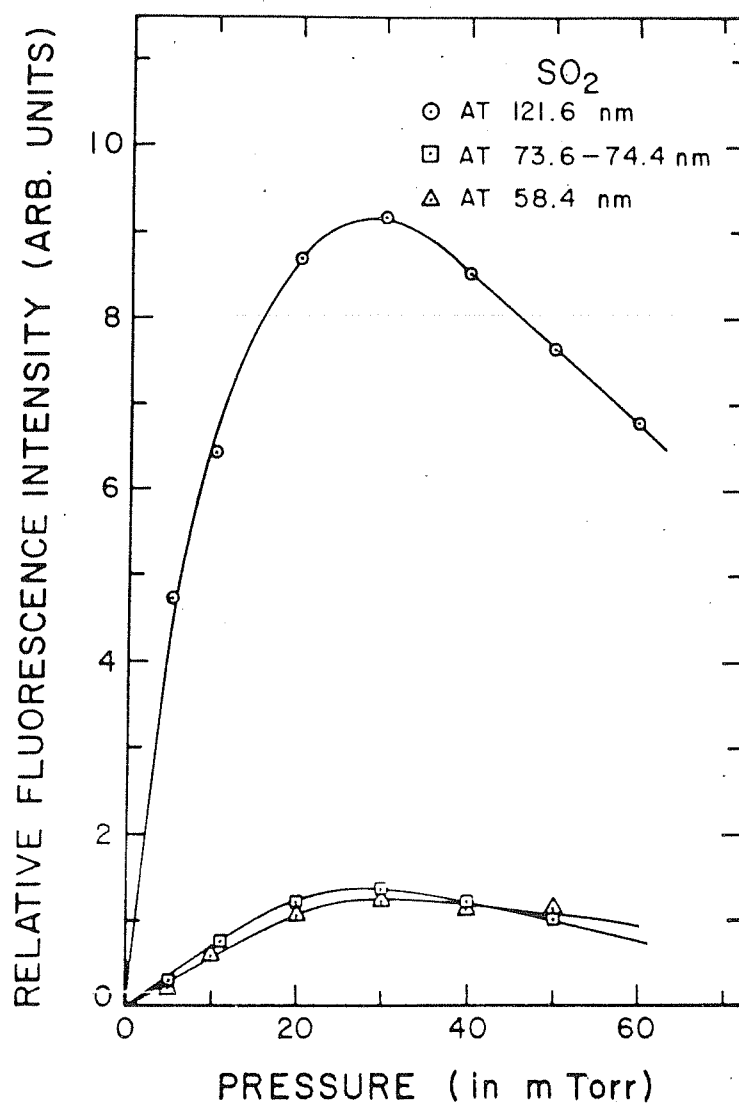
Figure 6.6 Total fluorescence for SO_2 as a function of pressure of the target gas at three incident photon wavelengths.

maximum fluorescence quantum yield of SO_2 at 121.6 nm is about 6.8 and 7.3 times larger than that obtained at 73.6-74.4 and 58.4 nm respectively.

The fluorescence spectra for SO_2 excited at three incident photon wavelengths 121.6, 73.6-74.4, and 58.4 nm were obtained in the emission wavelength region from 238 to 442 nm. The monochromator resolution of 0.7 and 1.3 nm at 253.7 and 404.6 nm respectively was adequate to identify most of the measured band heads in all the three fluorescence spectra shown in Fig.(6.7). The fluorescence spectrum at the incident photon wavelength of 121.6 nm (Fig. 6.7a) includes vibrational bands of two systems of SO emission. The A $^3\Pi \rightarrow$ X $^3\Sigma^-$ system of SO extends from 240 to 268 nm whereas the B $^3\Sigma^- \rightarrow$ X $^3\Sigma^-$ system covers the spectral range from 268 to 442 nm. The emission spectrum in the two regions has been identified and the assignment of bands has been carried out using the wavelength data reported by Rosen (1970). It may be noted that the dotted lines shown in the assignment chart in Fig.(6.7a) have not been observed and reported by Rosen (1970), but these have been shown in the figure based on simple calculations using molecular constants reported in literature.

The fluorescence spectrum at incident photon wavelength of 73.6-74.4 nm (Fig.6.7b) includes the bands of the same two systems of SO as observed in case of excitation at 121.6 nm but the emission spectrum is very much weaker. The fluorescence spectrum from SO_2^+ though energetically possible (Table 5.3) has not been observed. It is possible that the SO_2^+ fluorescence is very weak and could not be identified because of the presence of the stronger emission from SO. Dujardin and Leach (1981) have shown previously in their photoion-fluorescence photon coincidence study that the emission from SO fragments is about 100 times stronger than the SO_2^+ emission when excited at the NeI incident photon wavelength.
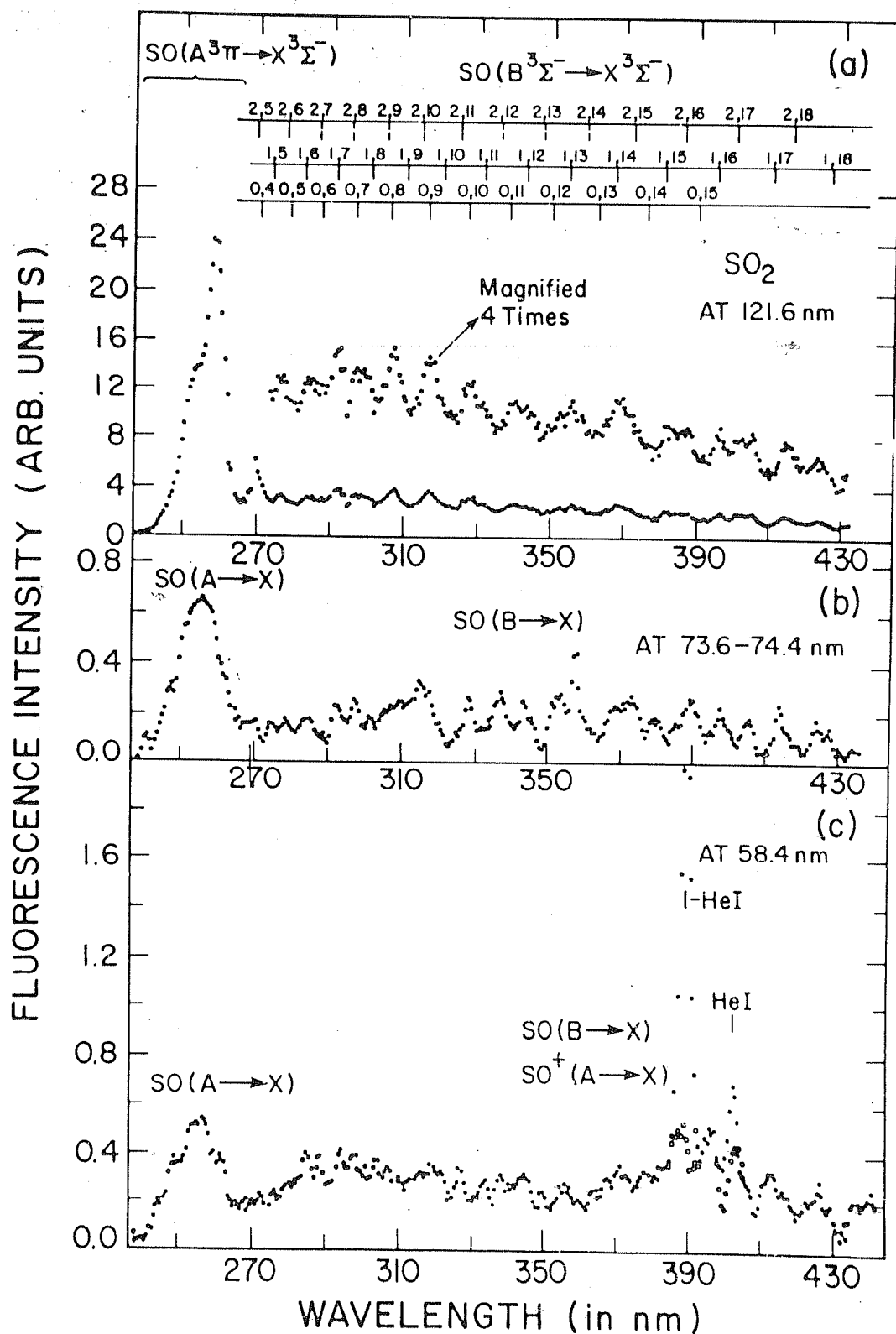
Figure 6.7 The fluorescence spectra of SO_2 at incident photon wavelengths of (a) 121.6 nm (b) 73.6-74.4 nm and (c) 58.4 nm.

The emission spectrum as shown in Fig.(6.7c) was obtained by photoionization of SO_2 at the incident photon wavelength of 58.4 nm. Some of the scattered neutral helium line emissions observed in the present work could be seen in the figure. These lines have been subtracted from the fluorescence spectra in the same way as in the case of CS_2. The remaining true fluorescence signals have been shown by open circles. This spectrum differs significantly from the spectra shown in Figs.(6.7a) and (6.7b). It consists of two components given below:

a) The first component of the emission spectrum is the same as for spectra excited at other two incident photon wavelength i.e. the A $^3\Pi \rightarrow$ X $^3\Sigma^-$ system of SO. This system is slightly weaker than that observed in Fig.(6.7b). But it is much stronger than that observed by Dujardin and Leach (1981) at the same excitation wavelength, 58.4 nm. Surprisingly, this system was not observed by Wu (1984) in the emission spectra obtained at the two excitation wavelengths, 68.6 and 55.5 nm.

b) The second component of the emission spectrum includes a broad continuum band with discrete bands of SO and SO^+ superimposed on it. The broad continuum band extends over the range from 260 to 440 nm with two apparent maxima at around 300 and 390 nm. One of the sets of bands superimposed over the continuum belongs to SO (B $^3\Sigma^- \rightarrow$ X $^3\Sigma^-$) system which extends almost over the whole spectral range from 268 to 442 nm. This system is relatively very weak. There is another set of bands superimposed over the continuum which is very weak from 250 to 380 nm but a few clearly resolved discrete bands were observed in the spectral region 380 to 440 nm. This set of bands belong to SO^+(A $^2\Pi \rightarrow$ X $^2\Pi$) system. The assignment for the bands of the system has recently been carried out by Tsuji et al (1980). The bands of the two

systems mentioned above are very close to each other; therefore some of the bands of the two systems appear to be a single broad band. Also, because of this type of merging and poor resolution, these bands appear to be superimposed over a continuum. It should be added that no emission due to SO_2^+ excitation was observed as shown in Fig. (6.7c). Threshold energies for formation of some electronic excited states of the products are given in Table (6.3) for the photoexcitation process of SO_2.

The relative production cross sections for SO (A $^3\Pi \rightarrow$ X $^3\Sigma^-$) and SO (B $^3\Sigma^- \rightarrow$ X $^3\Sigma^-$) systems have been calculated at the incident photon wavelengths of 121.6, and 73.6-74.4 nm. These cross sections include all the vibrational transitions for the two SO systems. No attempt has been made to calculate the relative cross sections for individual bands. For this purpose, the production cross section for the B→X system has been considered to be 1.00 and that for the A→X system has been calculated accordingly. It may be mentioned here that the relative production cross sections at the incident photon wavelength of 58.4 nm have not been computed, as at this wavelength, there are large number of interspaced bands belonging to a few systems mentioned above. The relative production cross sections at 121.6 and 73.6-74.4 nm are given in Table (6.4). The ratio of A→X system to B→X system have been found to be 0.57 and 0.35 at the excitation wavelengths of 121.6 and 73.6-74.4 nm. No comparison with any other data has been carried out as the production cross sections for these systems have not been reported in literature.

Table 6.3 Threshold energies for formation of various electronic
excited states of products for the photoexcitation
process of SO_2.

Products	Threshold Energies (eV)	Fluorescence Wavelength Observed in the present work (in nm)
SO_2^+ ($\tilde{X}\ ^2A_1$) + e^-	12.30	
SO_2^+ ($\tilde{A}\ ^2A_2$) + e^-	13.01	
SO_2^+ ($\tilde{B}\ ^2B_2$) + e^-	13.24	
SO_2^+ ($\tilde{C}\ ^2B_2$) + e^-	15.99	
SO_2^+ ($\tilde{D}\ ^2A_1$) + e^-	16.32	
SO_2^+ ($\tilde{E}\ ^2B_1$) + e^-	16.50	
SO_2^+ ($\tilde{F}\ ^2A_1$) + e^-	20.06	
SO^+ (X $^2\Pi$) + $O(^3P)$ + e^-	15.93	
SO^+ (a $^4\Pi$) + $O(^3P)$ + e^-	19.12	
SO^+ (A $^2\Pi$) + $O(^3P)$ + e^-	20.32	SO^+(A$\rightarrow$X): $\geq$ 250
SO^+ ($b^4\Sigma^-$) + $O(^3P)$ + e^-	20.56	
SO (X $^3\Sigma^-$) + $O(^3P)$	5.65	
SO (A $^3\Pi$) + $O(^3P)$	10.40	SO (A$\rightarrow$X): $\geq$ 240
SO (B $^3\Sigma^-$) + $O(^3P)$	10.81	SO (B$\rightarrow$X): $\geq$ 258

Table 6.4 The relative production cross sections for SO (A $^3\Pi \rightarrow$ X $^3\Sigma^-$) and SO(B $^3\Sigma^- \rightarrow$ X $^3\Sigma^-$) systems produced at incident photon wavelengths of 121.6 and 73.6-74.4 nm.

Incident Photon Wavelength in nm	Relative Production cross sections	
	SO : A→X System	SO : B→X System
121.6	0.57	1.00
73.6-74.4	0.35	1.00

CHAPTER - 7

CONCLUSION AND SCOPE FOR FUTURE WORK

7.1 CONCLUSION

The photoabsorption cross sections, fluorescence cross sections and fluorescence quantum yields were measured for sulphur dioxide using argon mini arc light source in the 188-231 and 278.7-320 nm regions. The cross sections were measured with the monochromator resolution of 0.2 nm. It was found that in most of the experiments reported so far, for the measurement of photoabsorption cross sections, the transmitted beam along the optic axis included the contribution of fluorescence from molecules. Therefore, the absorption cross sections measured were not accurate. This problem was taken care in the present experiment by using another monochromator after the transmitted beam so as to get rid of the fluorescence component being emitted along the optic axis. In view of this, it is suggested that more and more experiments should be done taking care of the fluorescence component along the optic axis so as to get accurate data on absorption cross sections of molecules. The measurement of fluorescence cross sections for SO_2 has confirmed the presence of a predissociating state in the present work. The threshold energy of incident photons responsible for predissociation has been found to be in the range between 218.9 and 220.6 nm.

The photoabsorption cross sections, fluorescence cross sections and fluorescence quantum yields were measured for

107

carbon disulphide in the 188.2-213 and 287.5-339.5 nm regions. The photoabsorption cross sections measured in the 188.2-213 nm region were found to be pressure dependent and such a measurement, to the best of our knowledge, has been carried out for the first time. The fluorescence cross sections in the present experiment, were measured along the photon-beam axis and a new mathematical approach was put forward to obtain fluorescence cross sections. In the spectral region 300-320 nm, the fluorescence cross sections as well as fluorescence quantum yields measured at the peaks of some vibrational bands of the V system were found to have a special type of pressure dependence. A possible mechanism for this phenomenon has been suggested.

It has been observed that the quantitative data on fluorescence of SO_2 and CS_2 in the spectral regions mentioned above are rather scarce. More experiments with better technology are needed to be taken up in this direction in near future.

The fluorescence spectra of CS_2 and SO_2 have been studied at three incident photon wavelengths of 121.6, 73.6-74.4, and 58.4 nm and relative production cross sections for different product states have been measured. The $CS(A \rightarrow X)$ system produced at 121.6 nm and $CS_2^+(B \rightarrow X$ and $A \rightarrow X)$ systems obtained at 73.6-74.4 and 58.4 nm have been analyzed in the present work whereas the $SO (A \rightarrow X$ and $B \rightarrow X)$ systems at 121.6 and 73.6-74.4 nm and the two systems of SO along with $SO^+(A \rightarrow X)$ system at incident photon wavelength of 58.4 nm have been studied carefully. In all these emission spectra, the relative production cross sections for fluorescence bands of different systems have been computed. It may be noted that not much work has been done in this direction. Therefore, a comprehensive comparison is not at all possible.

In all these measurements carried out in the present work, the monochromator resolution was not enough to resolve

all the bands individually. Instead, the relative production cross sections for different spectral regions consisting of large number of vibrational bands, were computed. It is felt that more measurements in this direction are required with much higher monochromator resolution without sacrificing the low level fluorescence intensities. Also, in the present experiment as well as in other studies reported by a few other researchers, the relative production cross sections have been measured at a few incident photon wavelengths only.

7.2 Scope for Future Work

Present measurement of photoabsorption and fluorescence cross sections of neutral species have been carried out at an instrumental resolution of 0.2 nm. This, relatively low, resolution has been chosen to accommodate very weak fluorescence fluorescence signals of target gases (SO_2 and CS_2) in certain spectral regions. A large number of photoabsorption cross section studies have been reported in the literature at high instrumental resolutions. Therefore, a direct comparison of cross sections measured in the present work, with the measurements reported at high resolutions is not possible. Hence there is a clear cut need to carry out these experiments at higher resolution. For this purpose, the same experimental set-up could be used to measure both photoabsorption and fluorescence cross sections at higher resolutions, as the 1-meter monochromator used for the selection of incident photon wavelengths can offer resolutions down to 0.05 nm, using much reduced slit widths for both entrance and exit slits of the monochromator. This exercise should be carried out only for those target molecules which have relatively higher absorption and fluorescence cross sections in the spectral regions under investigation.

The study of temperature dependence of photoabsorption

cross sections measured in the laboratory is extremely useful to aeronomers and astrophysicists for the understanding of terrestrial and extra-terrestrial atmospheres. The importance of such measurements has been emphasized by Belton (1982) in order to use the spectrum of SO_2 as a diagnostic remote sensing tool in understanding the atmospheres of Venus and Io. Such measurements can be taken up using the same experimental set-up described previously after making some meaningful modifications. The absorption chamber in this case could be cooled or heated using a cold finger-methyl alcohol system attached to the chamber.

In the spectral regions above 200 nm where the target gas is found to have high fluorescence quantum yield e.g., SO_2 in 200-230 nm, the fluorescence spectrum could also be obtained at large number of incident photon wavelengths and relative production cross sections for different product states could be studied. The study of total fluorescence cross section at a certain incident photon wavelength along with the study of energy analysis of this fluorescence (that is fluorescence spectrum) would give the partial fluorescence cross sections for different competing product channels. This would give a better insight about the primary photochemical process of absorption of target molecules.

In the present experiment on ionic fluorescence of molecules like SO_2 and CS_2, the resolution of the monochromator, used for dispersing the fluorescence signals, was varied from 0.48 to 1.3 nm to study various systems of emission corresponding to different product states. The disadvantage at these (relatively poor) resolutions is that a large number of vibrational bands which are closely spaced could not be resolved. As a result, the relative production cross sections for product states had contribution from different unresolved vibrational bands. In view of this, it is desired to study the fluorescence emissions from the product states at higher monochromator resolutions (0.2 to

0.4 nm) so as to obtain the relative production cross sections for individual vibrational bands. This could be achieved by using the same experimental set-up with a better focusing optics and dispersing unit.

The fluorescence emission arising due to the interaction of VUV radiation with target gases (SO_2, CS_2) has been studied at few incident photon wavelengths only. This does not give a complete picture about the possible change of production cross section as a function of incident photon energy. To get a better insight, the measurements are required to be carried out at a large number of incident photon wavelengths. To study the emission spectrum from different product states at higher resolutions, as mentioned above, and also at many incident photon wavelengths, a powerful continuum source in VUV region is needed. A synchrotron radiation source is the ideal one to suit these requirements. However, in the absence of continuum VUV source, a many-lined source emitting very closely spaced emission lines would be a good substitute. A thyratron-triggered sliding spark discharge source is available in our laboratory, which can give a large number of closely spaced VUV lines due to multi-ionized gas atoms used in the source . A grazing incidence VUV monochromator would be needed to disperse the closely spaced emission lines.

LIST OF PUBLICATIONS

1. Quantitative photoabsorption and fluorescence spectroscopy of sulphur dioxide at 188-231 and 278.7-320 nm.

   S.M.Ahmed and Vijay Kumar

   Submitted for publication to
   J.Atmos.Chem.

2. Measurement of photoabsorption and fluorescence cross sections for carbon disulphide at 188.2-231 and 287.5-339.5 nm.

   S.M.Ahmed and Vijay Kumar

   Submitted for publication to
   J.Atmos.Chem.

3. Fluorescence studies of CS_2 and SO_2 at 121.6, 73.6-74.4, and 58.4 nm.

   I.A.Prajapati, S.M.Ahmed and Vijay Kumar

   Submitted for publication to
   Pramana

REFERENCES

Ahmed, S.M. and Kumar, V. (1990) Submitted for publication to *J.Atmos.Chem.*

Baldwin, G.C. and Gaerttner, M.R. (1973) *J.Vac.Sci.Technol.* 10 , 215.

Barker, E.S. (1979) *Geophys.Res.Lett.* 6 , 117.

Beer, A.V. (1852) *Ann.Phys.Chem.* 86 , 78.

Belton, M.J.S. (1982) *Icarus* 52 , 149.

Bertaux, J.L. and Belton, M.J.S. (1979) *Nature* 282 , 813.

Black, G., Sharpless, R.L. and Slanger, T.G. (1977) *J.Chem. Phys.* 66 , 2113.

Bouguer, P. (1729) *Essai d'optique sur la graduation de la lumiere.* This work was reprinted in 1921 by *Gauthier-Villars, Eds., Librakries du Bureau des Longitudes, de l'Ecole Polytechnique, Quais des Grands-Augustine* , 55.

Boursey, E., Ronain, J-Y., Damany, H. and Damany, N. (1977) *Rev.Sc.Instrum.* 42 , 526.

Brand, J.C.D., Chiu, P.H. and Hoy, A.R. (1976) *J.Mol. Spectrosc.* 60 , 43.

Brand, J.C.D. and Srikameswaran, K. (1972) *Chem.Phys.Lett.* 15 , 130.

Brassington, D.J. (1981) *Appl.Optics* 20 , 3774.

Bridges, J.M. and Ott, W.R. (1977) *Appl.Optics* 16 , 367.

Brundle, C.R. and Turner, D.W. (1969) *Int.J.Mass Spectrom.Ion Phys.* 2, 195.

Brus, L.E. (1971) *Chem.Phys.Lett.* 12 , 116.

Brus, L.E. and McDonald, J.R. (1974) *J.Chem.Phys.* 61 , 97.

Callear, A.B. (1963) *Proc.Roy.Soc. (London)* A276 , 401.

Callomon, J.H. (1958) *Proc.Roy.Soc. (London)* A 244, 220.

Castex, M-C, Romand, J. and Vodar, B. (1968) *Rev.Sc.Instrum.* 39 , 331.

Clements, J.H. (1935) *Phys.Rev.* 47 , 224.

Codling, K., Hamley, J.R and West, J.B. (1977) *J.Phy.* B10 , 2797.

Conway, R.R., McCoy, R.P. and Barth, C.A.(1979) *Geophys.Res. Lett.* 6 , 629.

Coon, J.B., Elliott, P.M., Riggs, J.M. and Kim, S.U. (1967) *Bull.Amer.Phys.Soc.* 12 , 182.

Dalgarno, A. and Black, J.H. (1976) *Rep.Prog.Phys.* 39 , 573.

Dibeler, V.H. and Walker, J.A. (1967) *J.Opt.Soc.Am.* 57, 1007.

Douglas, A.E. (1966) *J.Chem.Phys.* 45 , 1007.

Douglas, A.E. and Zanon, I. (1964) *Can.J.Phys.* 42 , 627.

Duchesne, J. and Rosen, B. (1947) *J.Chem.Phys.* 15 , 631.

Dujardin, G. and Leach, S. (1981) *J.Chem.Phys.* 75, 2521.

Edmonds, T. and Hobson, J.P. (1965) *J.Vac.Sci.Technol.* 2 , 182.

Esposito, J.W.,Winick, J.R. and Stewart, I.A. (1979) *Geophys. Res.Lett.* 6 , 601.

Freeman, D.E., Yoshino K., Esmond, J.R. and Parkinson, W.H. (1984) *Planet.Space Sci.* 32 , 1125.

Freney, J.R., Ivanov, M.V.and Rodhe, H.(1983) *SCOPE* 21 , 56.

Goldsmith, P.F., Langer, W.D., Schloerb, F.P and Scoville, N.Z. (1980) *Astrophys.J.* 240 , 524.

Golomb, D., Watanabe, K. and Marmo, F.F. (1962) *J.Chem.Phys.* 36 , 958.

Hamada, Y. and Merer, A.J. (1975) *Can.J.Phys.* 53 , 2555.

Heicklen, J. (1963) *J.Am.Chem.Soc.* 85 , 3562.

Herzberg, G. (1966) *Electronic Spectra of Polyatomic Molecules, pp. 512, 605, Van Nostrand, Princeton, N.J.*

Hillier, I.H. and Saunders, V.R. (1971) *Mol.Phys.* 22 , 193.

Hubin-Franskin, M.J., Locht, R. and Katihabwa, J. (1976) *Chem.Phys.Lett.* 37 , 488.

Hudson, R.D and Carter, V.L. (1965) *Phys.Rev.* 137A , 1648.

Hui, M.H. and Rice, S.A. (1972) *Chem.Phys.Lett.* 17 , 474.

Jaechke, W., Schmitt, R. and Georgii, H.W. (1976) *Geophys.Res.Lett.* 3 , 517.

Jungen, Ch., Malm, D.N. and Merer, A.J., (1973) *Can.J.Phys.* 51 , 1471.

Kleman, B. (1963) *Can.J.Phys.* 41, 2034.

Kripalani, I.T. and Misra, R.N. (1988) *P.R.L. Tech.Note* TN-88-60

Krueger, A.J. (1983) *Science* 220 , 1377.

Kumar, V. and Dutta, A.K. (1979) *App.Optics* 18 , 1414.

Kurylo, M.J. (1978) *Chem.Phys.Lett.* 58 , 238.

Lambert, J.H.(1760) A German translation appeared as *"Lambert's Photometrie "* translated by E. Andig, (1892) *Leipzig : Verlag von Wilhelm Engelmann.*

Lambert, C. and Kimbell, G.H. (1973) *Can.J.Chem.* 51 , 2601.

Lee, L.C., Judge, D.L. and Ogawa, M. (1975) *Can.J.Phys.* 53, 1861.

Linke, R.A. and Goldsmith, P.F. (1980) *Astrophys.J.* 235 , 437.

Maroulis, P.J. and Bandy, A.R. (1980) *Geophys.Res.Lett.* 7 , 681.

McGee, T.J. and Burris Jr. J. (1987) *J.Quant.Spectrosc. Radiat.Transfer* 37 , 165.

Mettee, H.D. (1968) *J.Chem.Phys.* 49 , 1784.

Molina, L.T., Lamb, J.J. and Molina, M.J. (1981) *Geophys.Res. Lett.* 8 , 1008.

Noyes, W.A. and Leighton, P.A. (1966) *The Photochemistry of gases, Dover Publication, New York.*

Okabe, H. (1971) *J.Amer.Chem.Soc.* 93 , 7095.

Okabe, H. (1972) *J.Chem.Phys.* 56 , 4381.

Ott, W.R. and Bartoe, J. (1972) *J.Opt.Soc.Am.* 62 , 1372.

Pearse. R.W.B. and Gaydon, A.G. (1965) *The Identification of Molecular Spectra, Chapman and Hall, London.*

Pitz, E. (1969) *App.Optics* 8 , 257.

Rosen, B. *Spectroscopic Data Relative to Diatomic Molecules (Pergoman, Oxford, 1970), p 342.*

Sagawa, E. and Itoh, T. (1977) *Geophys.Res.Lett.* 4 , 29.

Samson, J.A.R. (1964) *J.Opt.Soc.Am.* 54 , 6.

Samson, J.A.R., and Haddad, G.N. (1974) *J.Opt.Soc.Am.* 64 , 47.

Sandalls, F.J. and Penkett, S.A. (1977) *Atmos.Environ.* 11 , 197.

Schmitt, R.G. and Brelun, R.K. (1966) *Appl.opt.* 5 , 1111.

Smythe, W.C., Nelson, R.M. and Nash, D.B. (1979) *Nature* 280 , 766.

Stewart, A.I., Anderson, D.E., Jr., Esposito, L.W. and Barth, C.A. (1979) *Science* 203 , 777.

Stuck, D. and Wende, B. (1974) in *Vacuum UV Radiation Physics*, E.Koch, R.Hansel, and C.Kunz, Eds (*Vieweg und Sohn, Braunshweig,* 1974), p.722.

Sze, N.D. and Ko, M.K.W. (1979) *Nature* 280 , 308.

Thompson, B.A., Harteck, P. and Reeves, R.R. Jr. (1963) *J.Geophys. Res.* 68 , 6431.

Tsuji, M., Yamagiwa, C., Endoh, M. and Nishimura, Y. (1980) *Chem.Phys.Lett.* 73, 407.

Turco, R.P., Whitten, R.C., Toon, O.B., Pollack, J.B. and Hamill, P. (1980) *Nature* 283 , 283.

Warneck, P., Marmo, F.F. and Sullivan, J.O. (1964) *J.Chem.Phys.* 40 , 1132.

Weissler, G.L., Ogawa, M. and Judge, D.L. (1971) *J.Phys. Paris, Suppl.* 32 C4-154.

Wine, P.H., Chameides, W.L. and Ravishankara, A.R. (1981) *Geophys.Res.Lett.* 8 , 543.

Wu, C.Y.R. (1981) *Unpublished data*, Private communication.

Wu, C.Y.R. and Judge, D.L. (1981) *Geophys.Res.Lett.* 8 , 769.

Wu, C.Y.R. (1984) *J.Phys. B : At.Mol.Phys.* 17, 405.

Young, A.T. (1978) *Bull.Amer.Astron.Soc.* 10 , 549.